Polymer-induced tumor immunotherapy by *in situ* activation of antigen-presenting cells

Dissertation

zur Erlangung des Grades

„Doktor der Naturwissenschaften“

(Dr. rer. nat.)

Am Fachbereich Biologie

Der Johannes Gutenberg-Universität Mainz

Vorgelegt von

Lara Stein

Geboren am 21.05.1994 in Neunkirchen Saar
Matrikelnummer: 2713093

Mainz, den 17.05.2024

Aus dem Institut für Immunologie der
Universitätsmedizin der Johannes Gutenberg-Universität Mainz

Dekan: Prof. Dr. Eckhard Thines

1. Berichterstatter:
2. Berichterstatter:

Tag der mündlichen Prüfung: 23.07.2024

Directory

1. Introduction

1.1 The immune system

In daily life, the body is surrounded by various environmental influences and harmful invaders such as viruses, bacteria, fungi, and other pathogens. Some of them can cause serious diseases and lead to lasting damage of the organism. To eliminate these pathogens, evolution developed a complex and highly sophisticated network of cells, tissues, and organs, called the immune system. The primary function of the immune system is to recognize and eliminate these foreign substances while distinguishing them from the body's own healthy cells. To ensure the best possible protection, the immune system is divided into two components – the innate "general" and the adaptive "specialized" immune response, which interact together through a series of coordinated responses.

1.1.1 The Innate Immune System

The first line of defense is given by the innate immune system. It prevents foreign substances from entering the body by providing immediate, non-specific protection against a broad range of pathogens. This diversity comes from a limited number of germline-encoded receptors, which are inborn. They recognize conserved products of microbial metabolism produced by the microbial pathogens but not by the host (Janeway and Medzhitov 2002). Skin and mucous membranes act as important first physical barriers. If a pathogen breaches one of the host's anatomical barriers, there are various cellular and soluble components that quickly respond to infection by immediately killing or attenuating the invaders. Herein, antimicrobial enzymes, interferons, different immune cell types, peptides and complement proteins play an important role. Complement proteins can be activated by both the innate and the adaptive immune system. However, the activated proteins follow a signal cascade. If a complement protein binds to a component on the surface of a microorganism or an antibody, the microorganism can be recognized and eliminated by phagocytes. This causes an inflammatory reaction and attracts more phagocytes to the site of infection, which in turn lyse the invaders with defensins, nitric oxide, and reactive oxygen derivatives (Kaplan, Heine, and Simmons 1999; Robinson 2008). On the other hand, cells infected by viruses release interferons to warn other non-infected cells. Additionally, microorganisms express specific ubiquitous structures that are recognized by germline-encoded PRRs (pattern recognition receptors) on macrophages and dendritic cells (DC). In general, with their overlapping sentinel and regulatory functions, macrophages and

DCs play central roles in anti-infectious defense. While macrophages are innate immune effector cells, DCs induce the adaptive immunity (Weisheit, Engel, and Kurts 2015). Toll-Like-Receptors (TLR), which belong to the PRR family, recognize pathogen associated molecular patterns (PAMPs) like conserved components of the bacterial cell wall or general virus (Janeway 1989; Medzhitov and Janeway 1997, 1998; Kawai and Akira 2010; Krishnaswamy, Chu, and Eisenbarth 2013). TLR3, TLR7/8 and TLR9 exclusively expressed in endosomes, recognize nucleic acids like double-stranded (ds)RNA, single-stranded (ss)RNA and ssDNA (deoxyribonucleic acid) (Wagner and Bauer 2006). In contrast, TLR2, TLR4, TLR5 and TLR11 reside on the cell membrane, detect lipopeptides, lipopolysaccharide, flagellin, and propellin (Wagner and Bauer 2006). Furthermore, natural killer (NK) cells, which are type of innate lymphocytes, are able to distinguish between infected cells from the body's own healthy cells and trigger apoptosis in degenerated target cells (Yokoyama 2005). The innate immune system reacts rapidly within minutes to hours to become fully activated and recognizes a broad spectrum of different classes of organisms or molecules. If a pathogen outwits the non-specific immune system and enters the body despite the external protective barriers, a specific response, e.g., one that is specifically tailored against a pathogen, must take place. This is where the adaptive immune system intervenes.

1.1.2 The Adaptive Immune System

Immunity, acquired by the adaptive immune system, enables the body to react specifically to pathogens. This process can take days to several weeks to occur, but it is long lasting. This is not only because of immunological memory but also because of antigen specificity, the ability to distinguish between endogenous and exogenous as well as to react against an enormous variety of exogenous molecules (Farber, Yudanin, and Restifo 2014). In general, the adaptive immune system is divided into humoral and cellular immune responses. The main players are B cells on one hand and T cells on the other. They can be activated simultaneously and can also act cooperatively. Both cell types originate from lymphoid precursor cells in the bone marrow, whereby B cells remain there for further differentiation and T cells migrate to the thymus to mature into T helper cells ($CD4^+$ T cells) or cytotoxic T cells ($CD8^+$ T cells). Before the first antigen contact, T cells are naïve and in some cases they need antigen presenting cells (APCs) to become activated. Professional APCs include DC´s, macrophages, and B cells. All types of APCs trigger another adaptive immune response. Mature DCs, for example, are essential for T cell priming and activate naïve, effector, and memory cytotoxic T cells (Tc) as well as helper T cells (Th) (Hilligan and Ronchese 2020). Whereas macrophages and B cells present antigens

exclusively to effector and memory T cells ('Chapter 7 - Antigen Processing and Presentation' 2014).

There are four major pathways (exogenous, endogenous, cross-presentation, and autophagic) to process and present an antigen to the desired immune cell ('Chapter 7 - Antigen Processing and Presentation' 2014).

Antigens derived from extracellular sources, such as pathogens or proteins, are uptaken by APCs through processes like phagocytosis, endocytosis, or pinocytosis; this describes the **exogenous** antigen presentation pathway. The degradation of antigens into peptide fragments by proteases takes place within the endosomal or lysosomal compartment of the APC. Afterwards the peptides are loaded onto MHC-II complexes, which are subsequently transported to the cell surface for specific recognition by the matching T cell receptor (TCR) of $CD4^+$ T cells (Zinkernagel and Doherty 1997). This represents the first step of T cell activation. Another signal T cells need to fully activate and differentiate into effector T cells is the engagement of co-stimulatory molecules, such as CD28 on T cells binding to the ligandsCD80/86 on APCs (Gizinski, Fox, and Sarkar 2010a; Gizinski, Fox, and Sarkar 2010b).

The **endogenous** pathway involves the presentation of antigens derived from intracellular pathogens or proteins synthesized within the cell. In the proteasome, these proteins are degraded into peptide fragments and transported into the endoplasmic reticulum (ER) with the transporter associated with antigen processing (TAP) molecules. Within ER, the peptides are loaded onto major histocompatibility complex class I (MHC-I) of APCs, which is then transported to the cell surface where it gets recognized by $CD8^+$ T cells (Blum, Wearsch, and Cresswell 2013; Pishesha, Harmand, and Ploegh 2022). This is the form of direct presentation of an antigen. The indirect presentation, where both endogenous and exogenous paths are used, is called **cross presentation**. Cross presentation is a specialized antigen presentation pathway where DCs are involved. They are able to present exogenous antigens on MHC-I and activate cytotoxic T lymphocytes (CTLs) against antigens not directly derived from the cytosol of the APC itself (Joffre et al. 2012).

In the context of specialized antigen presentation, there is also **autophagy**. Cytosolic antigens are delivered to lysosomal compartments for degradation. Out of this process, antigenic peptides are loaded onto both MHC molecules and presented on the cell surface for recognition by T cells. It´s an important process, for presenting antigens derived from intracellular pathogens, damaged organelles, or misfolded proteins to contribute to immune surveillance and maintain cellular homeostasis (Crotzer and Blum 2009).

Ultimately, the prevailing cytokine environment, in addition to antigen presentation, is also of decisive importance for T cell activation to indicate in which direction they should differentiate (Clarkson and Sayegh 2005). Functionally, cytokine release can be subdivided into pro- or anti-inflammatory immune responses. Depending on the environment, $CD4^+$ T cells develop into T helper cells (Th1, Th2, Th17 T and T follicular helper (Tfh) cells) or regulatory T cells (Tregs) (Reddy et al. 2004; Walker 2022). Activated T helper cells can influence other cells via cytokine release and are therefore also called T effector cells (Teff).

The proinflammatory cytokines IL-12, produced by DCs, and IFN-γ, from NK cells, give rise to Th1 cells, which express the specific transcription factor T-bet. Th1 cells secrete IFN-γ, IL–2, and TNF-α to protect the host against intracellular infections by viruses and bacteria as well as from cancer cells (Heufler et al. 1996; Kaiko et al. 2008; Raphael et al. 2015; Abdi et al. 2022). This empowers the Th1 cells to activate macrophages at the site of inflammation to create a cell-mediated immunity and phagocyte-dependent protective immune responses (Romagnani 1999).

As a counterpart to the proinflammatory Th1-mediated immune response, an anti-inflammatory immune response involving Th2-type cytokines can occur. In this case, IL-4, primarily produced by mast cells, eosinophils, and basophils, leads to the formation of Th2 cells, which express the transcription factor GATA-3. Th2 cells secrete IL-4, IL-5, as well as IL-13 and play an important role in B cell activation for the antibody response (Berger 2000; Kaiko et al. 2008; Gadani et al. 2012; Hsieh et al. 1992; Seder et al. 1992). Th2 cells are also able to produce TNF-α and some produce IL-9.

The third subset of CD4 effector cells are the pro-inflammatory Th17 cells which develop in the presence of TGF-β and IL-6 (Veldhoen et al. 2006). They produce IL-17a, IL-17f, IL-22, TNF-α, and express RORγT (Park et al. 2005; Zhu, Yamane, and Paul 2010). These cells play a role in tissue inflammation as well as in the activation of neutrophils (Kaiko et al. 2008).

Tfh cells help B cells by the formation of germinal centers (GC) that allow affinity maturation of antibody response (Walker 2022). Thus, they facilitate the production of high affinity antibodies through the secretion of effector cytokines, such as IL-21 and IL-4, and through cell-cell interactions (Jandl, Loetsch, and King 2017).

On the other hand, there are immunosuppressive $CD4^+Foxp3^+$Tregs which are crucial for immunological homeostasis and for preventing immune responses to autoantigens (Chen and Oppenheim 2014). IL-2 plays a pivotal role in maintaining immune balance by governing the formation, upkeep, and activity of Treg cells, while also influencing the proliferation and differentiation of effector cells (Hayes et al. 2020). Tregs express the high-affinity receptor

alpha chain CD25 (IL2RA) that grants them selective access to IL-2 to support their anti-inflammatory functions (Hayes et al. 2020). They also express anti-inflammatory cytokines like TGF-β, IL-10 and IL35 (Astarita et al. 2022). They are also able to block the costimulatory CD80/CD86 signals through expression of CTLA-4 and directly kill inflammatory or autoreactive cells with cytotoxic molecules like perforin and granzyme (Astarita et al. 2022; Josefowicz, Lu, and Rudensky 2012). Through these properties, Tregs regulate the adaptive and innate immune response.

Additionally, so-called tissue-resident Treg cells, which migrate and accumulate in non-lymphoid tissues, are important for regenerative function and promote tissue repair in an IL-33 dependent fashion (Delacher et al. 2017). These cells play a role in wound healing and skin barrier regeneration after UVB (ultraviolet B radiation) damage and are required for lung epithelial proliferation after acute lung injury (Nosbaum et al. 2016; Arpaia et al. 2015; Tan et al. 2019). In addition to this important function in the regeneration of tissues, tissue-resident Treg cells are also found in the tumor microenvironment and are increasingly induced during tumor development and growth. There, these cells can inhibit anti-tumor immunity and thus prevent the immune system from attacking the tumor (Li, Jiang, et al. 2020).

As already mentioned, Tregs are important in maintaining immune tolerance. TCRs need to be able to recognize a large diversity of antigens to ensure immunological defense. This TCR diversity is achieved by somatic recombination of already existing gene segments. They are generated by the random combination of TCR coding gene segments V(D)J (Variability, Diversity and Joining) to generate T cell clones with unique TCRs (Davis and Bjorkman 1988; Market and Papavasiliou 2003; Jung and Alt 2004). The finite set of receptor gene segments leads to an enormous number of foreign antigens that can be recognized (Buch et al. 2005; Kaye et al. 1991; Market and Papavasiliou 2003; Jung and Alt 2004). An existing danger in the complex process of TCR generation is an autoimmune reaction based on the fact that receptors can also be formed that recognize the body's own antigens (Germain 2012). To protect the body from such reactions against itself, T cells are selected positively or negatively depending on the binding of TCRs to MHC-peptides complexes and the recognition of MHC-self peptides complexes in the course of central tolerance. When a TCR binds endogenous MHC molecules expressed by thymic epithelial cells, positive selection occurs and all bound T cells continue their development (Chaplin 2010). If a TCR is unable to recognize endogenous molecules, the cell receives no survival signal and undergoes apoptosis. This positive selection process is also known as "death by neglect" (Hernandez, Newton, and Walsh 2010). However, to avoid self-reactivity, T cells with a TCR that binds too strongly to the MHC-self peptide complex will be

negatively selected. These cells are overactivated and also undergo apoptosis. Ultimately, selection ensures that only T cells with a moderate affinity for self-peptides presented on thymic MHC complexes survive, thus preventing the development of autoreactive cells as much as possible.

Nevertheless, some T cells manage to bypass selection and potentially recognize the body's own antigens. For this reason, peripheral tolerance has developed. On the one hand, there is anergy, which means that self-reactive T cells no longer react functionally or are eliminated after encountering self-antigens outside the thymus (Xing and Hogquist 2012). Anergy occurs when a T cell binds to an MHC-self peptide complex without inducing co-stimulatory signals. This cell continues to live but can no longer be activated. This is not possible even by subsequent antigen presentation on an APC. There is also a clonal deletion of the T cells. Here, too, T cells die by apoptosis if an antigen is presented in a too high concentration or is reactivated within a short time after activation (Xing and Hogquist 2012).

In addition, peripheral tolerance is induced by conventional $CD4^+CD25^+FoxP3^+$ Treg cells that suppress autoreactive cells (Starr, Jameson, and Hogquist 2003; Mueller 2010). They express TCRs and are activated by antigen-MHC complexes. They maintain homeostasis by mediating tolerance to endogenous antigens and help to differentiate between exogenous and endogenous peptide-antigens (Hernandez, Newton, and Walsh 2010).

Based on their development pathway Tregs can be divided into thymus derived Tregs (tTreg), peripheral-derived Tregs (pTreg), and *in vitro* induced Tregs (iTreg). tTregs appear to exert their suppressive effects by inhibiting the migration of Teff cells to target organs. On the other hand, antigen-specific induced iTregs primarily prevent T-cell activation by targeting DCs with IL-10, playing a crucial role in iTreg-mediated suppression by regulating the expression of MARCH1 and CD83 on DCs (Shevach and Thornton 2014). Furthermore, activated tTregs can induce infectious tolerance by transferring cell surface-bound TGF-β to naïve T cells, thereby converting them into pTregs (Shevach and Thornton 2014).

Even after the induction of specific immune defenses, interaction with components of the innate immune system persists during what is termed as "the effector phase" of the immune response. In this phase, the immune system actively works to protect the host against the recognized danger, whether it be a pathogen, toxin, or any foreign substance perceived as a threat. This interaction between innate and specific immune components remains evident in both antibody-based and cytotoxic effector mechanisms of immune defense (McCullough and Summerfield 2005).

As already mentioned, there are two MHC molecules that are recognized by two subgroups of T cells. $CD4^+$ T cells recognize MHC-II class molecules and, in combination with B cells, represent the humoral immune response. Humoral means "fluid", which describes the contact of antibodies with antigens in blood, lymph and interstitial fluids. Here too, the phagocytized antigen is taken up by a macrophage, degraded in the lysosome, and peptide fragments are presented on the cell surface via MHC-II complexes. $CD4^+$ T cells recognize this complex through their TCR, thereby inducing proliferation and T cell clone expansion (McCullough and Summerfield 2005). In the effector phase, cytokines released by T helper cells activate the proliferation of B cells. Binding of an antigen to the specific IgM receptor of the B cell triggers endocytosis and the associated degradation and presentation of the antigen or fragments of the antigen. These processed fragments on the B cell can now be recognized by TCRs. As a result, the B cell also acts as an APC. Before the first antigen contact, the B cell is naive. After getting in touch with the foreign antigen, proliferation of the B cells starts. The proliferating B cells differentiate, and B cell clones of plasma cells, which secrete antibodies, and memory cells, for the potential secondary immune response through a renewed infection with the pathogen, develop.

$CD8^+$ T cells can interrogate all cells in the body and thus recognize fragments of extracellular proteins presented by infected cells on MHC-I molecules via the TCR. They represent the cellular immune response. Binding to an infected cell stimulates the cytotoxic T cell to proliferate and form clones. In the effector phase, the TCR of the cytotoxic cell again recognizes the processed non-self antigen bound to the MHC-I molecules, and this specific binding leads to the lysis of the target cell through a granule-mediated cytotoxicity involving perforin and granzymes. This process triggers rapid target-cell death (Nicholson 2016).

Cellular and humoral immune responses are important players in our immune system. Dysregulation in their work processes and an immunosuppressive tumor microenvironment can allow degenerated cells to escape the controls of the immune system and cause serious diseases such as cancer (Anderson and Simon 2020). Researchers have therefore set themselves the task of gaining a better understanding of the immune system and the crucial microenvironment of tumors. The aim is to prevent existing dysregulations in diseases and tumor-associated stoma so that the immune system can fight and recognize cancer cells again.

1.2 Development of Cancer

As described before, the immune system recognizes pathogens or degenerated cells before they can harm the body. But in some cases, this naturel defense is lost, leading to uncontrolled cell growth and proliferation of these degenerated cells. Depending on the type of cancer, the exact mechanism underlaying cancer development can vary, there are several general stages and factors involved (Hanahan and Weinberg 2000, 2011; Hanahan 2022).

1.2.1 Cancer initiation

Typically, the initiation of cancer starts with mutations or alterations in normal cells, caused by various factors including exposure to carcinogens such as ultraviolet (UV) radiation, tobacco smoke, chemicals or infectious agents. These mutations may affect genes that regulate cell growth, DNA repair, apoptosis or other cellular processes. With mutations in proto-oncogenes, that promote cell growth, or tumor suppressor genes, that inhibit cell growth or promote cell death, cancer cells gain a selective growth advantage. Proliferation of the degenerated cells leads to the outgrowth of a population of clonally derived tumor cells. This results in uncontrolled cell growth and ends in the formation of neoplastic lesions or benign tumors (Cooper 2000). Additional genetic changes may occur, further driving the progression towards malignancy. The accumulation of mutations forms a tumor that becomes increasingly aggressive and invasive, resulting in metastasis. This is accompanied by angiogenesis where cancer cells release angiogenic factors that stimulate the proliferation of blood vessels, ensuring a sufficient blood supply to further support the tumor growth. Together with various cell types, including immune cells, fibroblasts, endothelial cells, extracellular matrix (ECM) components and signaling molecules, this forms the tumor microenvironment (TME), which also plays a crucial role in cancer development and progression (Whiteside 2008). The interaction between the cancer cells and the TME influences the growth, invasion, immune evasion and the response to cancer therapy. In the 2000s, Hanahan and Weinberg established the six "Hallmarks of cancer", which are still the gold standard for describing the complex development of cancer today (Hanahan and Weinberg 2000).

1. *Self-sufficiency in growth signals*: Cancer cells exhibit uncontrolled growth signaling, often due to mutations or dysregulation in genes involved in cell cycle control and growth factor signaling pathways.
2. *Insensitivity to anti-growth signals:* Normally, there are inhibitory signals for cell growth or inducing cell death. But tumor cells evade these signals, allowing them to continue proliferating despite adverse conditions.

3. *Evading apoptosis*: Tumor cells can resist the programmed cell death by acquiring mechanisms, enabling their survival even in the presence of cellular stress or damage.
4. *Limitless replicative potential*: By activating mechanisms that sustain telomere maintenance or alternative lengthening of telomeres (ALT), cancer cells can overcome the normal limits on cellular lifespan. This allows them to divide indefinitely.
5. *Sustained angiogenesis:* Tumors stimulate the growth of new blood vessels to ensure a steady supply of oxygen and nutrients, facilitating their growth and metastasis.
6. *Tissue invasion and metastasis:* Cancer cells acquire the ability to invade surrounding tissues and migrate to distant sites in the body, forming metastases and contributing to cancer progression.

Later in 2011, two provisional "emerging" hallmarks (7. + 8.) and two enabling characteristics were added (9. + 10.) (Hanahan and Weinberg 2011).

7. *Deregulating cellular metabolism*: To meet their increased energy demands and biosynthetic needs, tumor cells undergo metabolic reprogramming. As a result, aerobic glycolysis (Warburg effect) is often favored, and the function of the mitochondria is altered.
8. *Avoiding immune destruction:* Cancer cells can escape the normal immune surveillance. They have various mechanisms like inhibiting immune cell function, promoting an immune suppressive TME, or downregulating antigen presentation.
9. *Genome instability and mutation:* This hallmark emphasizes the propensity of cancer cells to accumulate genetic alterations, including mutations, chromosomal rearrangements, and DNA damage, which can drive tumorigenesis and tumor progression. Genome instability can arise from defects in DNA repair mechanisms, replication errors, exposure to mutagens, and other factors.
10. *Tumor-promoting inflammation:* Tumors can influence and manipulate the immune cells within TME, to contribute inflammatory processes to various aspects of cancer development.

In a 2022 review they added again two emerging hallmarks "unlocking phenotypic plasticity" and "senescent cells" as well as two enabling characteristics "nonmutational epigenetic reprogramming" and "polymorphic microbiomes" (Hanahan 2022).

11. Unlocking phenotypic plasticity: Phenotypic plasticity refers to the ability of cancer cells to adapt and switch between different phenotypic states, which can contribute to tumor heterogeneity, therapeutic resistance, and metastasis (Gupta et al. 2019).

12. *Senescent cells*: Normally, senescent cells are in a permanent cell cycle arrest to counteract cellular stress. In tumors they promote cancer cell proliferation, migration, invasiveness, angiogenesis, and EMT (Xiao et al. 2023).
13. *Nonmutational epigenetic reprogramming:* Changes in DNA methylation, modifications in histone proteins and shifts in the expression of non-coding RNAs within cancer cells lead to disruptions in the epigenetic programming of gene expression (Costa et al. 2023).
14. *Polymorphic microbiomes*: Furthermore, changes in the microbiome play a role in the development of cancer. They include the modulation of inflammation, the induction of DNA damage, and the production of metabolites that can either promote oncogenesis or suppress tumor growth (Bhatt, Redinbo, and Bultman 2017). Microbes have the potential to directly cause cancer and influence the host immune system to facilitate malignancy (Lythgoe et al. 2022).

All in all, the way the hallmarks of cancer have expanded over the last years shows the complexity involved in the development of cancer and its microenvironment.

1.2.2 The tumor microenvironment

As already mentioned, the TME plays a crucial role in cancer development and progression. It encompasses diverse cell types such as tumor cells, fibroblasts, endothelial cells, various immune cell populations, along with their secreted mediators, as well as blood vessels and the ECM providing structural support. It is composed in part of cancer cells and infiltrating immune cells. On the one hand, there are cancer cells that have escaped the normal immune surveillance and proliferate uncontrollably. On the other hand, there are various non-malignant cell types supporting the tumor progression. Depending on the origin of the tumor and the present cell types as well as other individual factors, the TME can be either tumor suppressive or tumor promoting. Early on, a substantial influx of immune cells from both the innate and adaptive immune system migrates to the tumor site. If these tumor cells evade immune elimination, they establish themselves, creating a complex, dynamic, and heterogeneous milieu, which influences the effectiveness of anti-cancer treatments (Bilotta, Antignani, and Fitzgerald 2022). Cytokines and chemokines released by tumor cells, host cells, and immune cells significantly influence the immune landscape within the TME (Li, Yu, et al. 2020). The cells of the TME relevant to this work are highlighted below.

Cancer cells

Cancer cells are the primary component of the tumor and drive tumor growth and progression. They exhibit various genetic and epigenetic alterations that confer proliferative advantages, evade immune surveillance, promote angiogenesis, as well as enable invasion and metastasis. They can evade immune surveillance through various mechanisms, including downregulating major histocompatibility complex (MHC) molecules, which are crucial for immune recognition, and secreting immunosuppressive factors that inhibit the activity of immune cells such as T cells and NK cells (Wu et al. 2023). Additionally, cancer cells may undergo genetic mutations that allow them to escape detection by the immune system or to create an immunosuppressive microenvironment that hampers immune responses (Jiménez-Morales et al. 2021).

Immune cells

Various immune cells such as neutrophils, T cells, B cells, NK cells, NKT cells, macrophages, and DCs can infiltrate the tumor microenvironment. These immune cells have complex interactions with the cancer cells and depending on their activations state as well as the cytokine milieu, these cells can either promote or suppress tumor growth. Among the infiltrating tumor-associated innate immune cells are macrophages and neutrophils, which interact with tumor cells and dampen the cytotoxic activity of both innate and adaptive killer cells, thereby promoting tumor growth and enhancing malignancy (Guc and Pollard 2021).

Neutrophils are cells of the innate immune system and inherently, constitute the highest population of immune cells within the blood stream. They are recruited to the primary tumor site and depending on the TME as well as their maturation status they can have pro- or anti-tumor functions (de Visser and Joyce 2023). Tumor associated neutrophils (TANs) enable tumor progression through the facilitation of angiogenesis, remodeling of the extracellular matrix, promotion of metastasis, and induction of immunosuppression. In turn, they are also able to kill tumor cells directly and support the anti-tumor inflammation (Jaillon et al. 2020; Guc and Pollard 2021).

Tumor-associated macrophages (TAMs) have multiple subsets that coexist, and they possess dual roles in cancer progression (de Visser and Joyce 2023). By fostering angiogenesis, immunosuppression, metastasis, and therapy resistance, they promote tumor growth (DeNardo and Ruffell 2019). However, they are also able to impede cancer progression through direct phagocytosis of cancer cells or by stimulating anti-tumor immune responses.

DCs are important APCs that initiate and regulate adaptive and innate immune responses (de Visser and Joyce 2023; Wculek et al. 2020). They provide information's about the TME to immune cells, especially to T cells, and shape anti-tumor immunity (Gerhard et al. 2021). Within an immunosuppressive TME, the activity of DCs shifts towards dysfunction and tolerogenicity, and thus cancer cells can evade their immune control mechanism (Del Prete et al. 2023).

$CD8^+$ T cells kill cancer cells through apoptosis induced by the release of granzymes and perforin proteins or FasL (Fas Ligand)-Fas mediated cell death (de Visser and Joyce 2023; Nagata and Golstein 1995; Nagata 1999). In cancer, this type of T cell is often in an exhausted or dysfunctional state (Philip and Schietinger 2022; van der Leun, Thommen, and Schumacher 2020). This means that the cells gradually lose their effector function after long-term exposure to antigens and provide inefficient protection against cancer (Kurachi 2019).

NK cells are cytotoxic cells from the innate immune system with the task to protect the body from viruses and cancer (Cerwenka and Lanier 2001). They recognize stress-induced autologous proteins on transformed or infected cells, kill them by lysis, as well as produce inflammatory chemokines and cytokines. A major advantage of NK cells is the recognition of degenerated cells regardless of neoantigen presentation or MHC class I expression what makes them really attractive for immunological therapy approaches (Wolf, Kissiov, and Raulet 2023). Due to resistance and mutations, tumor cells no longer express MHC I resulting in insufficient elimination through cytotoxic T cells (Vivier et al. 2011; Chan and Ewald 2022).

Invariant NKT cells (iNKT) are also cells from the innate immune system and are related toNK cells. But unlike NK cells, they are CD1d-restricted lipid specific T lymphocytes and build the bridge between the innate and adaptive immune system (Terabe and Berzofsky 2008; Kawano et al. 1997). They possess the ability to moderate numerous immune functions based on their distribution throughout various tissues. iNKT cells participate in cancer immunosurveillance by directly eliminating tumor cells or by coordinating the actions of immune cells that either promote or inhibit tumor growth (Fujii and Shimizu 2019). Cancer-related immunosuppression may alter iNKT cell behavior towards more regulatory roles (de Visser and Joyce 2023).

Cancer-associated fibroblasts

Cancer-associated fibroblasts (CAFs) are activated fibroblasts and one of key components of the tumor stroma (de Visser and Joyce 2023). They consist of various functionally diverse subtypes exhibiting considerable flexibility and contribute to tumor progression by secreting growth factors, cytokines, and ECM components that promote tumor cell proliferation,

invasion, and angiogenesis (Kalluri 2016). CAFs also play a role in remodeling the ECM and create a supportive niche for cancer cells, resulting in immune evasion (Sahai et al. 2020).

Extracellular matrix

The ECM is a complex network of fibrous proteins such as collagen, glycoproteins, and proteoglycans that provides structural as well as biochemical support to tissues and regulates cell behavior (Popova and Jücker 2022). In the TME, the ECM undergoes significant remodeling, leading to the deposition of stiff and dense matrix components that promote tumor cell survival, migration, and invasion (Kai, Drain, and Weaver 2019). Abnormal ECM remodeling can also impair drug delivery and contribute to treatment resistance (Kesh et al. 2020).

Angiogenic Factors and Hypoxia

Tumors require a sufficient blood supply to sustain their growth, and angiogenesis, the formation of new blood vessels, is a critical process in tumor progression. The TME is enriched with angiogenic factors such as vascular endothelial growth factor (VEGF), fibroblast growth factor (FGF), and angiopoietin, which promote the sprouting of new blood vessels from pre-existing ones (Lugano, Ramachandran, and Dimberg 2020). Because of the rapid growth, tumors often lack oxygen and nutrients, leading to the development of hypoxic regions within the TME. Hypoxia triggers adaptive responses in cancer cells and stromal cells, such as increased angiogenesis, altered metabolism, and resistance to apoptosis, which promote tumor survival and aggressiveness (Muz et al. 2015; Li, Zhao, and Li 2021).

Inflammatory Cytokines and Chemokines

Chemokines and cytokines are important mediators in the communication between immune cells. In the TME, they shape the immune status often towards pro-tumorigenic state (Bule et al. 2021). The TME is characterized by the presence of inflammatory cytokines and chemokines, such as interleukin-6 (IL-6), tumor necrosis factor-alpha (TNF-alpha), and interleukin-10 (IL-10), which contribute to tumor-associated inflammation, immune suppression, and tumor progress (Abdul-Rahman et al. 2024).

Understanding the interactions between tumor cells and their microenvironment is critical for developing new cancer therapies that target not only the cancer cells themselves but also the surrounding stromal and immune cells that support tumor growth and progression. Therapies

targeting the TME aim to disrupt pro-tumor signaling pathways, enhance anti-tumor immune responses, and normalize the abnormal vasculature to improve the delivery of chemotherapy drugs and other treatments to the tumor site.

1.3 Immunotherapies

In the development of cancer, immune cells lose control of degenerated cells. By the use of immunotherapies in the treatment of cancer, the body's own immune system is reactivated or boosted to recognize, fight, and eliminate tumor cells again. It is a promising approach for cancer treatment due to its potential for durable responses, reduced toxicity compared to traditional treatments, and applicability across a wide range of cancer forms. There are different immunotherapies types and approaches.

1.3.1 CAR T cell and TIL therapy

For example, *chimeric antigen receptor* (CAR) T cell therapy, pave a new way in the treatment of cancer. This type of therapy involves a genetic engineering of a patient's T cells to express synthetic receptors (CARs) that target specific antigens expressed by cancer cells. After this modification, the CAR T cells are infused back into the patient where they recognize and eliminate cancer cells in a highly targeted manner. CAR T cell therapy has shown impressive results but is associated with severe side effects such as severe life-threatening toxicities, modest anti-tumor activity, antigen escape, restricted trafficking, and limited tumor infiltration (Sterner and Sterner 2021).

Another immunotherapy based on *tumor infiltrating lymphocytes* (TILs) has also been developed. Here, immune cells, particularly T cells, from a patient's tumor tissue, are expanded and reinfused back into the patient. This kind of treatment harnesses the natural anti-tumor activity of T cells and showed good efficacy against solid tumors (Zhao et al. 2022).

1.3.2 Monoclonal antibodies and immune modulators

One form of therapy that is now considered as one of the main components of cancer treatment besides surgery, radiation, and chemotherapy is the injection of *monoclonal antibodies* (MABs). These MABs consist of laboratory-made proteins that target specific proteins on cancer cells, thereby triggering immune-mediated destruction of cancer cells. The majority of MABs exhibit direct anti-tumor effects by either prompting apoptosis or inhibiting receptor signaling when they bind to their designated antigen (Hubert and Amigorena 2012). But indirect killing by antibody-dependent cell cytotoxicity (ADCC) and complement dependent

cytotoxicity (CDC) also plays a crucial role (Narvekar et al. 2022). MABs can be used as standalone therapies or in combination with other treatments, such as chemotherapy or radiation therapy. Examples of monoclonal antibodies used in cancer immunotherapy include rituximab, trastuzumab, and cetuximab (Zahavi and Weiner 2020).

Immune modulators are a somewhat different approach, which modulate the activity of the immune system to enhance anti-tumor immune responses. These include cytokines such as interleukin-2 (IL-2) and interferon-alpha (IFN-α), which can stimulate immune cell proliferation and activation

1.3.3 Immune Checkpoint inhibitors

Immune checkpoint inhibitors (ICI) are also a popular form of therapy and very effective when patients respond to therapy. Immune checkpoints are used by cancer cells to block the immune system's control, allowing them to grow unhindered. To regain the control of the immune system and to reactivate already existing T cells, specific ICI have been developed in the context of this immune checkpoint blockade therapy (Dine et al. 2017). These drugs target inhibitory receptors or specific ligands on immune cells or tumor cells, thereby releasing the brakes on the immune response and enhancing anti-tumor immunity. Programmed cell death protein 1 (PD-1), programmed death-ligand 1 (PD-L1), and cytotoxic T-lymphocyte-associated protein 4 (CTLA-4) count as key checkpoints in this kind of therapy (Alturki 2023). The ICI treatment has been very successful over the last decade because of the reduced side effects compared to standard therapies, but there are also limits. If the tumor has a low tumor mutational burden (TMB), not enough neoantigens are expressed to trigger a robust immune response (Arora et al. 2019). In addition, anti PD-1/PD-L1 therapy may not respond if the tumor expresses only a small amount of PD-L1 (Uruga and Mino-Kenudson 2021). In an immunosuppressive TME, the effect of the inhibitors is also severely limited by Tregs, MDSCs, and other suppressive immune cells (Hou et al. 2020). Combination therapies have proven to be useful in overcoming these problems. The combinations of different ICI or ICI with other immunotherapies, chemotherapy, or targeted therapies are being investigated to improve response rates and overcome resistance mechanisms.

Anti-cancer vaccinations represent a new field of research. They aim to stimulate the immune system to recognize and attack cancer cells by presenting tumor-specific antigens to immune cells. There are several types of cancer vaccines, including peptide vaccines, DNA or RNA vaccines, and dendritic cell vaccines. Cancer vaccines can be prophylactic, targeting cancer-

causing viruses such as human papillomavirus (HPV), or therapeutic, targeting tumor-specific antigens expressed by cancer cells (Fan et al. 2023).

1.3.4 Nanoparticle based immunotherapies

Anti-cancer vaccinations also include nanoparticle-based approaches that offer a suitable platform for drug delivery by encapsulating active pharmaceutical ingredients to bring to the tumor site in a more efficient manner (Mundekkad and Cho 2022). Advantages of this type of treatment are the variability of size, shape, selective binding capacity, high permeability and surface modification of the particles (Sun et al. 2014). Besides this, by encapsulating the active ingredients, the particles are immunological silent, which results in lower toxicity and reduces the risk of unpredicted loss of function. Moreover, they are characterized by good biocompatibility and biodegradability (Wang, Li, and Nie 2021). As with all other forms of therapy, there are also difficulties that need to be overcome. Peptide- and protein-based anti-cancer vaccines suffer from insufficient immune activation with risk of tolerance and tumor relapse (Toes et al. 1996; Hailemichael et al. 2013; Joshi et al. 2012; Stickdorn et al. 2022). We have therefore developed in cooperation a nanoparticle (NP) that stimulates the immune system through a TLR7/8 ligand and induces a stable immune response through the simultaneous binding of an antigen.

1.4 Aim of this project

The aim of this project was to establish a nanoparticle based, personalized immunotherapy to overcome the immunosuppressive tumor microenvironment and to reactivate the inherent capacity of immune cells to recognize and eliminate tumor cells again.

Therefore our collaborators, former at the Max Planck Institute for Polymer Research at the Johannes Gutenberg-University Mainz and now Macromolecular Chemistry at the Julius-Maximilians-University Würzburg developed a nanoparticle, decorated with whole ovalbumin protein (OVA) as a model antigen and 1-(4-(aminomethyl)- benzyl)-2-butyl-1H-imidazo[4,5-c]quinolin-4-amine (IMDQ) as an immune stimulatory TLR7/8 agonist. With this particle, we vaccinated wild-type C57BL/6J mice in a therapeutic setting and challenged them with subcutaneously inoculated cancer cells unmodified or containing membranous or cytosolic OVA. Afterwards we checked if our NP based vaccination was able to induce a tumor-specific immune response.

2. Material and methods

2.1 Material

2.1.1 Laboratory Equipment

Table 1: Laboratory equipment

Device	Company
Amnis ImageStream Mk II	Luminex (Texas, USA)
Analytical scale	Sartorius CP64 (Göttingen Germany)
Attune NxT flow cytometer	Thermo Fisher Scientific (Darmstadt, Germany)
BD FACSymphony™ A3 Cell Analyzer BD FACSCanto™ BD LSR II™	BD Bioscience (Franklin Lakes, USA)
BD Rhapsody™ single cell analysis system	BD Bioscience (Franklin Lakes, USA)
Capacitance extender plus	Bio-Rad (California, USA)
CO_2 incubator	Sanyo (München, Germany) Thermo Fisher Scientific (Darmstadt, Germany)
Digital caliper	Thermo Fisher Scientific (Darmstadt, Germany)
Electric shaver	B. Braun (Melsungen, Germany)
ELISpot reader AiD iSpot (ELR08IFL)	AiD Diagnostika GmbH (Straßberg, Germany)
Freezer (-20 °C, -80 °C)	Liebherr (Biberach an der Riß, Germany)
Gene-Pulser II	Bio-Rad (California, USA)
Heraeus Biofuge fresco	Thermo Fisher Scientific (Darmstadt, Germany)
Heraeus Megafuge 40R Centrifuge, Megafuge ST Plus Series Centrifuge	Thermo Fisher Scientific (Darmstadt, Germany)
Incubation waterbath (Aqualine AL12)	Lauda (Königshofen, Germany)
Infrared lamp (INFRARED-H95E)	Philips (Hamburg, Germany)
Injection cage	Kent Scientific (Torrington, USA)
MACS seperator	Miltenyi Biotec (Bergisch-Gladbach, Germany)
Microscope Motic AE20 series	Motic (Wetzlar, Germany)
Mini centrifuge (MCF-2360)	LMS (Tokyo, Japan)
Multichannel pipette	Eppendorf (Hamburg, Germany)

Continuation of Table 1: Laboratory equipment

Device	**Company**
Nalgene CO2 euthanasia chamber	Thermo Fisher Scientific (Darmstadt, Germany)
Neubauer counting chamber	Roth (Karlsruhe, Germany)
Pipetboy comfort	INTEGRA bioscience (Fernwald, Germany)
Pipettes	Gilson (Berlin, Germany) Eppendorf (Hamburg, Germany) Thermo Fisher Scientific (Darmstadt, Germany)
Platform shaker (Titramax 100)	Heidolph (Schwabach, Germany)
Refrigerator (4 °C)	Liebherr (Biberach an der Riß, Germany) Bosch (Gerlingen, Germany)
SI-200 Series Stuart Shaking Incubator	Cole-Parmer® (Illinois, USA)
Tecan GENios plate reader	Tecan (Männedorf, Schweiz)
Thermal mixer	Thermo Fisher Scientific (Darmstadt, Germany)
UniVet anesthesia Induction chamber	Groppler Medizintechnik (Deggendorf, Germany)
UniVet Porta anesthesia machine	Groppler Medizintechnik (Deggendorf, Germany)
Vet Animal blood counter	Scil veterinary excellence (Viernheim, Germany)
Vortex mixer 230V	VWR (Leuven, Belgium)

Table 2: Reagents

Reagent	**Company**
3-Amino-9-ethyl-carbazole (AEC)	Sigma-Aldrich (Steinheim, Germany)
5,6-Carboxyfluorescein Diacetat Succinimidyl Ester (CFSE)	Thermo Fisher Scientific (Waltham, USA)
Accutase® solution	Sigma-Aldrich (Missouri, USA)
Albumin	Sigma-Aldrich (Steinheim, Germany)
Anti CD45 beads (TIL)	Miltenyi Biotec (Bergisch-Gladbach, Germany)
Aqua	Fresenius Kabi Deutschland GmbH (Bad Homburg, Germany)
BSA	PAN Biotech (Aidenbach, Germany)
Calcein AM	Thermo Fisher Scientific (Waltham, USA)
Collagenase-4	Worthington Biochemical Corporation (New Jersey, USA)
Dimethyl sulfoxide (DMSO)	Sigma-Aldrich (Steinheim, Germany)
DMEM (1X)	Gibco (Darmstadt, Germany)
DNase-I	Sigma-Aldrich (Steinheim, Germany)
Ethanol (96 %)	Merck (Darmstadt, Germany)
Ethylenediaminetetraacetic acid (EDTA)	Sigma-Aldrich (Steinheim, Germany)
Fetal calf serum (FCS)	Gibco (Darmstadt, Germany)
Fixable Viability Dye eFluor^{TM} 780	Thermo Fisher Scientific (Waltham, USA)
Fucoidan	Sigma-Aldrich (Steinheim, Germany)
Geneticin G-418 Sulphate	Gibco (Darmstadt, Germany)
Glutamax	Gibco (Darmstadt, Germany)
HRP anti IgG1 KT91 ab170487	Abcam (Cambridge, UK)
HRP anti IgG2a KT92 ab170489	Abcam (Cambridge, UK)
HRP anti IgM KT95 ab170492	Abcam (Cambridge, UK)
Hydrogen peroxide (30 %)	Merck (Darmstadt, Germany)
IMDM (1X)	Gibco (Darmstadt, Germany)

Continuation of Table 2: Reagents

Reagent	**Company**
Isopropanol (2-Propanol)	Hedinger (Stuttgart, Germany)
$OVA_{257-264}$ (SIINFEKL) and $OVA_{323-337}$ (ISQAVHAAHAEINEAGR)	Peptides & elephants (Henningsdorf, Germany)
pcDNA3.1+P2A-eGFP	Genscript Biotech (New Jersey, USA)
Penicillin/Streptomycin	Serva (Tübingen, Germany)
pIRES2-EGFP	Clontech (Mountain View, USA)
Rompun 2 % (Xylazin hydrochloride)	Bayer (Leverkusen, Germany)
RPMI Medium 1640	Gibco (Darmstadt, Germany)
Sodium pyruvate	Serva (Tübingen, Germany)
Sterican® cannulas	Braun (Melsungen, Germany)
Trypan blue solution	Calbiochem (Darmstadt, Germany)
Tumor dissociation kit	Miltenyi Biotec (Bergisch-Gladbach, Germany)
Tween-20	Roth (Karlsruhe, Germany)
Vectastain ABC-Kit	Maravai Life Sciences (San Diego, USA)

Table 3: Consumables

Device	**Company**
Autoclavable bags	Roth (Karlsruhe, Germany)
C-Chip Counting Chamber	Nanoentek (Waltham, USA)
Cell culture flask (25 cm^2, 75 cm^2, 175 cm^2)	Greiner (Frickenhausen, Germany)
Cell strainer (40 µm, 70 µm)	Greiner (Frickenhausen, Germany)
Cell strainer (70 µm)	Miltenyi Biotec (Bergisch-Gladbach, Germany)
Centrifuge tubes (15 ml, 50 ml)	Greiner (Frickenhausen, Germany)
ELISA plates	Greiner (Frickenhausen, Germany) Thermo Fisher Scientific (Waltham, USA)
ELISpot plates	Merck Millipore (Darmstadt, Germany)
Glas pipettes	Hirschmann (Eberstadt, Gemany)
Latex and nitril gloves	L&R (Wien, Austria) VWR (Pennsylvania, USA)
Multi-well plates (F-, U- or V-bottom)	Greiner (Frickenhausen, Germany)
Petri dishes	Sigma-Aldrich (Steinheim, Germany)
Pipette tips	Starlab (Hamburg, Germany)
Reagent reservoir	Corning incorporated (New York, USA)
Reagent tubes (0,5 ml, 1,5 ml, 2 ml)	Eppendorf (Hamburg, Germany)
Reagent tubes for Flow Cytometry	Greiner (Frickenhausen, Germany)
Scale dishes	VWR (Leuven, Belgium)
Scalpels	Dahlhausen (Halberstadt, Germany)
Syringes (1 ml, 30 ml)	B. Braun (Melsungen, Germany)

2.1.2 Kits, buffer and media

1. Kits

Table 4: Kits

Kit	Company
BD Rhapsody™ Targeted mRNA and AbSeq Amplification Kit	BD Bioscience (Franklin Lakes, USA)
BD Rhapsody™ Whole Transcriptome Analysis (WTA) Amplification Kit	BD Bioscience (Franklin Lakes, USA)
BD® Single-Cell Multiplexing Kit	BD Bioscience (Franklin Lakes, USA)
Cytometric Bead Array (CBA) Flex Kit	BD Bioscience (Franklin Lakes, USA)
CytoTox96 Non-Radioactive Cytotoxicity Assay kit	Promega (Wisconsin, USA)
eBioscience™ Foxp3/Transcription Factor Staining Buffer Set	Thermo Fisher Scientific (Waltham, USA)
ELISpot Vectastain ABC Kit	Vector Laboratories (Burlingame, USA)
Tumor Dissociation Kit (TDK)	Miltenyi Biotec (Bergisch-Gladbach, Germany)

2. Buffer

1x PBS (phosphate buffered saline)

Desalted water (pH 7,3 and sterile filtrated 0,2 µm)

8.18 g/l sodium chloride

1.56 g/l sodium hydrogen phosphate dihydrate

ACK Buffer

pH 7.3 and sterile filtrated 0,2 µm

8.02 g/l Ammonium chloride

0.1 g/l Potassium hydrogen carbonate

0.037 g/l Ethylene diamine tetra acetate (EDTA)

AEC complex solution for ELISpot (for 50 ml)

Sodium acetate buffer

1 AEC tablet

2.5 ml Dimethyl formamide

(afterwards sterile filtrated)

Coating buffer

pH 9.3 filtered 0,2 µm

0.1 M Di-Natriumhydrogenphosphat-Dihydrat (Na_2HPO_4 x $2H_2O$)

Citrate buffer

pH 4.4 and sterile filtered 0,2 µm

40 mM citrate acid monohydrate

60 mM Di-Natriumhydrogenphosphat-Dihydrat (Na_2HPO_4 x $2H_2O$)

EDTA blood buffer

1 x PBS

30 mM EDTA

0.01 % sodium azide

ELISA wash buffer

1 x PBS

0.1 % TWEEN 20

ELISA blockbuffer

1 x PBS

1 % BSA

0.2 % TWEEN 20

FACS buffer

1 x PBS

0.5 % BSA

5 mM EDTA

Gey´s lysis buffer

Desalted water (pH 7,3 and sterile filtrated 0,2 µm)

150 mM ammonium chloride

1 mM Potassium hydrogen carbonate

1 mM EDTA

MACS buffer

1 x PBS

0,5 % BSA

5 mM EDTA

PBS-EDTA

1 x PBS

0.5 % EDTA (0,5 M stock solution)

Trypan blue staining solution

Desalted water (pH 7,3 and sterile filtrated 0,2 µm)

Mixing ratio 1:5

0.2 % trypan blue

4.25 % sodium chloride

3. <u>Media</u>

DMEM high glucose (for B16-F10, MC38 and also their transfected cell counterparts)

10 % FCS

2 mM L-Glutamine

200 mg/ml penicillin

200 U/ml streptomycin

1 mM sodium pyruvate

RPMI 1650 (OTI splenocytes)

10 % FCS

2 mM L-Glutamine

200 mg/ml penicillin

200 U/ml streptomycin

50 µM β-mercaptoethanol

1:250 dilution of IL2 supernatant from XL-63 cells

1 µg/ml $OVA_{257-264}$ peptide

IMDM (DC2.4)

5 % FCS

2 mM L-Glutamine

200 mg/ml penicillin

200 U/ml streptomycin

50 µM β-mercaptoethanol

IMDM or TM10/TM5 (Iscoves Modified Dulbeccos Medium) (primary cells)

10 % or 5 % FCS

2 mM L-Glutamine

200 mg/ml penicillin

200 U/ml streptomycin

1 mM sodium pyruvate

2.1.3 Antibodies

Table 5: Antibodies

antibody	fluorochrome	clone	dilution	manufacturer	usage
αIFN-γ	biotinylated	R4-6A2	1:500	Mabtech	ELISpot
αIFN-γ	purified	AN-18	1:200	Mabtech	
αIgG1	HRP	KT91 ab170487	1:000	Abcam	ELISA
αIgG2a	HRP	KT92 ab170489	1:2000	Abcam	
αIgM	HRP	KT95 ab170492	1:1000	Abcam	
CD4	APC	RPA-T4	1:400	BD Bioscience	FACS
CD44	BV785	IM7	1:400		
CD45(TIL)	Magnetically labeled		1:10	Miltenyi	
CD62L	FITC	MEL-14	1:400		
CD8	APC-Cy7	SK1	1:200	BioLegend	
CFSE	FIT-C	/	1:200	Thermo Fisher Scientific	
Goat anti-rabbit IgG		AlexaFluor647	1:500		FACS
Live/dead	APC-Cy7	/	1:1000	Thermo Fisher Scientific	

Continuation of Table 5: Antibodies

antibody	fluorochrome	clone	dilution	manufacturer	usage
Ovalbumin polyclonal	HRP		1:300	Thermo Fisher Scientific	
SIINFEKL-H2K^b	PE	25.D1.16	1:133	Own production	

2.1.4 Cell lines

All the following text passages have been copied from our own publication, partially rewritten and marked as such (Stickdorn et al. 2022).

MC38 colon adenocarcinoma cells were kindly provided by H.-C. Probst (Institute for Immunology, University Medical Center, Johannes Gutenberg-University Mainz). The cells were isolated from a colon tumor in a C57BL/6 mouse after prolonged exposure to the carcinogen DMH (1,2-dimethylhydratinedihydrochlorid) (Tan, Holyoke, and Goldrosen 1976). Tumors arising from the cell line are immunogenic and are useful for exploring in vivo adjuvant immunotherapies and chemoimmunotherapies (Belnap et al. 1979).

B16-F10 melanoma cells were purchased from ATCC (USA) and the cell line was generated out of a spontaneously melanoma from C57BL/6 (H-2b) mice (Brown et al. 2001).

DC2.4 cells, kindly provided by V. Mailänder (Department of Dermatology, University Medical Center, Johannes Gutenberg-University Mainz) were generated by immortalizing murine DCs by transduction of BMDCs with retrovirus vector expressing murine GM-CSF, Myc and Raf oncogenes (Shen et al. 1997). They have the same cell morphology as normal DCs and express specific markers. Because of their feature characteristics like the ability of phagocytosis and present antigens to MHC I as well as II, they are ideal to study DC activity *in vitro*.

OT-I splenocytes were isolated from the spleen of OT-I or C57BL/6-Tg(TcraTcrb) 1100Mjb/Crl (Charles River) mice. These mice contain transgenic inserts for the murine

Tcrα-V2 and Tcrβ-V5 genes. This transgenic TCR is able to recognize the OVA-specific peptide SIINFEKL ($OVA_{257-264}$) restricted by the murine MHC class I molecule H-$2K^b$.

2.1.5 Mouse strains

Wildtype mice

- C57BL/6 (own breeding)
- C57BL/6JOlaHsd (Envigo)

Transgenic mice

- OT-I (own breeding, kindly provided from working group Reddehase Institute of Virology, University Medical Center)
- C57BL/6-Tg(TcraTcrb)1100Mjb/Crl (Charles river)

2.1.6 Nanoparticle

The NPs were produced by our cooperation partners of the Nuhn group (predominantly by Judith Stickdorn) at the Max Plank Institute for Polymer Research located at the Johannes Gutenberg-University Mainz but now based at the Julius-Maximilians-University in Würzburg, Chair for Macromolecular Chemistry. The particles were pH-responsive, core functionalized with 1-(4-(aminomethyl)- benzyl)-2-butyl-1H-imidazo[4,5-c]quinolin-4-amine (IMDQ), a TLR-7/8 agonist and they contain the ovalbumin (OVA) antigen on the particle surface. One injection of 100 µl NP contains 120 µg of the particle and is functionalized with 30 µg OVA and 10 µg IMDQ.

Table 6: Declaration of the NP compositions and its meaning

NP composition and notation	**meaning**
NP(IMDQ+OVA)	IMDQ and OVA covalently attached to the NP
NP(IMDQ)+sOVA	IMDQ covalently attached to the NP, soluble OVA
sIMDQ+sOVA	soluble IMDQ and soluble OVA, **NOT** attached to the NP

2.2 Methods

2.2.1 Cell line culture

Cells get cultured in different media (compare 2.1.2). After feeding and splitting in different ratios the cells were incubated by 37°C, 95 % humidity und 5 % CO_2. Cells need to get feed every two or three days depending on the splitting ratio. Adherent cells can be removed from the bottom by using the cell-detach solution accutase. For DC2.4 cells 5mM PBS-EDTA (0.5 M Stock solution) was used instead. Afterwards they are ready to split and for experimental use.

Calculating cell viability with trypan blue

To calculate the viability, 10 µl of cell suspension get mixed with 90 µl of a 0.05 % trypan blue solution (1:10), whereof 10 µl get pipetted into a Neubauer counting chamber. Trypan blue is able to pass the cell membrane when the cell is damaged and stains the cytoplasm of dead cells blue. Total cell number per ml is calculated according to the following equation:

Counted cells * dilution * total capacity * Neubauer chamber constant = total cell number per ml

All steps were carried out according to the manufacturer's instructions. The following text passages has been copied from our own publication, partially rewritten and marked as such (Stickdorn et al. 2022).

2.2.2 Engineered cell lines – Transfection with membranous or cytosolic OVA

Both cell lines (MC18 and B16-F10) expressing membrane-bound OVA (MC38mOVA, B16-F10mOVA) were generated by electroporation using expression plasmids (pIRES2-EGFP (Clontech) for MC38 and pcDNA3.1+P2A-eGFP (GenScript Vectors) for B16-F10) containing cDNA encoding full-length OVA protein linked to the transmembrane region of H-2D^b, which was generously provided by T. Tedder (Department of Immunology, Duke University School of Medicine, North Carolina). To obtain stable B16-F10 cells expressing cytosolic OVA (B16-F10cOVA), B16-F10 cells were electroporated using the pcDNA3.1+P2A-eGFP vector containing cDNA encoding full-length OVA. Cells expressing EGFP were selected by two rounds of screening using a FACS Aria (BD Biosciences) at the Core Facility of the Research Center for Immunotherapy (University Medical Center, Johannes Gutenberg-University Mainz). Cells were maintained in DMEM high glucose supplemented with 10 % FBS, 2 mM

L-Glutamine, 200 mg/ml penicillin, 200 U/ml streptomycin and 1 mM sodium pyruvate. To maintain EGFP and OVA expressions, transfected cell cultures were supplemented with G418 (400 µg/ml for MC38mOVA, MC38cOVA; 1000 µg/ml for B16-F10mOVA and B16-F10cOVA) (Stickdorn et al. 2022). The MC38mOVA transfection was established and done by Dr. Danielle Arnold-Schild.

2.2.3 *In vitro* experiments

2.2.3.1 Quantification of the successful transfection

To verify whether the transfection of the cancer cells with the OVA and EGFP containing vector was successful, we performed some quantitative and functional experiments.
Some following text passages have been copied from our own publication, partially rewritten and marked as such (Stickdorn et al. 2022).

Surface and cytosolic OVA expressing tumor cell line

Illustrating FACS staining

For surface OVA staining, MC38 or B16-F10 cells, MC38 mock-transfected cells expressing only EGFP or MC38mOVA or B16-F10mOVA cells were incubated for 20 min at 4°C with a rabbit polyclonal antibody against OVA (dilution 1:300), which was kindly provided by H.-C. Probst (Institute for Immunology, University Medical Center, Johannes Gutenberg-University Mainz) and K. Schäkel (Department of Dermatology, University Hospital Heidelberg). After secondary antibody staining using a goat anti-rabbit IgG (H+L) conjugated to Alexa Fluor 647 (Thermo Fisher Scientific, dilution 1:500), data were acquired on an Amnis ImageStream Mk II flow cytometer (Luminex) at the Core Facility of the Research Center for Immunotherapy (University Medical Center, Johannes Gutenberg-University Mainz) and analyzed using the IDEAS software (Luminex). Dead cells were gated out using DAPI (Thermo Fisher Scientific, dilution 1:10,000) (Stickdorn et al. 2022).

Cytotoxic Assay

For recognizing and eliminating OVA-expressing cells by effector T cells, OT-I transgenic mice were used to generate $CD8^+$ T cells that respond to peptide 257-264 of OVA. Cytotoxicity activity was measured using the CytoTox96 Non-Radioactive Cytotoxicity Assay kit (Promega) and by following the manufacturer's instructions. In brief, target cells were incubated with varying numbers of effector cells for 4 hours, and supernatants were then analyzed for lactate dehydrogenase release. The results are expressed as percent specific lysis, calculated as

(Experimental release – Spontaneous release)/(Total release – Spontaneous release) x 100% (Stickdorn et al. 2022).

Coculture assay with transfected cancer cells and OT-I splenocytes

Transfected B16-F10 cells were cocultured with isolated and CFSE stained OT-I splenocytes to measure their proliferation initiated by the antigen presentation of the $OVA_{257-264}$ epitope (SIIINFEKL) on the cancer cells MHC-I molecules. SIINFEKL presentation only occurs when OVA is processed from the transfected cancer cells. OT-I cells were labeled with 5 µM CFSE in 1x PBS for 4 min at 37°C in the water bath. Afterwards cells were washed with pure FCS and resuspended in RPMI medium. B16-F10, B16-F10mOVA as well as B16-F10cOVA were prepared as described in 2.2.1 and 2.2.2. Both cell types were adjusted to a concentration of $1x10^7$ cells/ml and the target cancer cells were incubated with varying numbers of CFSE-labeled effector OT-I T cells for 48 hours. Non-transfected B16-F10 and OT-I cells not cocultured with cancer cells served as negative control and both supplemented with 1 µg/ml SIINFEKL peptide as positive control. After the 48 hours of coincubation cells were harvested and stained with FACS antibodies for the epitopes CD45, CD8, CD90.2 and Vb5.1/5.2 for flow cytometry analysis of proliferated OT-I cells.

2.2.3.2 Quantification of the successful NP uptake in dendritic cells

The following text passages have been copied from our own publication, partially rewritten and marked as such (Stickdorn et al. 2022).

Nanoparticles and dendritic cells (DCs) were incubated together to ensure the NP internalization within cellular compartments. It was also checked whether the NP were taken up when internalization was inhibited. Cells were stained afterwards and measured under the confocal microscope or on an imaging flow cytometry system (Stickdorn et al. 2022).

<u>NP internalization assay with DC2.4</u>

Confocal fluorescence microscopy of DC2.4

DC2.4 dendritic cells (50,000 cells/well, suspended in 0.18 ml of the culture medium) were seeded into Ibidi µ-slide eight-well confocal microscopy chambers and left to adhere overnight. Afterwards, cells were incubated with 20 µl nanogel sample with soluble or covalently attached OVA sample (yielding a total nanogel concentration of 40 µg/ml) for 16 hours. Then, culture medium was aspirated and cells were washed three times with PBS. Next, 200 µl of 4 % paraformaldehyde was added and allowed to fixate for 15 minutes at 37°C. Subsequently, cells

were washed again three times with PBS and their nuclei were stained with 200 µL of 4′,6-diamidino-2-phenylindole (DAPI) (50 µg/mL in PBS) for 15 min at 37°C. Finally, cells were washed three times with PBS and stored under an aqueous mounting medium. Fluorescence confocal laser scanning microscopy images were recorded on a Leica SP5 confocal microscope system with a 63× immersion objective. All images were finally processed by the ImageJ software package (Stickdorn et al. 2022).

Internalization and inhibition of NP(IMDQ+OVA-FITC) and sOVA by dendritic cells

For internalization experiments, 1 x 10^6 DC2.4 cells were incubated with NP(IMDQ+OVA) at a dilution of 1:150 in the presence of 2 % mouse serum for 30 min at 37°C after 1 hour starvation in serum-free X-VIVO medium. For inhibition experiments, 300 µg/ml Fucoidan (Sigma) was added. Analysis of the internalized NP by DC2.4 cells was performed using an Amnis ImageStream Mk II flow cytometer (Luminex) at the Core Facility of the Research Center for Immunotherapy (University Medical Center, Johannes Gutenberg-University Mainz). Data were evaluated using the IDEAS software (Luminex). Dead cells were gated out using DAPI (Thermo Fisher Scientific) at a dilution of 1:10,000 (Stickdorn et al. 2022).

2.2.4 *In vivo* experiments

2.2.4.1 Toxicity and immunization experiments

For a comparison of administration routes and to check the tolerance, different nanoparticle formulations were injected either subcutaneously (*s.c.)* into the neck fold or intravenously (*i.v.)* into the tail vein of mice. Therefore 100 µl of NP were injected, containing 120 µg particles with 10 µg IMDQ and 30 µg OVA, either covalently bound to the NP or soluble. The respective control groups received 100 µl PBS. 14 days later, the immunization was repeated the same way as a boost. Mice were sacrificed on day 28 to analyze antibody titers in the blood and cytotoxic T cells in the spleen for the immunization study. In addition, for the toxicity experiments, the body weight from mice and the liver values out of blood serum was recorded at different intervals (Figure 1) (Text passage copied and modified from our publication (Stickdorn et al. 2022)).

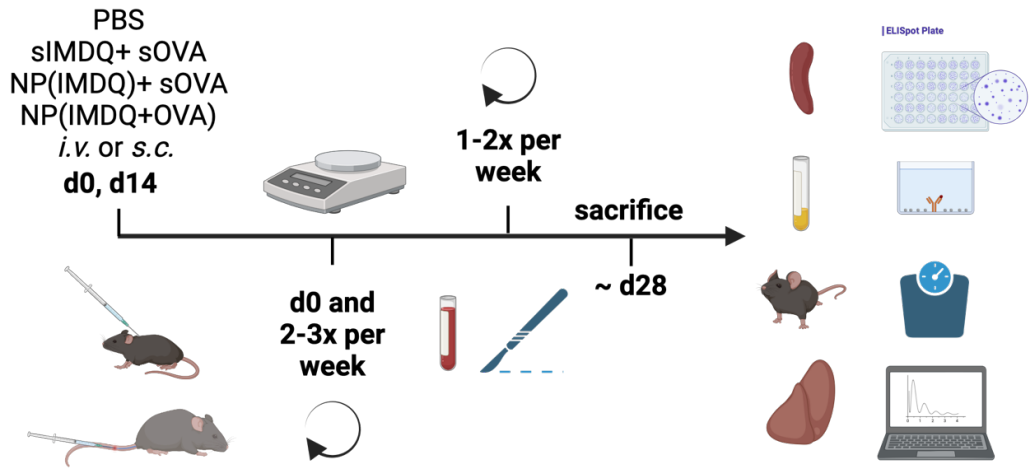

Figure 1: general workflow toxicity and immunization experiment - Created with BioRender.com

2.2.4.2 Preparing therapeutic tumor experiments

Cells get prepared as described above. After removing them from the flasks bottom cells were washed 3 times in PBS and counted. Then they were adjusted to the desired concentration and drawn into a syringe with a 0,4x12 mm cannula (27 gauge). In the meantime, the mice were anesthetized with isoflorane and the right flank of the animals were shaved. For the isoflurane anesthesia the UniVet Porta anesthesia device from Groppler Medizintechnik with a forene volume of 2.8% and an oxygen supply of 0.5 l/min was used. After the animals felt asleep, 100 µl of the prepared tumor cell suspension (cell number depends on cell line see Table 7) was injected subcutaneously. We only used C57BL6/J female mice in the age of 8-12 weeks due the homogeneous constitution of the skin. Three times a week the tumor size was measured with a digital caliper and the volume calculated based on the following equation:

$$\text{tumor volume } [mm^3] = \text{width}^2\ [mm] * \text{length}\ [mm] * 0{,}5$$

The health of the mice, including the tumor size, was monitored by a scoresheet. If the tumor ulcerated or exceeded 600 mm^3 as well as other health risks were detected, the mice were sacrificed with CO_2.

Table 7: cell lines and associated cell numbers

Cell line	Cell number
B16-F10	100.000 cells per injection
B16-F10mOVA	500.000 cells per injection
B16-F10cOVA	100.000 cells per injection
MC38	500.000 cells per injection
MC38mOVA	500.000 cells per injection

General workflow for therapeutic tumor experiments

As described before, tumor cells were earned, mice prepared and cells inoculated on day 0 (d0). For the therapeutic tumor setting, when the tumor was pulpable, mice were vaccinated *i.v.* in the tail vein on day 3, 5, 7 with 100 µl of the NP solution (for a more detailed description see Figure 2). Every two or three days the volume was measured and blood was obtained once or twice a week by scratching the tail vein of the mice. When the termination criteria were reached mice were sacrificed and different analysis followed.

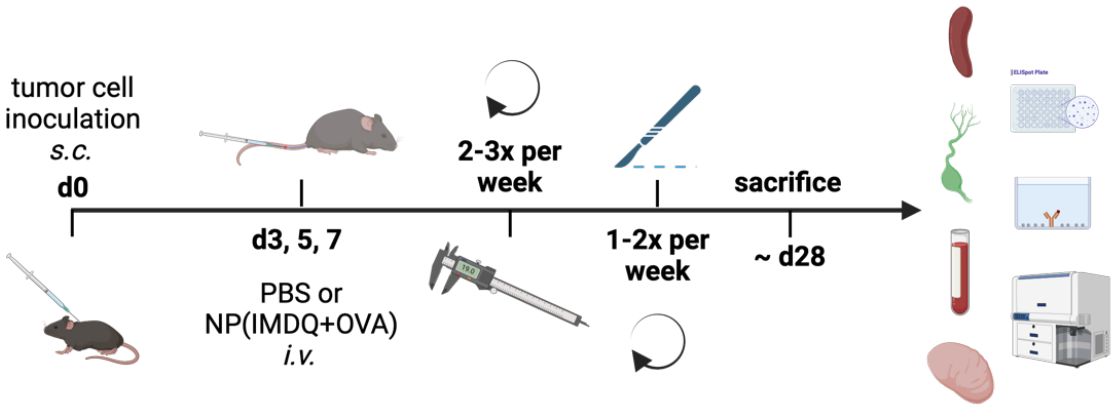

Figure 2: general workflow tumor experiment - Created with BioRender.com

2.2.4.3 Cell suspensions from organic mouse material

Spleen

Spleen gets smashed on a 70 µM filter and rinsed with 5 ml PBS into 50 ml falcon. After centrifuging for 5 minutes at 1700 rpm, spleen was treated for 2 minutes with Gey's hypotonic solution for erythrocyte lysis. Afterwards reaction was stopped with 15 ml PBS, cells centrifuged and counted.

Tumor Dissociation with Miltenyi Kit to generate single cell suspension

After the tumors were harvested, they were transferred to gentleMACS™ tubes for tissue dissociation and pre-cut into small pieces. The tubes already contained the enzyme mixture

from the kit in RPMI medium, all according to the manufacturer's protocol. Afterwards, samples were placed on the gentleMACS™ device and digested with the program "soft/medium tumor – 37C_m_TDK_1". When the digestion was complete, the samples were filtered (70 µM), washed twice and taken up in FACS buffer.

2.2.4.4 Blood samples from mice

Blood cells for FACS staining

50 µl of collected blood was mixed with 500 µl 1x PBS + 30 mM EDTA to prevent clotting. For erythrocyte lysis 3 ml ACK buffer was added and incubated for 10 minutes. Then samples were centrifuged (1700 rpm, 3 minute) and the lymphocyte pellets were transferred into a 96 well plate, ready for FACS staining.

Serum for ELISA and CBA

Serum was obtained from coagulated blood, which was allowed to rest 20 minutes after collection. Then blood was centrifuged at 11,000 g for 15 minutes. The serum obtained was transferred to new tubes and stored at 4°C until use.

2.2.4.5 ELISA

ELISA analyses were performed using sera from immunized mice before and after immunization with different kind of nanoparticles. In brief, 96-well plates were coated with 25 mg/ml OVA at 4°C overnight. After blocking the 96-well plate, the serum was added 1:100 in the first well and titrated serially 1:2 over the plate. After 1 hour of incubation at 37°C, detection of OVA-specific antibody production was performed using anti-IgG1-HRP, anti- IgG2a-HRP and anti-IgM-HRP antibodies (all received from Abcam, Cambridge, United Kingdom), which were incubated for 30 min at 37°C. After washing the plate, 5 mg/mL ABTS was added and after 10 – 15 min of incubation at room temperature, the absorbance was measured at 410 nm. As a positive control, an anti-OVA-HRP antibody (Sigma Aldrich, St. Louis, Missouri, United States) was used (Stickdorn et al. 2022).

2.2.4.6 Cytokine analysis via cytometric bead array (CBA)

Cytokine concentrations were determined by cytometric bead array (CBA; BD Biosciences, San Jose, CA) as recommended by the manufacturer. For this, bead populations with distinct fluorescence intensities were conjugated with cytokine-specific capture antibodies. Recombinant cytokines were used to prepare standard dilutions. Diluted serum samples (1:4)

were mixed with capture beads, subsequently incubated with PE-conjugated detection antibodies for 1 hour (all at room temperature in the dark) and subjected to flow cytometric analysis. Samples were measured with an Attune NxT flow cytometer (Thermo Fisher) and analyzed after filtering with the FCAP FCS filter v.1.0.4.@2005-2008, soft flow with the FCAP Array software v.1.0.1.@2006, soft flow (Stickdorn et al. 2022).

2.2.4.7 ELISpot

96-well plates (MultiScreenHTS IP, 0.45 mm, Merck Millipore, Darmstadt, Germany) were coated with 10 µg/mL of anti-IFN-γ antibody (clone AN18, Mabtech, Nacka Strand, Sweden) at 4 °C overnight. After blocking the plate, splenocytes were plated. Therefore, mice were sacrificed and the spleen was removed. After isolating the splenocytes by using a cell strainer and lysis of erythrocytes, cells were counted and plated at $5x10^5$ per well. They were restimulated with either 1 µM $OVA_{257-264}$, 1 µM $OVA_{323-337}$ or left untreated and incubated at 37 °C for 20 hours. After washing the plate, 2 mg/mL of a biotinylated anti-IFN-γ antibody (clone R4-6A2, Mabtech) was added and incubated for 2 hours at 37 °C. Afterwards Vectastain ABC Kit (Vector Laboratories, Burlingame, USA) / AEC (Sigma-Aldrich, Taufkirchen, Germany)-Complex was added according to manufacturer ‘s constructions. After spots were visible plates were washed with water and dried overnight. Spot counting was performed on an AID iSpot ELISpot Reader (AID AutoimmunDiagnostika, Straßberg, Germany) (Stickdorn et al. 2022).

2.2.4.8 Flow cytometry

For our flow cytometry analysis, we used different antibodies (find on the table 2.1.3).

Extracellular staining

Live/dead (L/D) staining

After the cells have been washed 3 times with PBS, they were stained with FVD 780 (Fixable Viability Dye, APC-Cy7) 1:1000 in PBS for 20 minutes at 4°C.

CFSE proliferation staining

For CFSE staining cells were labeled with 5 µM CFSE in 1x PBS for 4 min at 37°C in the water bath. Afterwards cells were washed with pure FCS, resuspended in FACS buffer and ready for use.

Tetramer

Peripheral blood samples were collected and incubated with the following antibodies: BV421conjugated anti-CD8, APC-conjugated anti-CD44 and FITC-conjugated anti-CD62L (all from eBioscience) after hypotonic lysis. H-2K^b-OVA$_{257-264}$-specific T cells were detected by H2-K^b tetramers containing OVA$_{257-264}$ peptides as described.[9] The samples were analyzed by flow cytometry.

Intracellular staining and cell fixation

After extracellular staining cells were washed 3 times (1700 rpm, 2 minutes) with FACS buffer and permeabilized with 50 µl FixPerm solution (1:4 concentrate to diluent, eBioscience™ Foxp3/Transcription Factor Staining Buffer Set) for 20 minutes at 4°C. Here, also overnight is possible. Then cells were washed 2 times with perm-buffer (1:10 dilution with ddH_20, eBioscience™ Foxp3/Transcription Factor Staining Buffer Set) and also stained in perm-buffer (20 min, 4°C). When the incubation period was over, cells were washed (2x) and resuspended with FACS buffer. Samples can be stored at 4°C for several days without any problems, they are still measurable after few days.

2.2.4.9 MACS (magnetic cell separation) from cell suspensions

Out of the tumor single cell suspensions from paragraph 2.2.4.3, the CD45$^+$ tumor infiltrated lymphocytes (TILs) were isolated using the magnetic cell separation (MACS) technology. All steps were carried out according to the manufacturer's protocol.

2.2.4.10 Single Cell RNA sequencing (scRNAseq)

scRNAseq was performed out of CD45$^+$ TILs from *ex vivo* treated and untreated B16-F10, B16-F10cOVA and B16-F10mOVA tumors to characterize the immune cells in the TME. After the MACS separation (2.2.4.9) cell concentration was adjusted to 1x10^6 cells/ml in BD sample buffer and stained with calcein AM (1:1000, BD Bioscience) as well as DRAQ7 (1:1000, BD Bioscience) for 10 minutes at 37°C to check the cell viability. 10 µl of the stained cell suspension were pipetted into C-Chip counting chamber (Nanoentek, Waltham, USA) and viability measured with BD Rhapsody™ scanner. If the viability was above 80 %, each sample was tagged with a unique sample tag allowing multiplexing of all samples on one cartridge. According to the manufacturer's protocol “BD Rhapsody System mRNA whole Transcriptome

Analysis (WTA) and Sample Tag Library Preparation protocol", the DNA libraries for whole transcriptome analysis (WTA) and sample tag (ST) were created using the BD WTA Amplification Kit (BD Bioscience). The whole scRNAseq process was performed in cooperation with the Core Facility Next Generation Sequencing (NGS) of the University Medical Center of the Johannes Gutenberg-University Mainz.

Sequencing of the WTA and ST DNA library was perfomed by Novogene Co., Ltd. (Cambridge, USA). The fastq-files were processed with the BD Rhapsody WTA analysis pipeline (BD Biosciences, Franklin Lakes, USA), resulting in a csv-file in the form of "molecules_per_cell" for each biological replicate of a scRNAseq experiments. Afterwards, these files were used for further biostatistical analysis platforms.

Analysis and visualization of the scRNAseq data

The first analysis of the scRNAseq data was in cooperation with Federico Marini (Institute for Medical Biostatistics, Epidemiology and Informatics (IMBEI) of the University Medical Center of the Johannes Gutenberg-University, Mainz) with the statistical program R studio. In order to visualize the data, it was subjected to a biostatistical quality control as follows:

- Cell type annotation by setting up gene level annotation
- Quality control and processing for each sample (formatting row and table data, exclusion of 1. cell doublets, 2. cells with low library size, 3. cells with high mitochondrial count and 4. cells with low feature count)
- Calculation of PCA, t-SNE and UMAP visualization (reduced dimensionality plots)
- Immune cell type prediction based on samples
- Generate one data set by integration of every dataset from each sample
- Cluster calculation
- Final cell type annotation for the whole data set
- Safe the file as rds-file for data exploration

To visualize the data the interactive Summarized Experiment Explorer (iSEE) program was used (Rue-Albrecht et al. 2018). Therefore, the bioconductor and iSEE package were installed in RStudio. To explore the whole B16-F10 data set, the following commands were entered in RStudio:

```
>Library("iSEE")
>getwd()
>setwd("/Users/Lara/Desktop")
```

>sce <- readRDS("sce_merged_allsets.RDS")

>iSEE(sce)

2.2.5 Statistical analysis, software and p-values

GraphPad Prism 7™ was used to analyze, visualize and statically check the data (except scRNAseq data).

Table 8: Software

Software	Usage	Copmany
AiD ELISpot 8.0	ELISpot	AiD Diagnostika GmbH (Straßberg, Germany)
Bioconductor package	scRNAseq Data	Open source software
FCAP Array software	FACS from CBA Kit	BD Bioscience (Franklin Lakes, USA)
Flow Jo	FACS Data	BD Bioscience (Franklin Lakes, USA)
GraphPad Prism 10.1.1	Data Analysis	GraphPad Software (Boston, USA)
IDEAS	Image based FACS	Luminex (Texas, USA)
iSEE	scRNAseq Data	Open source software
MS Office 2016	Word, PowerPoint, Excel	Microsoft Corporation (Redmond, USA)
PartekFlow	scRNAseq Data	Partek Incorporated (St. Louis, USA)
R, R Studio	scRNAseq Data	Open source software

Table 9: Explanation of p-values

p-values	significance	meaning
$p > 0,05$	ns	not significant
$p \leq 0,05$	*	significant
$p \leq 0,01$	**	high significant
$p \leq 0,001$	***	highly significant

3. Results

In order to establish a personalized immune vaccination system, the functionalized particles with IMDQ as immune stimulant and OVA as model antigen, made by our cooperation partners, needed to be tested both *in vitro* and *in vivo*. Therefore, we first checked the particle internalization into DCs, followed by creating antigen transfected cell lines to link the NP function to the cancer antigen, ending in the *in vivo* testing in two tumor models.

3.1 The particles

The first step to get a personal vaccination approach is to create a system to bring the immune stimulant and the antigen together to antigen presenting cells. Therefore, our cooperation partners designed a nanoparticle core functionalized with IMDQ a TLR7/8 agonist as immune stimulant (Figure 3 B) and OVA (Figure 3 C), the egg protein, on the NP surface as model antigen to address the cancer cells. Thoughts behind the system is to reactivate the own immune system with the stimulant and at the same time show attending immune cells the caner antigen to recognize and attack the tumor again. The particles are characterized by pH sensitivity, which means that they are able to disassemble and all the components get released (Figure 3 A).

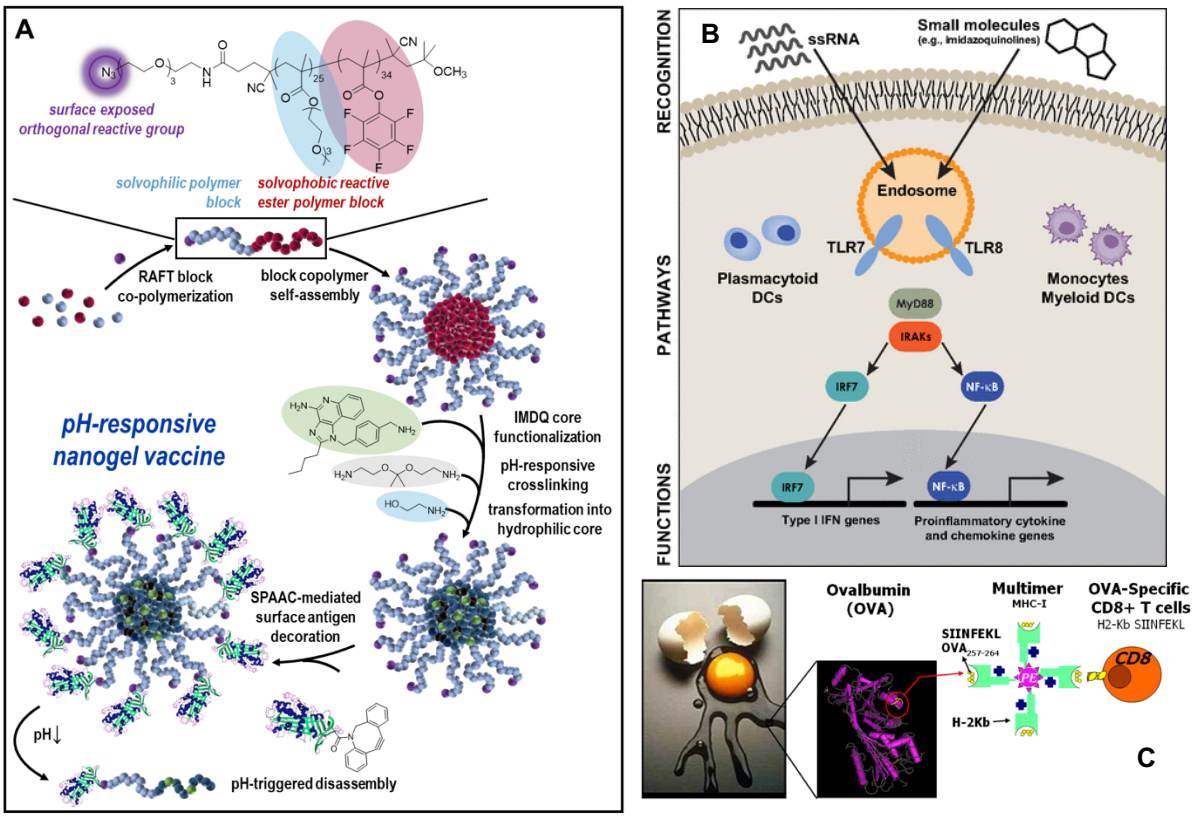

*Figure 3: **A** shows the chemical production and design of the NP; in **B** the IMDQ-induced immune response is mapped via TLR7/8 (Dowling 2018); **C** represents the concept of the model antigen OVA with the SIINFEKL TCR receptor (Pimentel 2010).*

For this purpose, several particle variations were developed to test their potential both *in vitro* and *in vivo*.

3.1.1 *In vitro* internalization study in DCs

The first step was to test whether OVA is better absorbed by APCs when covalently bound to the particles or when it is soluble. For this purpose DCs and NPs (NP(IMDQ+OVA)) or soluble OVA (sOVA) were incubated together and checked for antigen uptake and localization.
Figure 4 show the results of the coincubation analyzed with ImageStream, an imaging flow cytometry system. Here, an intracellular localization of the antigen could be determined for the soluble as well as the NP bound OVA. No signal could be detected in the untreated control.

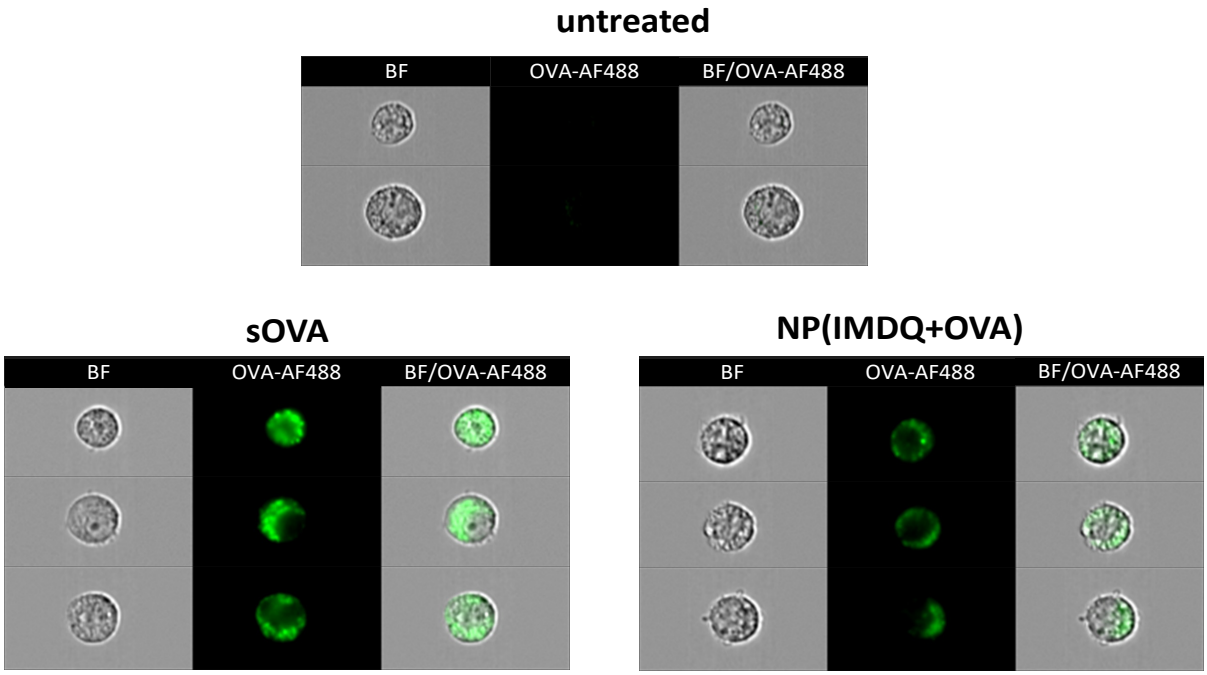

Figure 4: Results of imaging flow cytometry of DCs incubated with sOVA and OVA-conjugated IMDQ-nanogel formulations. ImageStream recorded images of bright field (BF), Alexa Fluor 488 derived OVA fluorescence and overlay of untreated DC2.4 or incubated with sOVA and NP(OVA+IMDQ) (magnification 40x) (Stickdorn et al. 2022).

With confocal microscopy in Figure 5 a colocalization of IMDQ and OVA in the same DC cell compartment could be observed but not for sOVA. Also, no signal and uptake for the untreated control.

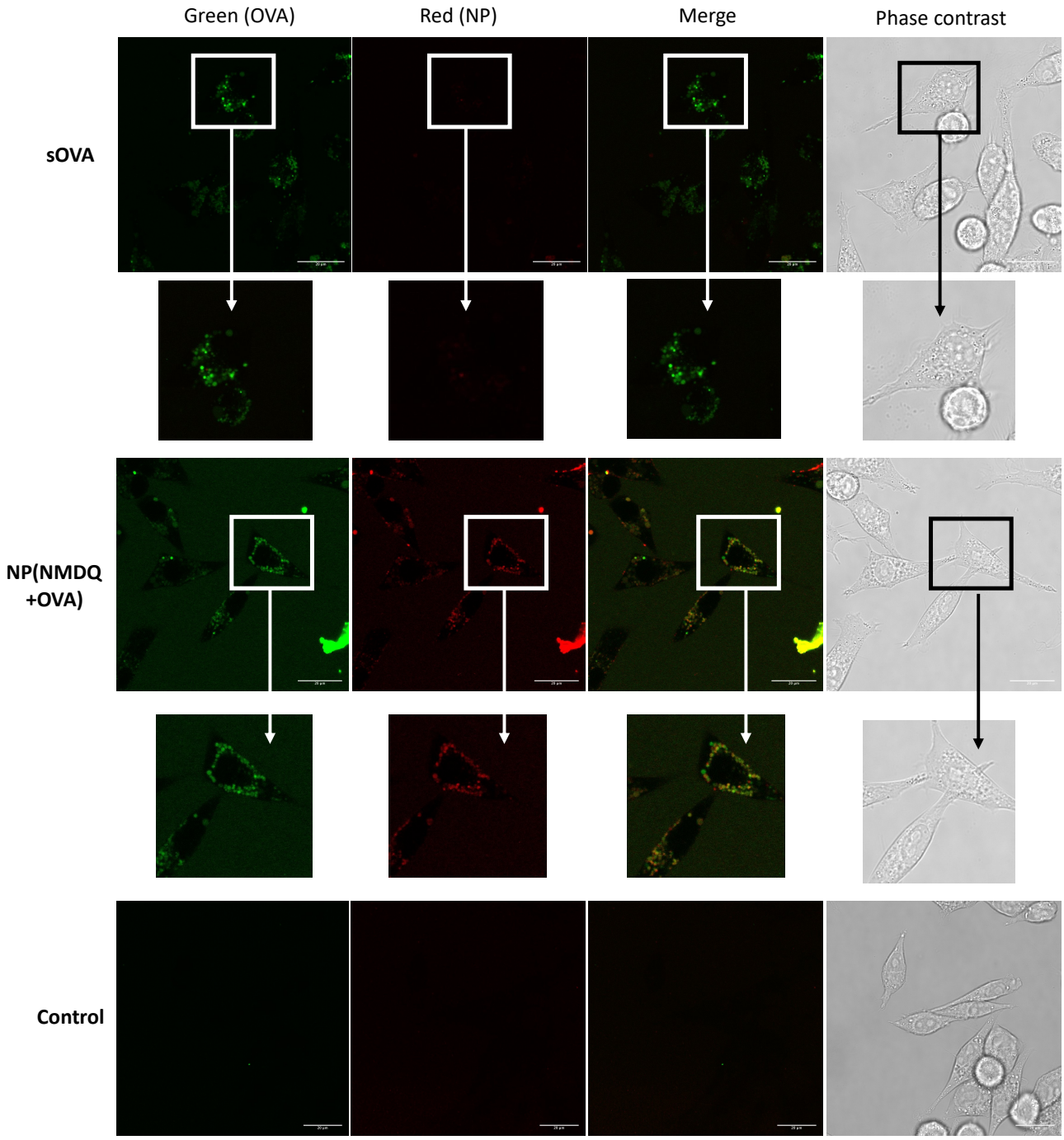

Figure 5: Fluorescence confocal microscopy image of DC2.4 dendritic cells incubated with sOVA and IMDQ- and OVA- loaded nanogels NP(IMDQ+OVA). Nanogels could be identified by their Texas Red label (red), while OVA could be visualized by the Alexa Fluor 488 label (green) (Stickdorn et al. 2022).

Based on these two experiments, it was possible to classify the binding of OVA to the particle as useful. OVA is also taken up in its soluble form (Figure 4), but by binding to the NP, colocalization can be achieved in the same cell compartment (Figure 5).

3.1.2 *In vitro* inhibition of the NP internalization

Here too, sOVA or NP(IMDQ+OVA) were incubated together with DCs, but additionally treated with 300 µg/ml fucoidan (FU). Fucoidan is an inhibitor of the scavenger receptor, which causes the intracellular uptake. Figure 6 shows, that there is no or a reduced uptake for sOVA, when treated with FU.

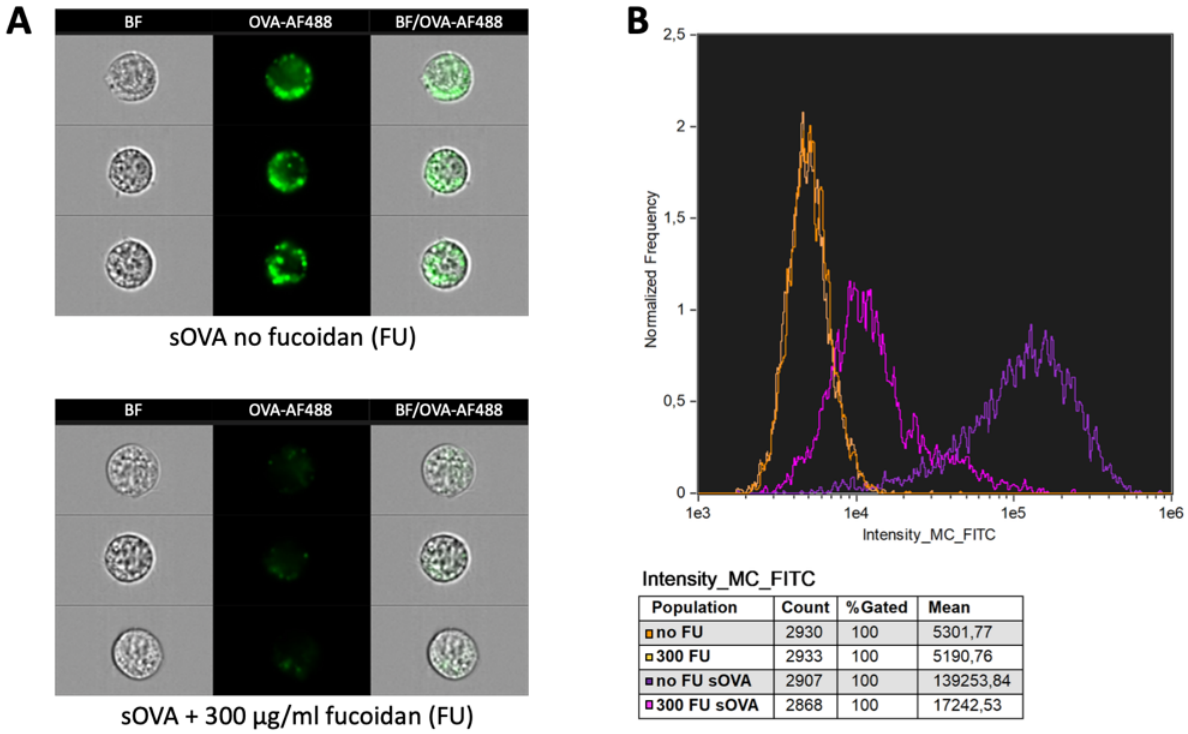

Intensity_MC_FITC

Population	Count	%Gated	Mean
no FU	2930	100	5301,77
300 FU	2933	100	5190,76
no FU sOVA	2907	100	139253,84
300 FU sOVA	2868	100	17242,53

Figure 6: Results of imaging flow cytometry of DCs incubated with sOVA with and without 300 µg/mL fucoidan (FU). (A) ImageStream recorded images of bright field (BF), Alexa Fluor 488 derived OVA fluorescence and overlay (magnification 40x). (B) Derived histogram for the samples with and without 300 µg/mL fucoidan (FU) (Stickdorn et al. 2022).

In contrast, the NP is also widely internalized by DCs despite fucoidan blocking the scavenger receptor (compare Figure 7).

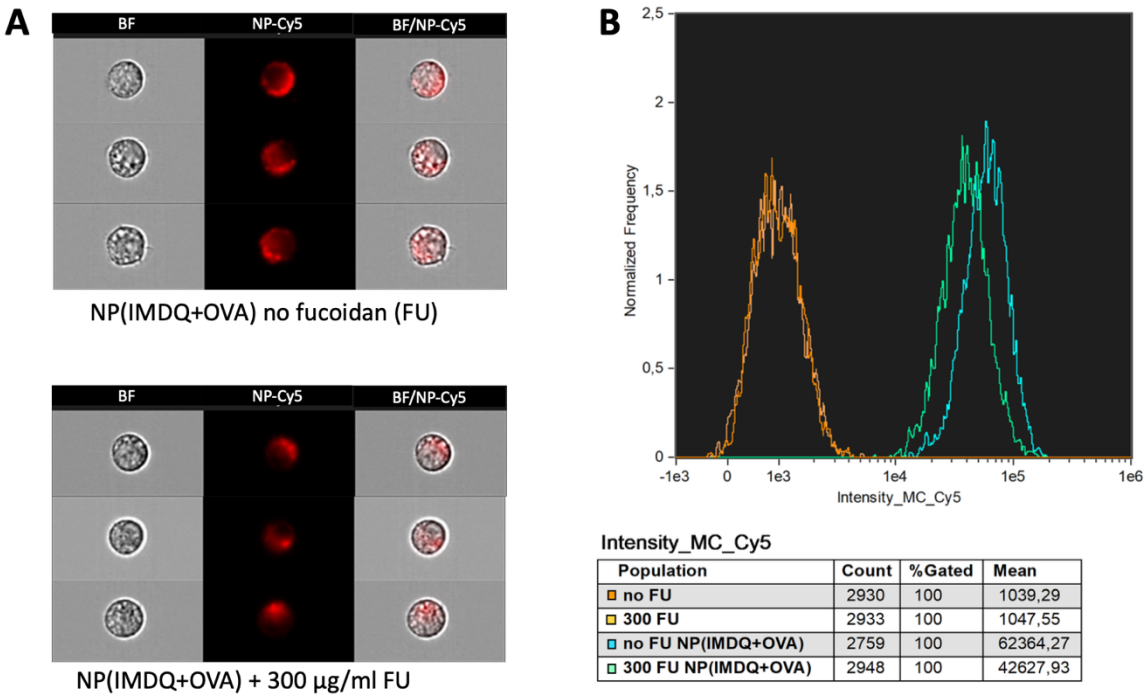

Intensity_MC_Cy5

Population	Count	%Gated	Mean
no FU	2930	100	1039,29
300 FU	2933	100	1047,55
no FU NP(IMDQ+OVA)	2759	100	62364,27
300 FU NP(IMDQ+OVA)	2948	100	42627,93

Figure 7: Results of imaging flow cytometry of DCs incubated with NP(IMDQ+OVA) with and without 300 µg/mL fucoidan (FU). (A) ImageStream recorded images of bright field (BF), Cy5 derived NP fluorescence and overlay (magnification 40x). (B) Derived histogram for the samples with and without 300 µg/mL fucoidan (FU) (Stickdorn et al. 2022).

In this case, blocking the scavenger receptor with fucoidan once again demonstrated the necessity of the covalent binding of OVA to the NP. In contrast to sOVA, the NP(IMDQ+OVA) were still internalized.

3.2 The cell lines

To ensure that the particles with the antigen also recognize the cancer cells, the cell lines B16-F10 and MC38 were transfected with either cytosolic or membrane-bound OVA (Figure 8). Various in vitro assays were used to confirm the successful transfection. The transfection system could be seen in Figure 8. After a successful transfection with the vector, new cells containing GFP and membranous OVA (mOVA) or cytosolic OVA (cOVA) were generated.

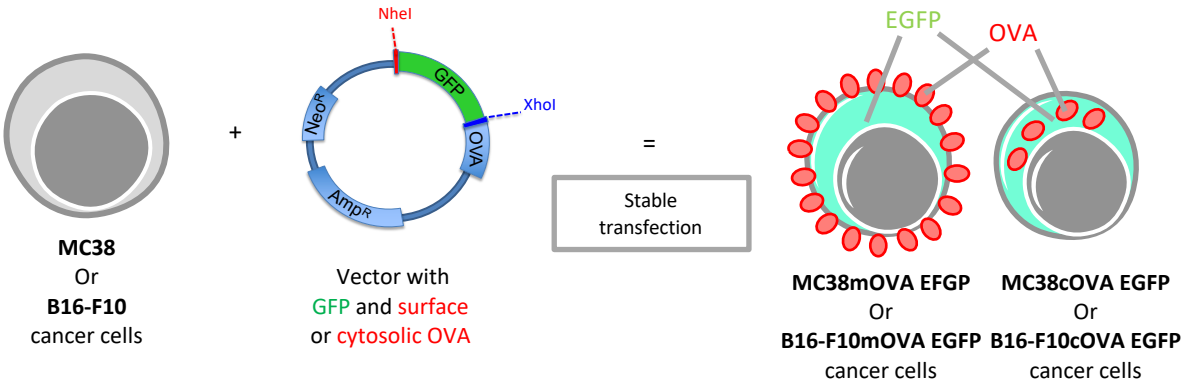

Figure 8: Cell line MC38 or B16-F10 transfected with the vector containing GFP as well as cytosolic or membranous bound OVA results in new engineered cell lines with the antigen on the membrane or in the cytosol.

3.2.1 OVA surface staining of MC38 and B16-F10 transfected cells

To control the successful transfection, the transfected cells were stained for OVA expressed on the membrane and analyzed by imaging flow cytometry. In Figure 9 the red OVA ring around the surface of MC38mOVA (A) and B16-F10mOVA (B) cells is visible. The expression of EGFP which is also encoded by the vector is shown in green for both transfected cell lines. In this staining experiment wild-type cancer cells served as negative controls: no signal could be detected, neither for the surface OVA expression, nor for the EGFP expression. If the vector without OVA was transfected, only a signal for EGFP but not for OVA could be measured.

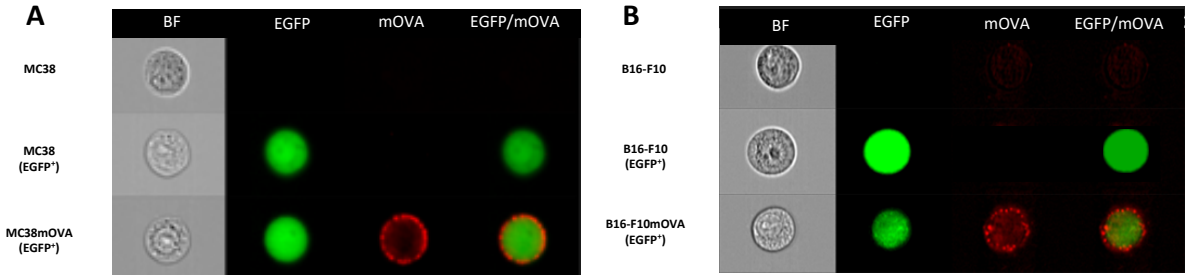

*Figure 9: ImageStream analysis of wild- type (**A**) MC38 or (**B**) B16-F10 cells (top), (**A**) MC38 or (**B**) B16-F10 cells expressing only EGFP (middle) and (**A**) MC38mOVA or (**B**) B16-F10mOVA (EGFP$^+$, bottom) stained for surface OVA by OVA- specific antibodies. Image panels (left to right) show brightfield (BF, magnification 40×), EGFP expression (green), surface OVA expression (Alexa Fluor 647, red), and overlay image (EGFP/surface OVA); copied and modified by (Stickdorn et al. 2022).*

3.2.2 Cytotoxicity Assay

To further conform the transfected antigen in the cell lines, killing assay was performed. After a successful transfection the expressed OVA protein is degraded or processed by the transfected

tumor cells before the resulting SIINFEKL peptide gets presented on MHC-I (H-2K^b) of the cancer cells and recognized by the specific, cytotoxic OT-I CD8$^+$ splenocytes. Different amounts of OT-I cells (effector) were incubated with a constant number of cancer cells (target), resulting in a cytotoxicity curve (% of killing). As negative control non-transfected cells and as positive control non-transfected cells loaded with the SIINFEKL peptide ($OVA_{257-264}$, 1 µg/ml) were used. For MC38mOVA and the positive control a specific killing round about 60 % could be observed. MC38cOVA has a lower killing rate in the beginning because there may be too many effector cells meeting target cells. All in all, a nice cytotoxicity curve was seen, with no killing in the negative control. The stimulated B16-F10 cells showed a cytotoxicity of about 75 % whereas the transfected B16-F10cOVA cells just get killed by 18 %. But also, no unspecific cytotoxicity for the unstimulated negative control.

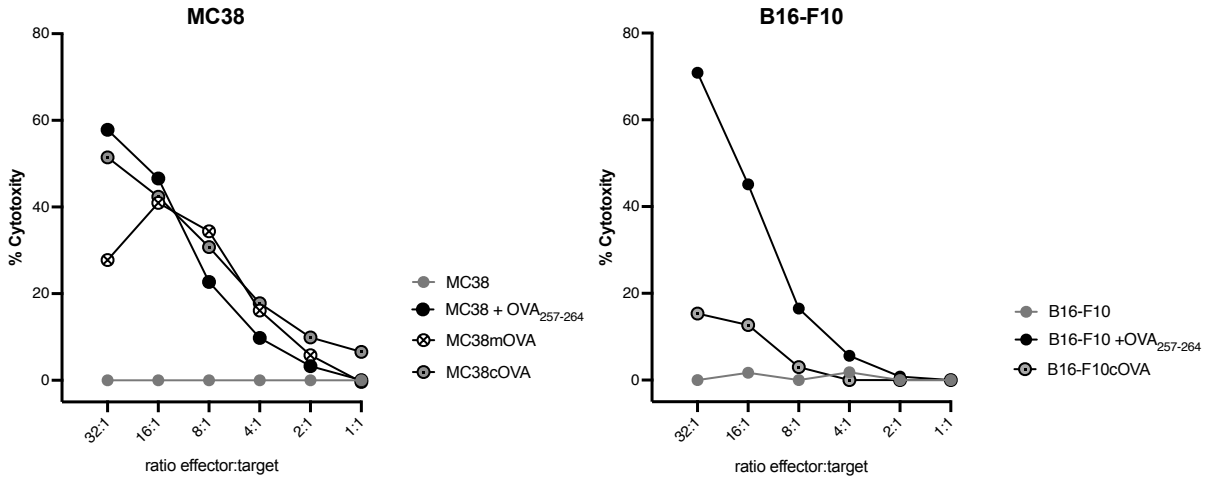

Figure 10: transfected (MC38mOVA, MC38cOVA; B16-F10cOVA) and non-transfected (MC38; B16-F10) cancer cells were incubated with OT-I cells, which are able to recognize the OVA-specific SIINFEKL peptide with their transgenic CD8$^+$ TCR.

3.2.3 Coculture

For the coculturing experiment OT-I splenocytes were cultivated with the transfected (MC38mOVA, MC38cOVA; B16-F10mOVA, B16-F10cOVA) or the non-transfected cancer cells (MC38; B16-F10) using different cell ratios. After 48 hours the specific proliferation, triggered by the expression and processing of the OVA antigen was measured. Figure 11 (left graph) shows a specific OVA-induced proliferation of OT-I cells, at least for the MC38 transfected tumor cells. For the negative control, MC38 wild-type cells were incubated with the splenocytes and no proliferation could be detected. In the positive controls, OT-I cells stimulated with 1 µg/ml SIINFEKL (SIIN) showed nice proliferations when incubate with or

without the non-transfected MC38 tumor cells. The same experiment was repeated with the B16-F10 cells. In this case, no specific OVA-induced proliferation of OT-I cells could be detected in the cocultures with the OVA transfected lines, although a good proliferation could be observed in the positive control: coculture of B16-F10 and OT-I cells stimulated with the SIINFEKL peptide (Figure 11, right graph).

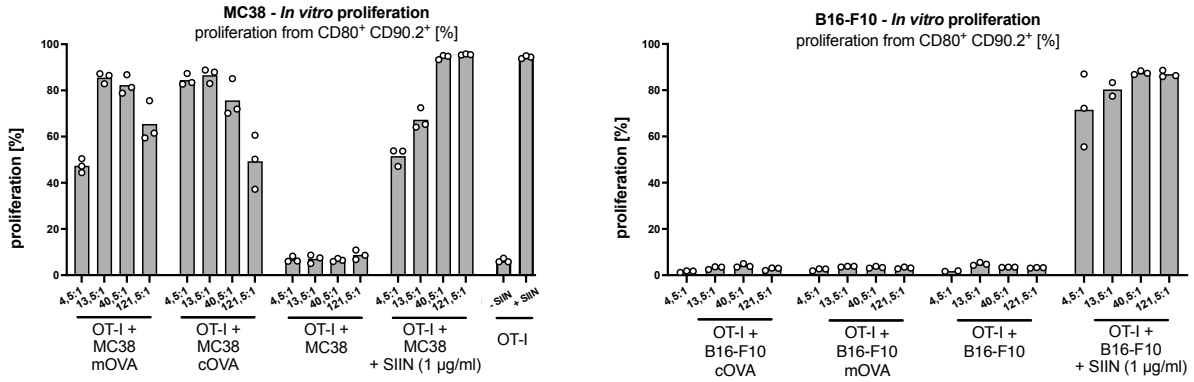

Figure 11: transfected (MC38mOVA, MC38cOVA; B16-F10cOVA) and non-transfected (MC38; B16-F10) cancer cells were cocultured with OT-I cells and the specific proliferation of the OT-I cells measured after 48 h.

3.2.4 PCR

To finally show that the B16-F10cOVA transfected cells also contain the cytosolic OVA transgene, a PCR using the extracted genomic DNA of the transfected cells was carried out. In Figure 12, a specific band for OVA is clearly visible in the transfected cells, whereas the wild-type cell line shows no band.

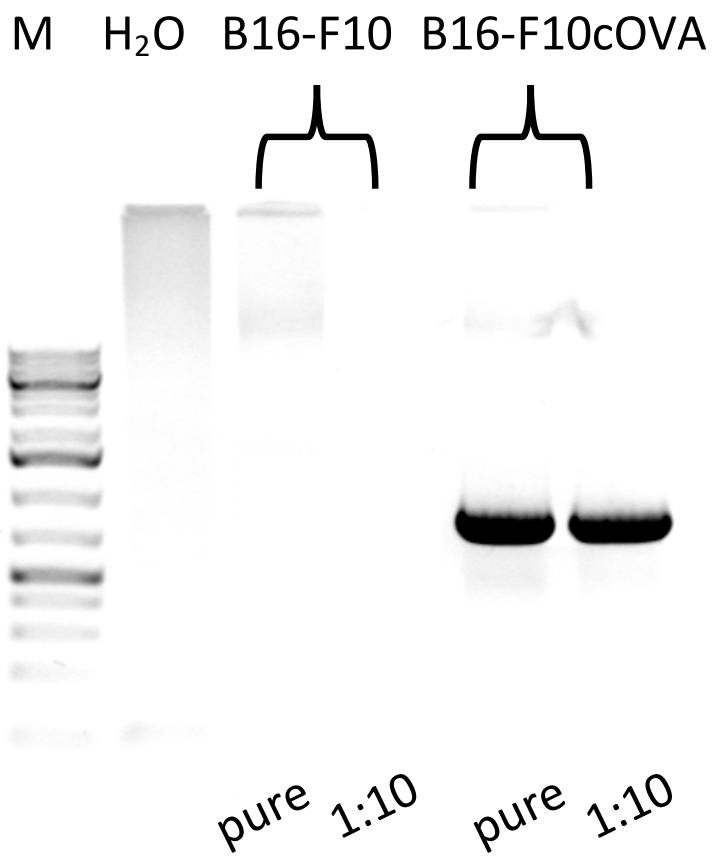

Figure 12: PCR of transfected B16-F10cOVA and non-transfected B16-F10 tumor cells.

3.3 *In vivo* tolerability

After the expression of OVA in the transfected cancer cells had been experimentally proven, it was necessary to investigate the compatibility of the particles in the mice. The first step was to find the best application route and demonstrate the necessity of covalently attachment from IMDQ to the NP. To do this, different variations of particles were injected *s.c.* or *i.v.* into the mice and the animals' health was monitored. Afterwards, the mice were sacrificed and the antibody and T cell responses were investigated.

The weight of the mice was monitored as an indicator of health. Figure 13 shows the change in weight within 17 days after two applications *s.c.* or *i.v.* of the soluble particle components (sIMDQ+sOVA) or bound to the NP (NP(IMDQ+OVA)). For both application routes, the sIMDQ+sOVA (red line in Figure 13) vaccination leads to a drop-in weight after the boost injection on day 12 followed by a slower recovery compared to the NP(IMDQ+OVA) injection form. These results show clearly that the IMDQ attachment to the particle is necessary for the

health of the mice. No major weight loss is seen here and the animals health quickly return to the PBS curve (in grey, control injection) after the injection.

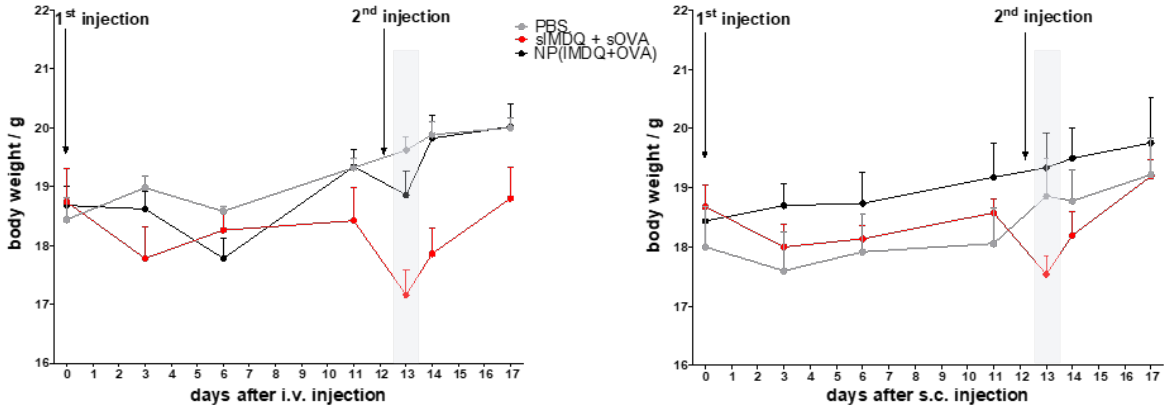

Figure 13: Body weight of wild-type mice after i.v. (left) or s.c. (right) administration of IMDQ-containing formulations. Independent of the application route sIMDQ+sOVA lead to a drop in body weight after the boost injection and slower recovery (Stickdorn et al. 2022).

The statement that IMDQ must be bound to the NP and that an *i.v.* injection is the better application route could be confirmed by the fact that at least the number of OVA-specific $CD8^+$ T cells is increased after the NP(IMDQ+OVA) injection (Figure 14). For the $CD4^+$ T cells, there is a higher amount of $CD4^+$ T cells after *i.v.* compared to the *s.c.* injection of sIMDQ+sOVA and NP(IMDQ+OVA), but no difference between the two NP groups. Subcutaneous injection of the NP leads to a lower number of $CD4^+$ T cells for the soluble components as well as for the NP bound. This experiment showed that it makes sense to bind IMDQ to the particle and that *i.v.* administration is probably the better form of application.

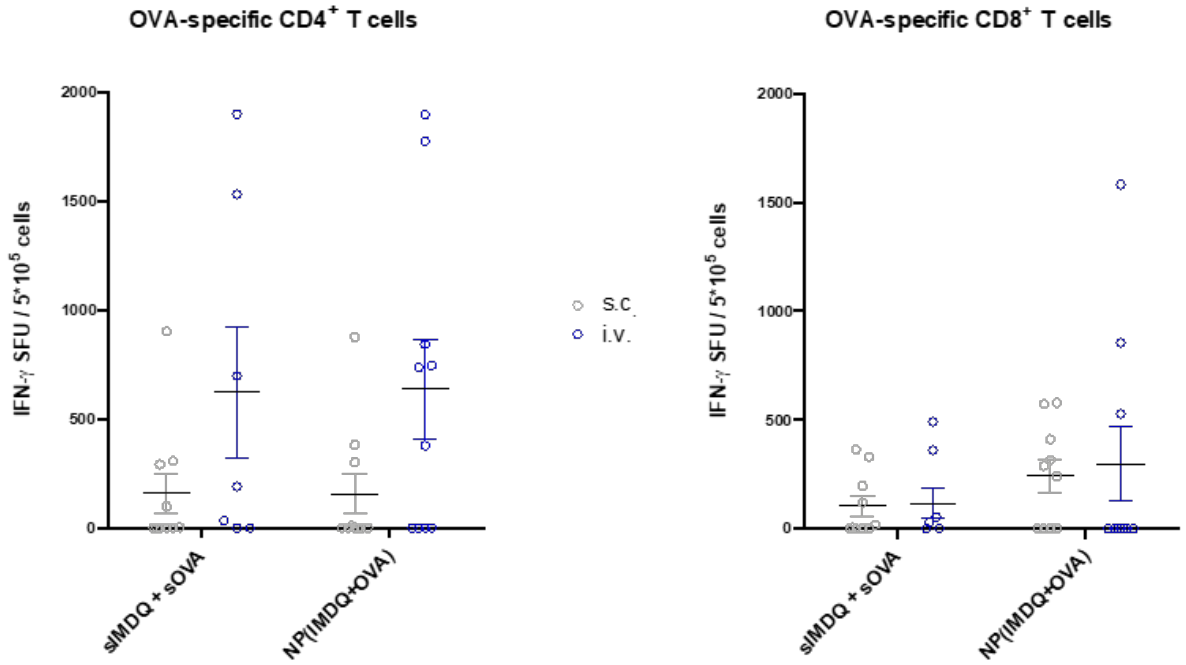

Figure 14: ELISpot analysis of on day 25 isolated spleen cells after i.v. or s.c. injection of sIMDQ+sOVA or NP(IMDQ+OVA) (Stickdorn et al. 2022).

In order to strengthen the initial indications of the previous experiments on *i.v.* application, the blood of the animals was stained for the OVA specific peptide SIINFEKL. For both injection routes a level of about 8 % SIINFEKL tetramer positive $CD8^+$ T cells could be detected (Figure 15).

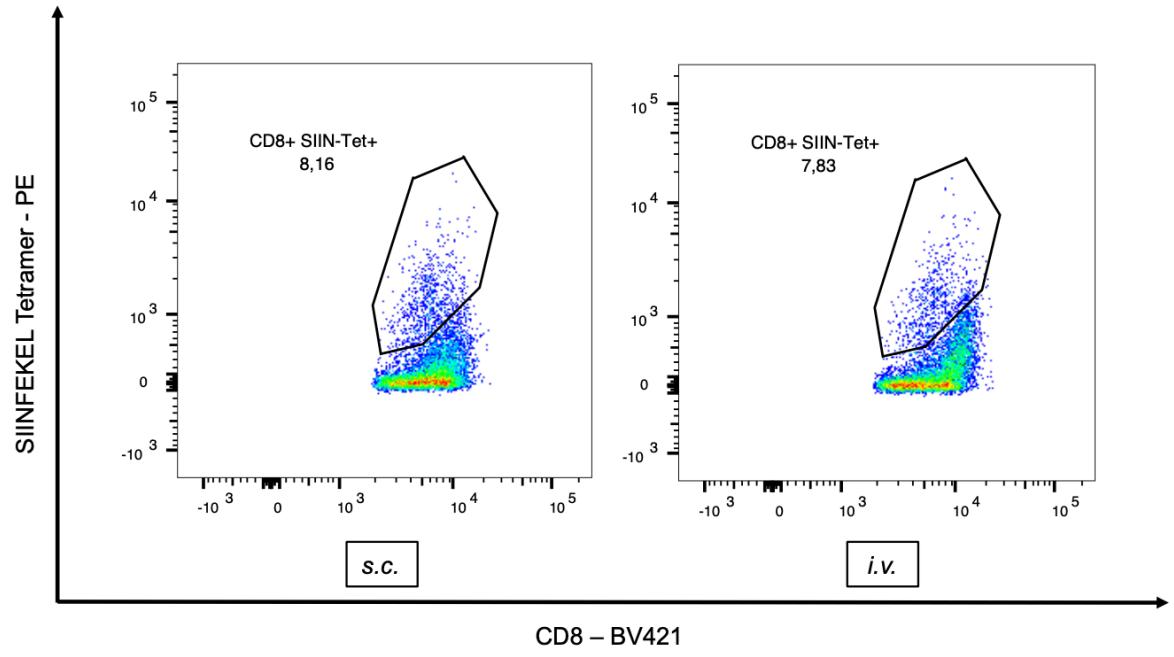

Figure 15: FACS plots from flow cytometry gated for OVA-specific CD8+ T cells in blood after s.c. (left) and i.v. (right) injection of NP(IMDQ+OVA) determined by tetramer staining (Stickdorn et al. 2022).

Finally, the benefits for *i.v.* application became clearer with the analysis of the OVA-specific antibodies generation and the $CD4^+$ and $CD8^+$ T cell immune responses. For *i.v.* injection a significantly higher amount of IgG2a antibodies could be detected (Figure 16 A). Furthermore, the number of $CD4^+$ and $CD8^+$ OVA-specific T cells was also increased in this experiment after the *i.v.* compared to the *s.c.* injection form (Figure 16 B).

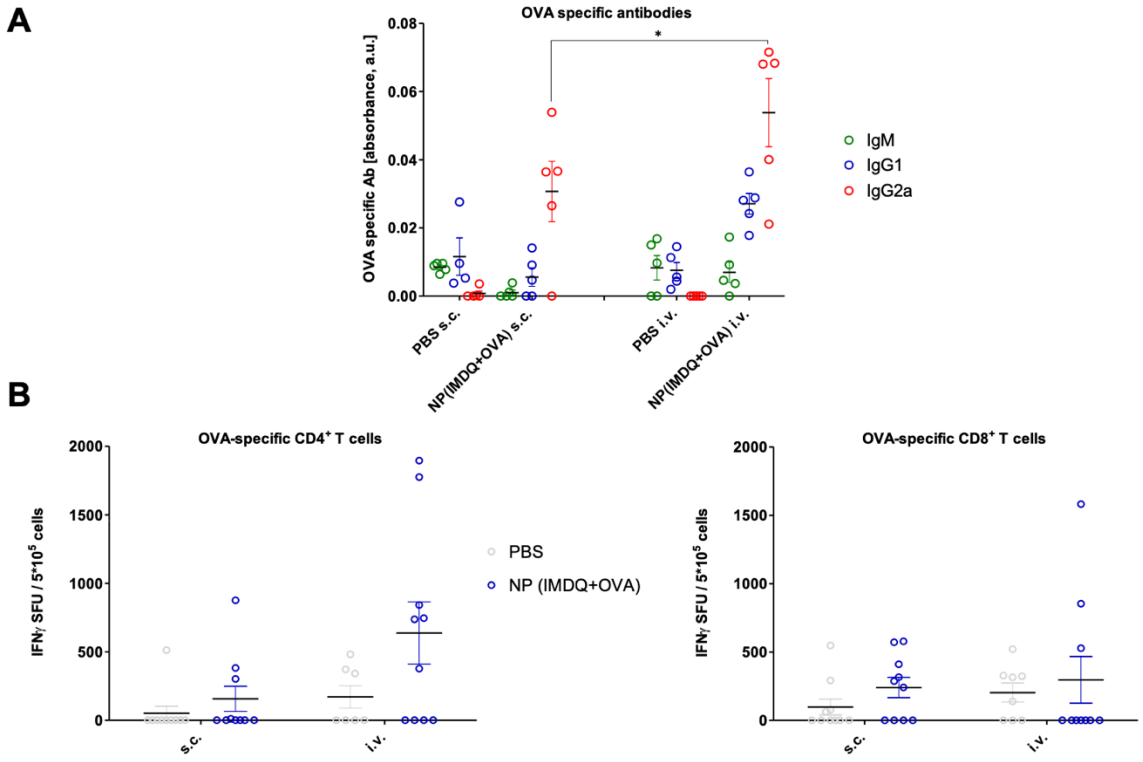

Figure 16: Humoral and cellular immune responses after s.c. and i.v. administration of NP(IMDQ+OVA). A) OVA specific antibodies determined by ELISA of the blood serum, (B) corresponding T cells determined by ELISpot of the isolated spleen cells of mice (Stickdorn et al. 2022).

Based on the results of these experiments it could be justified to inject the particles *i.v.* for the following experiments, as stable T cell and antibody responses could be generated. Additionally, these experiments demonstrated that IMDQ should not be injected in its soluble form but covalently attached to the particle.

Now that the efficacy and tolerability as well as the injection route of the particles have been confirmed, both *in vitro* and *in vivo*, the next step was to test the particles in a therapeutic tumor model. Based on the previous results, the particles will subsequently always be applied intravenously and only the particles with covalently bound IMDQ and OVA were further used.

3.4 *In vivo* tumor experiment – therapeutic vaccination against MC38 and B16-F10 cancer cells

In previous experiments it has been shown that the NPs are safe for *i.v.* application. The OVA-transfected cells carry their model antigen either on the cell surface or in the cytosol. Thus, the recognition of the tumor cells should be guaranteed by the vaccination system. The effect of the particles was therefore tested in three different tumor models. The first step was to inoculate tumor cells into wild-type C57BL/6 mice and vaccinate them on day 3, 5 and 7 with NP(IMDQ+OVA) (compare Figure 17 A). For the study, MC38 and its counterpart MC38mOVA as well as B16-F10 and its counterparts B16-F10mOVA and B16-F10cOVA were used. For all three tumor models a reduced tumor volume after the NP vaccination could be observed (Figure 17 B, D and G). And there is no impact on the tumor growth from the vaccination on the non-transfected cancer cells. The growth of these wild-type tumors followed the control group just treated with PBS.

The MC38 tumor model, establish by Dr. Jennifer Hahlbrock and the modified cells generated by Dr. Danielle Arnold-Schild, also showed a significantly higher number of $CD45^+$ (immune cells), $MHCII^+CD11c+$ (DCs), $CD11b^+GR\text{-}1^+$ (myeloid-derived suppressor cells - MDSCs) and $MHCII^+F4/80^+$ (macrophages) after nanogel vaccination (compare Figure 17 C). There was also a higher amount of $CD3^+$ (T cells) cells. They can also be divided into $CD4^+$ and $CD8^+$, whereby the number of T cells also increases after NP application.

In both B16-F10 models, a significant increase in IgG2a antibodies (Figure 17 E+H) as well as a higher number of OVA-specific $CD4^+$ and $CD8^+$ T cells (Figure 17 F+I) can be recorded after vaccination. It was striking that tumor growth in the cytosolic B16-F10 tumor model stagnated after vaccination (Figure 17 G).

The effectiveness of the NP vaccination system could therefore be confirmed for two independent tumor models *in vivo*.

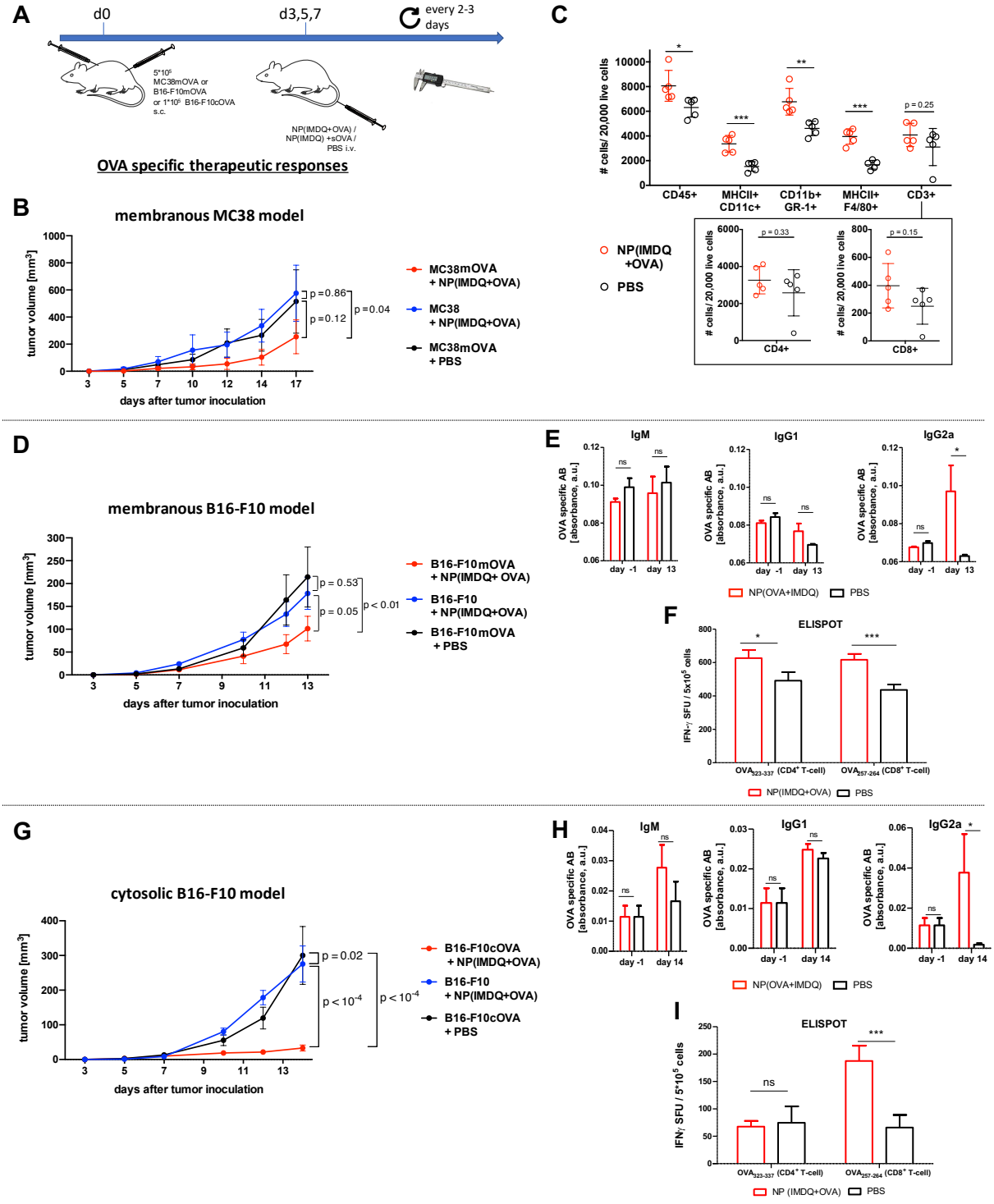

Figure 17: IMDQ- and OVA-loaded nanogels provide antigen-specific tumor immunity by induction of Th-1-biased immune responses with respect to increasing levels of antigen-specific IgG2a titers, increasing numbers of antigen-specific $CD8^+$ and $CD4^+$ T cells and increasing numbers of tumor-infiltrating immune cells. (A) Therapeutic schedule for the treatment of mice challenged with both MC38mOVA and wild-type MC38, B16-F10mOVA and wild-type B16-F10, or B16-F10cOVA and wild-type B16-F10 tumor cells. (B) Results of the MC38mOVA or MC38 tumor sizes after treatment either with NP(IMDQ+OVA) or PBS (n = 10). (C) Flow cytometric analysis of single-cell tumor suspensions derived from MC38mOVA tumors treated with NP(IMDQ+OVA) or PBS. (D) Results of B16-F10mOVA or B16-F10 tumor sizes after treatment with NP(IMDQ+OVA) or PBS (n = 9−11). (E) ELISA analysis of blood serum samples taken on day −1 (so before tumor inoculation and treatment with the nanogel)

and day 13 after tumor inoculation from B16-F10mOVA-bearing mice treated with NP(IMDQ+OVA) or PBS. (F) ELISpot analysis of the isolated spleen cells taken on day 13 after tumor inoculation from B16- F10mOVA-bearing mice treated with NP(IMDQ+OVA) or PBS. (G) Results of B16-F10cOVA or B16-F10 tumor sizes after treatment with NP(IMDQ+OVA) or PBS (n = 10). (H) ELISA analysis of blood serum samples taken on day −1 and day 14 after tumor inoculation from B16-F10cOVA-bearing mice treated with NP(IMDQ+OVA) or PBS. (I) ELISpot analysis of the isolated spleen cells taken on day 14 after tumor inoculation from B16-F10cOVA-bearing mice treated with NP(IMDQ+OVA) or PBS (Stickdorn et al. 2022).

In addition, during the B16-F10mOVA tumor experiment, a cytokine analysis was carried out to better classify the immunological processes. Blood from mice was analyzed on day -1 before and day 13 after tumor cell inoculation. Together with the findings from Figure 17 E, the increased level of the proinflammatory cytokines TNF-α and IFN-γ from Figure 18 indicating a Th1-mediated immune response.

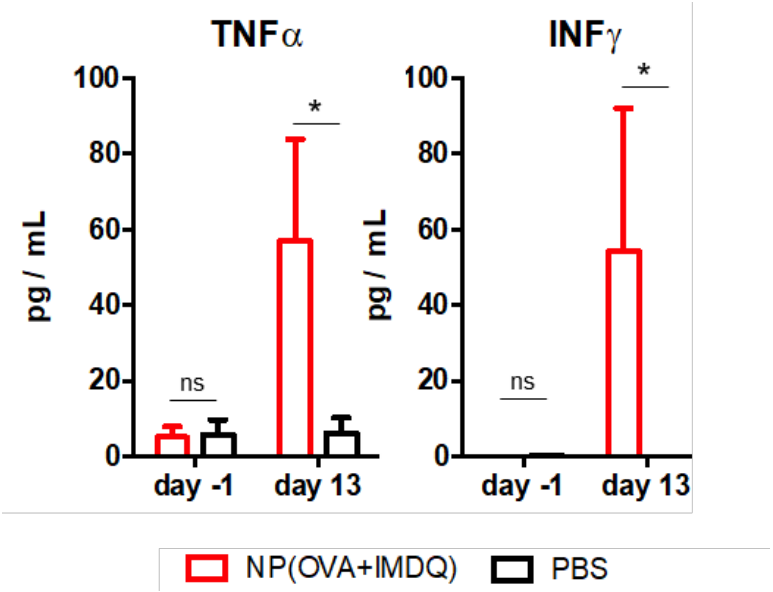

Figure 18: Cytokine analysis of blood serum samples taken on day -1 and day 13 after tumor inoculation from B16-F10mOVA bearing mice treated with NP(IMDQ+OVA) or PBS (Stickdorn et al. 2022).

All in all, a successful anti-tumor vaccination could be established with the test series. The results confirm that the *i.v.* application of NP(IMDQ+OVA) guarantees a fully selective antigen-specific antitumor responses in wild-type mice, independent from the tumor source (Stickdorn et al. 2022). A stable humoral and cellular immune response could be observed both *in vitro* and *in vivo* resulting in an enhanced antitumor efficacy.

On the other hand, the results also raised questions, especially why the B16-F10 tumor model with cytosolic expressed OVA showed such good tumor control compared to the OVA on the membrane. Therefore, a more detailed analysis was needed.

3.5 Single cell RNA sequencing of B16-F10 tumors

In order to better understand these anti-tumor mechanisms, single cell analysis was added for the B16-F10 model. On day 11, the day of the strongest tumor control, single cell suspensions from NP(IMDQ+OVA) treated as well as untreated PBS tumors out of B16-F10, B16-F10cOVA and B16-F10mOVA were generated. The $CD45^+$ TILs were then further processed with the BD Rhapsody, sequenced by Novogene and finally analyzed with iSEE.

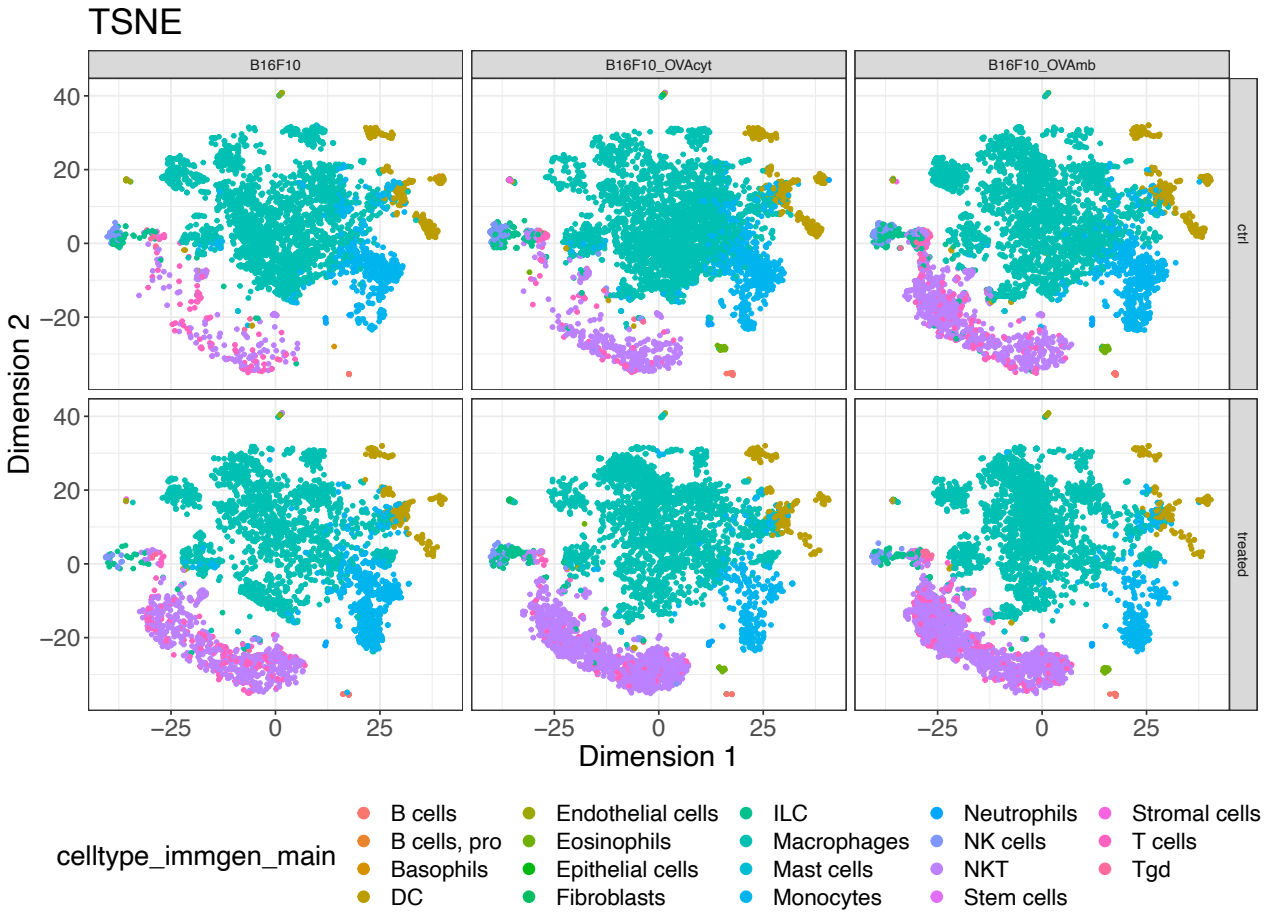

Figure 19: two dimensional tSNE plot of TILs out of NP treated (bottom row) vs. PBS untreated (top row) B16-F10, B16-F10cOVA and B16-F10mOVA tumors (from left to the right) clustered in different immunological cell types by ImmGen.

In Figure 19 the two-dimensional tSNE plot of the scRNAseq analysis from the B16-F10 model is shown. The different tumors were plotted as follows: from left to the right B16-F10, B16-F10cOVA and B16-F10mOVA each with PBS control (crtl, top row) and treated with the nanogel (treated, bottom row). The different colors are assigned to different cell types. Classification of the cell types was created using the immunological data bank ImmGen (immunological genome project). Five main clusters can be identified in the figure: the mint

green cluster in the center with macrophages, the small yellow cluster in the upper right which contains DCs, the blue cluster in the lower right with neutrophils and the mixed cluster with the T cells in pink and the NKT cells in purple. There is also a cluster that only appears in the modified B16-F10cOVA and B16-F10mOVA models. The small cluster at the bottom right below the neutrophils in yellow/green which, according to ImmGen, are the esosinophils. In order to work out the differences between all models, all conspicuous clusters need to be analyzed and compared with each other. With iSEE it is possible to display and compare the expression of signature genes in the different clusters as well as across clusters. In addition, differential gene expression and abundance analyses provide details about the activity of the cells. The first thing that is noticeable in this figure is the increasing number of the T as well as NKT cells before and after the NP treatment, especially for the cytosolic model (Figure 19, graphic in the middle). Here, in the PBS control, a few NKT cells and T cells are already present, but after vaccination the number of NKT cells in particular, but also that of T cells, increases sharply. For the non-transfected B16-F10 group (Figure 19, left graph) only a few T and NKT cells are seen in the untreated PBS control. After nanogel treatment, the number of both cell types increases. For the B16-F10mOVA variant (Figure 19, right plot), the difference between treated and untreated in terms of the increase in T and NKT cell population is present but less pronounced than for B16-F10 and B16-F10cOVA.

The second cluster that clearly differs between untreated and treated are the neutrophils, even if only for the modified versions of B16-F10 cells (Figure 19, blue cluster). After treatment with NP(IMDQ+OVA), the number of neutrophils in B16-F10cOVA and B16-F10mOVA increases. For B16-F10 there is no difference in the presence of neutrophils between PBS and NP treatment.

4. Discussion

Cancer stands as one of the most formidable challenges of modern medicine. Despite significant strides in research and treatment over the past decades, the burden of cancer continues to increase, fueled by an aging population, environmental factors, and lifestyle changes. The inherent heterogeneity in cancer, manifested through diverse molecular alterations, cellular phenotypes, and clinical behaviors, underscores the complexity of the disease and the difficult obstacles it presents to effective prevention, diagnosis, and treatment.

Cancer immunotherapies are a promising new treatment strategy. This approach harnesses the body's own immune system to recognize and eliminate cancer cells, presenting a promising alternative or complement to traditional treatments such as chemotherapy and radiation therapy. Cancer vaccines, a type of immunotherapy, aim at eliciting a specific immune response against tumor specific antigens. However, the development of therapeutic cancer vaccines is a challenging act because of the inherent low immunogenicity of the target antigens to provoke a clinical response (Morse, Gwin, and Mitchell 2021). It is necessary to stimulate the immune system with adjuvants to improve antigen uptake and presentation. This allows an immune response to be initiated and T cells to be primed. This is important as the development of high quality-tumor-specific T cells plays a crucial role in anti-tumor response (Liu et al. 2022).

To build on this idea, we developed together, with our cooperation partners, a nanoparticle-based anti-cancer vaccine, including the OVA antigen and the TLR7/8 agonist IMDQ, as an immune stimulant.

The first step was to ensure that the particles were absorbed so that they could exert their effect. Here, the particle size plays an important role. When particles exceed a size of 50 nm, this is accompanied by poorer distribution and rapid clearance, resulting in an insufficient immune activation (Chenthamara et al. 2019; Foroozandeh and Aziz 2018). In our study, where the particles had a size around 58 nm, we could show a NP uptake in DCs and macrophages (Stickdorn et al. 2022). It was also shown that a covalent binding of both components (NP(IMDQ+OVA)), instead of administration in a soluble form (sIMDQ or sOVA) is of great advantage. By blocking the scavenger receptor with fucoidan, we were able to show that the particles NP(IMDQ+OVA) carrying covalently bound both components were better internalized compared to soluble administration and could confirm a receptor independent NP uptake (Bermudez, Parker, and Goodman 1997).

To establish a system for later *in vivo* experiments, where the tumor cells and the vaccine contain the identical antigen (OVA), we transfected tumor cells with the OVA antigen and generated a nanoparticle vaccine containing OVA to induce an immune response that

recognizes our model target antigen on tumor cells. OVA is a well-known model antigen in immunological research and allows the detailed analysis of an induced immune response. To be able to differentiate between an immune response mediated by a combination of $CD8^+$ T cells and antibodies or $CD8^+$ T cells alone, tumor cells were either transfected with OVA that localized on the surface membrane or in the cytosol of the cells. If the cells express OVA on the plasma membrane, the antigen is directly accessible to antibodies. In addition, these can also be recognized by $CD8^+$ T cells, which detect peptide fragments generated by intracellular antigen processing as well as presentation events and presented by MHC class I molecules (Blum, Wearsch, and Cresswell 2013; Pishesha, Harmand, and Ploegh 2022). On the other hand, the presence of OVA in the cytosol only allows the recognition and activation of cytotoxic $CD8^+$ T cells. In several experiments, we were able to show that the transfection of tumor cells was successful, as shown by OVA-specific PCR for B16-F10 cancer cells, and that they were effectively recognized by cytotoxic OT-I T cells for MC38 cancer cells. Lysis of B16-F10 cells by cytotoxic OT-I T cells was less pronounced than of MC38 cells. In line with this, B16-F10 cells, as a classic melanoma cancer model, are known to have a lower MHC-I expression, which might explain the reduced recognition by OT-I cells (Lee et al. 2020).

After the model system was established, the nanoparticles were tested in mice. As already mentioned above, the particles contain IMDQ, a small-molecule imidazoquinoline-based TLR7/8 agonist, as an immune stimulant. TLR agonists play a critical role in tumor defense and can activate innate immune cells and thereby adaptive immune responses. IMDQ is well known to trigger the production of proinflammatory cytokines like TNF-α, INF-γ, IL-6, IL-12 and type-I interferons resulting in a Th1-mediated immune response and in the activation of cytotoxic T cells against intracellular pathogens (Dowling 2018). However, it is also known that it can cause systemic inflammation with severe side effects (Engel, Holt, and Lu 2011). This became apparent in our experiments. When IMDQ was not bound to the NP, the animals were not well and suffered from weight loss after administration. On the other hand, when IMDQ was attached to the NPs, it induced less side effects and was uptaken by APCs, underlining the importance of covalent attachment. In addition, the NP(IMDQ+OVA) showed an improved T cell and antibody response in our study compared to the administration of our compounds in solution. The packaging of drugs in particles also has the advantage that they strongly resemble pathogens due to their morphological and compositional properties (Lepeltier et al. 2015). In addition, improved circulation and pharmacokinetics can be achieved (Sultana et al. 2022; Alghamdi et al. 2022; Joseph et al. 2023). As a result, the particles accumulate in lymphatic organs and are better absorbed by immune cells (Lynn et al. 2015; Nuhn et al. 2016).

Together with the fact that the polymer platform ensures that both components are provided to the same APCs, it also promotes the necessary priming of the essential cytotoxic T cells (Schlosser et al. 2008; Wilson et al. 2013).

We also tested the *s.c.* versus *i.v.* application route in mice. Here, too, we were able to report good tolerability and an improved immune response with the *i.v.* route compared to *s.c.* injection. Similarly, amongst others, Ramirez-Valdez et al. have shown that *i.v.* injection induces a 4-fold stronger antigen specific $CD8^+$ T cell response compared to mice injected intramuscular (Ramirez-Valdez et al. 2023). We also detected a higher frequency of antigen-specific T cells in the blood of the mice after our prime boost.

After we were able to demonstrate the functionality of our particles *in vivo*, we wanted to see whether we could also induce an anti-tumor response. Therefore, we inoculated two different types of cancer cells: MC38 colon carcinoma cells and B16-F10 melanoma cells.

MC38 is a typical "hot tumor" with a strong immune infiltration, and it responds well to immune checkpoint inhibitors such as anti-PD1 blockade therapy. On the other side, we utilized poorly immunogenic B16-F10 as a classic cold tumor, with very low immune cell infiltration and known resistance to immunological treatments (Kim et al. 2023; Homet Moreno et al. 2016).

Within the B16-F10 model, a distinction was made between B16-F10 (B16-F0 with no OVA expression) and B16-F10 with membrane (B16-F10mOVA) or cytosolic (B16-F10cOVA) expression of OVA. In MC38, only untransfected (MC38 with no OVA expression) and the OVA membrane expressing cells (MC38mOVA) were used. Afterwards, we vaccinated the mice three times with our previously tested and approved nanogel. We could observe in all tumor models an antigen-specific reduction of tumor growth based on the nanoparticle induced immune response. For all entities, we saw an increased $CD8^+$ T cell response combined with a higher amount of IgG2a antibodies. Together with the increased levels of the proinflammatory cytokines, TNF-α and IFN-γ, a Th1-mediated immune response can be inferred here.

Particularly striking was the almost stagnant, strongly suppressed growth in the B16-F10cOVA group, where OVA was expressed in the cytosol. Due to the expression of OVA in the cytosol, the antigen is only recognized by $CD8^+$ T cells. Compared to this, expression of OVA at the cell membrane can be assumed to be detectable by OVA-specific cytotoxic T cells and antibodies. To understand this in more detail, we carried out single cell RNA sequencing analysis of these three tumors. We removed the tumors from treated and untreated mice on day 11, where the strongest inhibition of tumor growth was observed in all models compared to untreated control animals, and analyzed the tumor infiltrating $CD45^+$ immune cells. For B16-F10cOVA and B16-F10mOVA tumors, we saw again an increased number of a T cell

population in the TSNE-plot after nanogel vaccination. Interestingly, in the vaccinated B16-F10 control group, we also observed more T cells, which shows that nanoparticle therapy, even without recognition of the antigen, ensures that the immune system is stimulated and T cells with unknown specificity are activated.

Surprisingly, the number of NKT cells in both B16-F10mOVA and B16-F10cOVA treated groups was also increased. In the untreated group, the number of NKT cells for B16-F10 was very low. B16-F10cOVA also shows a low NKT number before treatment, but slightly more than untreated B16-F10 tumors. In B16-F10mOVA, the number of NKT cells was already high before vaccination and increased further after treatment. These results led to the most frequently asked question, whether it is advantageous if there is B cell involvement or if a dominant $CD8^+$ T cell response alone is more effective in controlling tumor growth. It is known that an increased number of functional cytotoxic T cells is associated with a better prognosis in cancer patients. However, these cells lose their functionality during cancer progression and adopt an exhausted phenotype, in which they are unable to fight cancer cells anymore (Kurachi 2019; Dolina et al. 2021). Furthermore, recent publications show that B cells also appear to play an important role in anti-tumor immunity. However, the functionality of B cells in the tumor microenvironment is still controversial; they can act in both a pro- or anti-tumoral manner. On the one hand, tumor-infiltrating B cells (TIL-Bs) have anti-tumor effects by activating T cells in tumor tissue through antigen presentation (de Visser and Joyce 2023; Laumont et al. 2022). In addition, tumor-reactive antibodies promote tumor killing by NK cells and phagocytosis by macrophages to prevent the tumor progression (Yuen, Demissie, and Pillai 2016). On the other hand, B cells can have pro-tumor effects through the secretion of anti-inflammatory and pro-angiogenic mediators, which promote tumor growth (de Visser and Joyce 2023). In addition, so called regulatory B cells (Bregs) are able to directly or indirectly suppress the inflammatory, anti-tumoral, Th1 T cell response (Yuen, Demissie, and Pillai 2016).

In order to relate the above findings about T cells and B cells to our data, the question is whether the B cells prevent the activity of the cytotoxic cells. In our data, only a negligible B cell population was detected, which also showed no differences in all B16-F10 tumor models either before or after treatment. Therefore, no statement can be made about B cells with regard to this scRNAseq data. However, considering the difference in tumor growth between immunized mice carrying B16-F10cOVA and B16-F10mOVA tumors, it could be concluded that existing cytotoxic T cells are inhibited by B cells in the B16-F10mOVA model. B cells can activate antigen-specific $CD4^+$ and $CD8^+$ T cells and modulate their regulatory or cytotoxic effects (Rastogi et al. 2022). Depending on their differentiation, $CD4^+$ T cells are known to either

suppress or support anti-tumor cytotoxic T cells (Ben Khelil et al. 2022). It is therefore possible that the increased $CD4^+$ T cell numbers in the B16-F10mOVA tumor model reduces the activity of the cytotoxic $CD8^+$ T cells. This hypothesis is supported by the fact that significantly more $CD4^+$ T cells were observed in the *in vivo* experiment with B16-F10mOVA after treatment with NP(IMDQ+OVA) (Stickdorn et al. 2022). In B16-F10cOVA tumors, no difference in the $CD4^+$ count was detected. Here, only significantly higher amounts of $CD8^+$ T cells were detected (Stickdorn et al. 2022). In conclusion, in the B16-F10mOVA model B cells may activate more $CD4^+$ T cells, which exert inhibitory effects on the $CD8^+$ T cells that are also present. This still results in a reduction in tumor growth, but not to the same extent as in the B16-F10cOVA tumors. This also supports the suggestion, that in the B16-F10cOVA model, the higher amount of cytotoxic $CD8^+$ T cells may be responsible for the differences in the reduced tumor growth. In order to support these hypotheses, the $CD4^+$ T cells and the B cells must be characterized more closely in future experiments.

In addition to the cell populations described so far, NKT cells are present in high numbers in the different tumors analyzed. NKT are T cells that recognize endogenous and exogenous lipid antigens over TCRs presented via the unconventional MHC-I molecule, CD1d (Terabe and Berzofsky 2008; Kawano et al. 1997). There are NKT type I and type II cells based on TCR rearrangements and glycolipid reactivity (Godfrey et al. 2004; Nelson, Lukacs, and Johnston 2021). The inflammatory and protective Type I invariant NKT (iNKT) cells produce INF-γ to activate $CD8^+$ T cells and APCs (La Cava, Van Kaer, and Fu Dong 2006). This selectively activates DCs via the CD1d-TCR complex and the interaction between CD40 and CD40L, which triggers DC maturation and the secretion of IL-12 (Terabe and Berzofsky 2008). IL-12 stimulates NK and NKT cells to produce more IFN-γ, which in turn leads to the activation of even more effector cells such as NK cells, $CD8^+$ T cells and γδ T cells (Terabe and Berzofsky 2008; Paget et al. 2012). As the name already indicates, they express an invariant TCRα chain using Vα14Jα18 in mice and Vα24Jα18 in humans paired with a restricted repertoire of TCRβ chains (Lantz and Bendelac 1994). Type II NKTs have variable TCRs and recognize self-lipids over a repertoire of Vα rearrangements (Macho-Fernandez and Brigl 2015; Cardell et al. 1995). In contrast to anti-tumoral type I NKT cells, type II cells are pro-tumorigenic and promote metastasis as well as tumor growth (Renukaradhya et al. 2008; Robertson, Berzofsky, and Terabe 2014). What makes NKT cells special compared to conventional T cells is that one single unconventional T cell clone can respond to various ligands (Vogt and Mattner 2021). In our study we observed especially after NP vaccination, a higher amount of NKT cells in the B16-F10cOVA tumors, which could also explain, in combination with the increasing cytotoxic

T cell number, the improved control of tumor growth. However, it is important to note that in the B16-F10mOVA model an increased number of NKT cells was detected before and after vaccination. For the control group B16-F10, there were hardly any of either NKT or T cells, which changed after vaccination. To conclude, this could mean that the vaccination is able to promote the formation of NKT and T cells. The fact that after vaccination these cell types increase in numbers and tumor control is improved in the antigen-dependent tumor models suggests that our vaccination strategy works and induces an antigen-specific anti-tumor response. The question that remains is: are the cells functionally different and what accounts for such a difference in tumor volume growth? As already mentioned, normally, NKT recognize lipids presented by CD1d molecules. Therefore, it remains currently unclear, why so many NKT cells can be detected before and after NP application in tumors where the OVA is located on the membrane (B16-F10mOVA). There is some evidence suggesting that they can also recognize certain extracellular antigens. Gernardi et al., for example, identified NKT subtypes as important players in *Staphylococcus aureus* (SA) infection (Genardi et al. 2020). Surprisingly, Type II cells were sufficient to control bacterial burden, but both subsets were activated by antigens derived from APCs and produced IFN-γ. Other studies suggest that lipid antigens derived from pathogens may be released into the extracellular environment during infection where they interact with the NKT cells. It is discussed whether NKT cells might directly recognize certain extracellular antigens (Kim, Cho, and Kim 2023). Whether or not recognition of membrane-expressed OVA by NKT cells might play a role and thereby explaining the increasing numbers in the B16-F10mOVA model remains to be analyzed.

The fact that B16-F10cOVA and B16-F10mOVA tumors displayed no obvious difference in NKT and T cell numbers in the TSNE-plots after vaccination but a big difference when mice were untreated lead us to ask the following questions: what is the difference in these types of cells? What are their functions?

To solve this problem, we plan to reanalyze our data with a focus on NKT and T cell populations using bioinformatical tools. In addition, new experiments will be performed in which the TCRs of $CD4^+$ and $CD8^+$ T cells in different organs and in the tumors of tumor-bearing animals will be analyzed on different days. We now hope to understand what distinguishes the T cells in the different B16-F10 models and how we can adapt our NP vaccination in the future to achieve even better control of tumor growth.

Our single cell analysis revealed that in addition to T cells also neutrophils were affected in numbers by our vaccination protocol. A decrease in the number of neutrophils was observed in both B16-F10mOVA and B16-F10cOVA tumors but not in the control B16-F10 tumors.

Neutrophils have a diverse and plastic phenotype that makes them immune suppressive or immune supportive depending on the TME. Tumor-associated neutrophils (TANs) play a crucial role suppressing anti-tumor immune responses. They promote ECM remodeling, which supports metastasis (Jaillon et al. 2020). This behavior supports tumor growth and malignancy (Guc and Pollard 2021). In our case, this could mean that the vaccination supports the anti-tumor response by reducing the number of tumor-infiltrating suppressive neutrophils. Here, too, only assumptions can be made on the basis of the data available to date. We are in the process to analyze this phenomenon in more detail in follow-up experiments and plan to perform a more detailed analysis of the scRNAseq data.

At our institute, the collogues Bartneck et al. have been working on a similar question. Using transcutaneous immunization (TCI), they could also detect reduced tumor growth in the MC38 model expressing OVA on the membrane (MC38mOVA) of the inoculated cancer cells. Their vaccination system, called DIVA^2, contains the adjuvants dithranol and the TLR7-agonist imiquimod (IMQ) as well as the antigen OVA to induce an antigen-specific immune response (Sohl et al. 2022; Hartmann et al. 2023). They also performed scRNAseq analysis out of CD45$^+$ TILs from MC38mOVA tumors. Unlike our study, the analyzes were performed at two different time points: during the immune control phase as well as in the immune evasion phase. While the immune system controlled the tumor growth, CD8$^+$ T cells in particular played a decisive role (Bartneck et al. 2023). These results are comparable to the results presented here and emphasize once again the importance of cytotoxic T cells in the TME. The presence of CCR2$^+$ monocytes expressing immunosuppressive markers correlated with the loss of tumor control. Bartneck et al. also showed that the depletion of these suppressive CCR2$^+$ monocytes in combination with the DIVA^2 therapy, they could prolong the survival of the mice. This shows the importance of identifying cell types that influence the long-term effect of a treatment. In turn, it enables an improved and more effective therapy, for example by working with a combination of preparations. In our study, we are also working on identifying the functional mechanisms and thus improving our vaccination strategy. Whether or not suppressive CCR2$^+$ monocytes play a role in our vaccination strategy and contribute tumor growth remains to be analyzed. If so, a combination of CCR2$^+$ monocytes depletion with the NP-based vaccination might improve the control of tumor growth.

In addition, replacing our model antigen OVA by tumor-associated or -specific antigens in our NP formulation will be the next step in the development of tumor-specific vaccination approaches relevant for the treatment of cancer patients.

Our vaccination system was able to elicit a stable cellular as well as humoral antigen-specific immune response allowing control of tumor growth. We could show that its necessary to combine the antigen and immune adjuvant in the same carrier system in order to get the full range of functional antigen-specific $CD8^+$ cytotoxic T cells. Furthermore, we could show the functionality of the NP system in different tumor models *in vivo*, where we observed reduced tumor growth after treatment. Which cells, in addition to $CD8^+$ T cells, play an important role in our vaccination strategy will be analyzed in further experiments. This will provide valuable information on how to adapt our vaccination strategy.

It has also been observed that a loss of tumor immune control occurs over time (Stickdorn et al. 2022; Bartneck et al. 2023). It is therefore important to know which cells play a role here and to counteract this loss, for example with a combination therapy. In addition, we continue to ask ourselves what role B cells and antibodies play in our vaccination protocol. The results to date suggest that a cellular response alone (antigen expressed in the cytosol) is associated with a better immune response, demonstrated by strong reduced tumor growth, than the combination of both responses (antigen expressed on the membrane). We will closely analyze the results of the existing single cell data and decode the key cell types to understand what exactly the differences are in the immune response of both systems also compared to the control tumor not expressing any antigen. In addition, we are looking at the TCR distribution in the different tumors and tissues to understand even more precisely how the antigen receptors of the $CD4^+$ and $CD8^+$ T cells change during tumor growth. With these planned experiments, some of which have already been initiated, we will hopefully be able to answer many of our remaining questions and improve our vaccination strategy. Nevertheless, we have been able to ensure successful tumor protection with our NP treatment. Our nanogel method stands out as a remarkably adaptable immunocarrier platform capable of activating anti-tumor capabilities. It holds promise for crafting tailored nanovaccines not only for prevalent clinical tumors but also for combating other viral pandemics (Stickdorn et al. 2022).

5. Abstract

Cancer is one of the most common diseases with a global incidence of 20 million people, responsible for 10 million deaths in 2020. The tendency is increasing. Normally, our immune system recognizes mutated cells and eliminates them. Cancer cells, however, are able to develop escape strategies that interfere with their elimination. Cancer immunotherapies aim at reinstalling the inherent capacity of immune cells to recognize and eliminate tumor cells. To induce a tumor-specific immune response able to eliminate cancer cells in the presence of an immunosuppressive tumor microenvironment, we established an immune stimulating and antigen-presenting nanoparticle (NP) platform. The NPs are decorated with ovalbumin (OVA) as model antigen and 1-(4-(aminomethyl)- benzyl)-2-butyl-1H-imidazo[4,5-c]quinolin-4-amine (IMDQ) as an immune stimulatory TLR7/8 agonist. They are characterized by pH sensitivity, well toleration and safety for intravenous injection.

To analyze the potential of our NPs *in vivo*, we inoculated B16-F10 or MC38 tumor cells either expressing membranous or cytosolic bound OVA or without expressing the antigen as control subcutaneously in the flank of C57BL/6 wild-type mice. When the tumor was pulpable with a size of about 0,25 mm^3 mice were vaccinated intravenously three times (on day 3, 5 and 7) with our nanogel to develop an immune response against our model antigen OVA in a therapeutic setting. Every two days we measured the tumor volume and once a week we took blood from the mice to determine the antibody titer. After approximately two weeks we sacrificed the mice and analyzed the immune responses concerning cytokines, T cell and B cell production. Furthermore, we analyzed the sera, splenocytes and lymphocytes from the mice via flow cytometry. We could show that our NP therapy was able to reduce the tumor growth in two different tumor models. The particles provided an antigen specific tumor immunity by inducing a Th1-mediated immune response and a high production of $CD8^+$ T cells. These results were also confirmed by single cell RNA analysis. Further evaluation and experiments are needed to decipher the differences in the T cell response and the role of the involvement of B cells in combination with T cells in the different models.

6. Summary – Zusammenfassung

Krebs ist noch immer eine der häufigsten Krankheiten mit einer weltweiten Inzidenz von 20 Millionen Menschen. Im Jahr 2020 war Krebs für über 10 Millionen Todesfälle verantwortlich. Die Tendenz ist steigend. Eine Ursache für die Entstehung von Krebs ist, dass unser Immunsystem entartete Zellen nicht mehr erkennen und zerstören kann. Tumorzellen sind in der Lage die natürlichen Kontrollsysteme des menschlichen Körpers zu übergehen und sich somit einer Eliminierung zu entziehen. Krebsimmuntherapien zielen darauf ab, diese schützenden Mechanismen des Immunsystems wieder zu reaktivieren, sodass eine aktive antitumorale Antwort gewährleitet werden kann. Um diesen Ansatz zu verfolgen und eine tumorspezifische Immunantwort auszulösen, die in der Lage ist, Krebszellen in Gegenwart einer immunsuppressiven Tumormikroumgebung zu eliminieren, haben wir eine immunstimulierende und Antigen-präsentierende Nanopartikel-Plattform (NP) entwickelt. Die NPs sind mit Ovalbumin (OVA) als Modellantigen und 1-(4-(Aminomethyl)-benzyl)-2-butyl-1H-imidazo[4,5-c]chinolin-4-amin (IMDQ) als immunstimulierender TLR7/8-Agonist funktionalisiert. Sie zeichnen sich durch pH-Sensivität und gute Verträglichkeit aus. Zudem können sie ohne Bedenken intravenös appliziert werden.

Um das Potenzial unserer NPs *in vivo* zu analysieren wurden C57BL/6 Wildtyp Mäusen Tumorzellen subkutan appliziert. Entweder MC38 oder B16-F10 Zellen ohne Antigen, als Kontrolle oder mit OVA-modifizierte Zellen, welche das Antigen entweder auf der Membran oder im Zytosol exprimierten. Bei einer Tumorgröße von etwa 0,25 mm^3 wurden die Tiere dreimal an den Tagen 3, 5 und 7 durch die intravenöse Gabe der Partikel behandelt. Alle zwei Tage wurde das Tumorvolumen gemessen und einmal pro Woche wurde den Mäusen Blut abgenommen, um den Antikörpertiter zu bestimmen. Nach etwa zwei Wochen wurden die Mäuse euthanasiert und die Immunreaktionen in Bezug auf Zytokine, T-Zell- sowie B-Zell-Produktion analysiert.

Mit der Reihe unserer Experimente konnten wir zeigen, dass unsere Nanopartikel Therapie in der Lage war, das Tumorwachstum in zwei unterschiedlichen Tumormodellen zu reduzieren. Die Partikel sorgten für eine antigenspezifische Tumorimmunität, indem sie eine Th1-vermittelte Immunantwort und eine hohe Produktion von $CD8^+$ T-Zellen induzierten. Diese Ergebnisse konnten wir auch durch Einzelzell-RNA-Analysen bestätigen. Es bedarf weiterer Auswertung und Versuche um die Unterschiede in der T-Zell Antwort, sowie die Rolle der Beteiligung von B- in Kombination mit T-Zellen in den unterschiedlichen Modellen zu entschlüsseln.

7. Appendix

7.1 List of abbreviations

Table 10: List of abbreviations

abbreviation	meaning
ADCC	Antibody-dependent cell cytotoxicity
AEC	3-Amino-9-ethyl-carbazole
ALT	alternative lengthening of telomeres
APC	Antigen presenting cell
B16-F10	B16-F10 without transfected OVA
B16-F10mOVA	B16-F10 transfected with OVA on the membrane
B16-F10vOVA	B16-F10 transfected with OVA on the cytosol
BMDC	Bone marrow-derived DCs
Bregs	Regulatory B cells
BSA	Bovine serum albumin
CAR	Chimeric antigen receptor
CBA	Cytometric Bead Array
CDC	Complement dependent cytotoxicity
CFSE	5,6-Carboxyfluorescein Diacetat Succinimidyl Ester
cOVA	Cytosolic OVA
CTL	Cytotoxic Lymphocyte
CTLA-4	Cytotoxic T-lymphocyte-associated Protein 4
ctrl	Control
DC	Dendritic cells
DHM	1,2-dimethylhydratinedihydrochlorid
DIVA	Dithranol/IMQ based vaccination approach
DMEM	Dulbecco´s Modified Eagle Medium
DMSO	Dimethyl sulfoxide
DNA	Deoxyribonucleic acid
dsRNA	Double stranded RNA
ECM	Extracellular matrix
EDTA	Ethylenediaminetetraacetic acid
ER	Endoplasmic reticulum
FACS	Fluorescence activated cell sorting
Fas-L	Fas-Ligand
FBS	Fetal Bovine Serum
FCS	Fetal calf serum
GC	Germinal centers
GM-CSF	Granulocyte-macrophage colony-stimulating factor
HRP	Horseradish peroxidase
IL2RA	Interleukin 2 receptor subunit aplha
IMDM	Iscove´s Modified Dulbecco´s Medium

Continuation of Table 10: List of abbreviations

abbreviation	meaning
IMDQ	1-(4-(aminomethyl)- benzyl)-2-butyl-1H-imidazo[4,5-c]quinolin-4-amine
iNKT	Invariant NKT
iSEE	Interactive Summarized Experiment Explorer
iTreg	in vitro-induced Treg
MABs	Monoclonal antibodies
MACS	Magnetic cell separation
MC38	MC38 without transfected OVA
MC38mOVA	MC38 transfected with OVA on the membrane
MDSC	Myeloid-derived suppressor cells
mOVA	Membranous OVA
Myc	Myc proto-oncogene protein
NK	Natural killer cells
NKT	Natural Killer T
NP	Nanoparticle
NP(IMDQ+OVA)	IMDQ and OVA covalently attached to NP
OVA	Ovalbumin
PAMPs	Pathogen associated molecular patterns
PBS	Phosphate buffered saline
PD-L1	Programmed cell death ligand 1
PD1	Programmed cell death protein 1
PRR	Pattern recognition receptors
pTreg	Peripherally-derived Tregs
Raf	RAF proto-oncogene serine/threonine-protein kinase
RPMI	Roswell Park Memorial Institute
scRNAseq	Single cell RNA sequencing
SIIN	SIINFEKL
sIMDQ	Soluble IMDQ
sOVA	Soluble OVA
ssDNA	Single stranded DNA
ssRNA	Single stranded RNA
ST	Sample Tag
TAM	Tumor-associated macrophage
TAN	Tumor-associated neutrophil
TAP	Transporter associated with antigen processing
Tc	Cytotoxic T cell
TCI	Transcutaneous immunization

Continuation of Table 10: List of abbreviations

abbreviation	**meaning**
TCR	T cell receptor
TDK	Tumor Dissociation Kit
Teff	T effector cell
Tfh	T follicular helper
Th	T helper cell
TIL	Tumor infiltrated lymphocytes
TIL-Bs	Tumor-infiltrating B cells
TLR	Toll like receptor
TMB	Tumor mutational burden
TME	Tumor microenvironment
Treg	Regulatory T cell
tSNE	t-distributed stochastic neighbor embedding
tTreg	Thymus-derived Treg
UVB	Ultraviolet B radiation
V(D)J	Variability, diversity and joining
WTA	Whole transcriptome analysis

7.2 Figure directory

7.3 Table directory

7.4 Literature directory

Abdi, K., K. Laky, M. Abshari, E. M. Hill, L. Lantz, N. J. Singh, and E. O. Long. 2022. 'Dendritic cells Trigger IFN-gamma secretion by NK cells independent of IL-12 and IL-18', *Eur J Immunol*, 52: 1431-40.

Abdul-Rahman, Toufik, Shankhaneel Ghosh, Sarah M. Badar, Abubakar Nazir, Gafar Babatunde Bamigbade, Narjiss Aji, Poulami Roy, Hajar kachani, Neil Garg, Lukman Lawal, Zarah Sophia Blake Bliss, Andrew Awuah Wireko, Oday Atallah, Favour Tope Adebusoye, Tetiana Teslyk, Kateryna Sikora, and Viktoriia Horbas. 2024. 'The paradoxical role of cytokines and chemokines at the tumor microenvironment: a comprehensive review', *European Journal of Medical Research*, 29: 124.

Alghamdi, M. A., A. N. Fallica, N. Virzì, P. Kesharwani, V. Pittalà, and K. Greish. 2022. 'The Promise of Nanotechnology in Personalized Medicine', *J Pers Med*, 12.

Alturki, N. A. 2023. 'Review of the Immune Checkpoint Inhibitors in the Context of Cancer Treatment', *J Clin Med*, 12.

Anderson, N. M., and M. C. Simon. 2020. 'The tumor microenvironment', *Curr Biol*, 30: R921-r25.

Arora, S., R. Velichinskii, R. W. Lesh, U. Ali, M. Kubiak, P. Bansal, H. Borghaei, M. J. Edelman, and Y. Boumber. 2019. 'Existing and Emerging Biomarkers for Immune Checkpoint Immunotherapy in Solid Tumors', *Adv Ther*, 36: 2638-78.

Arpaia, N., J. A. Green, B. Moltedo, A. Arvey, S. Hemmers, S. Yuan, P. M. Treuting, and A. Y. Rudensky. 2015. 'A Distinct Function of Regulatory T Cells in Tissue Protection', *Cell*, 162: 1078-89.

Astarita, Jillian L, Claudia X Dominguez, Corey Tan, Jovanny Guillen, Mariela L Pauli, Rosario Labastida, Jose Valle, Melanie Kleinschek, Jesse Lyons, and Ali A Zarrin. 2022. 'Treg specialization and functions beyond immune suppression', *Clinical and Experimental Immunology*, 211: 176-83.

Bartneck, J., A. K. Hartmann, L. Stein, D. Arnold-Schild, M. Klein, M. Stassen, F. Marini, J. Pielenhofer, S. L. Meiser, P. Langguth, M. Mack, S. Muth, H. C. Probst, H. Schild, and M. P. Radsak. 2023. 'Tumor-infiltrating CCR2(+) inflammatory monocytes counteract specific immunotherapy', *Frontiers in immunology*, 14: 1267866.

Belnap, L. P., P. H. Cleveland, M. E. Colmerauer, R. M. Barone, and Y. H. Pilch. 1979. 'Immunogenicity of chemically induced murine colon cancers', *Cancer Res*, 39: 1174-9.

Ben Khelil, M., Y. Godet, S. Abdeljaoued, C. Borg, O. Adotévi, and R. Loyon. 2022. 'Harnessing Antitumor CD4(+) T Cells for Cancer Immunotherapy', *Cancers (Basel)*, 14.

Berger, A. 2000. 'Th1 and Th2 responses: what are they?', *Bmj*, 321: 424.

Bermudez, L. E., A. Parker, and J. R. Goodman. 1997. 'Growth within macrophages increases the efficiency of Mycobacterium avium in invading other macrophages by a complement receptor-independent pathway', *Infect Immun*, 65: 1916-25.

Bhatt, A. P., M. R. Redinbo, and S. J. Bultman. 2017. 'The role of the microbiome in cancer development and therapy', *CA Cancer J Clin*, 67: 326-44.

Bilotta, M. T., A. Antignani, and D. J. Fitzgerald. 2022. 'Managing the TME to improve the efficacy of cancer therapy', *Frontiers in immunology*, 13: 954992.

Blum, J. S., P. A. Wearsch, and P. Cresswell. 2013. 'Pathways of antigen processing', *Annu Rev Immunol*, 31: 443-73.

Brown, D. M., T. L. Fisher, C. Wei, J. G. Frelinger, and E. M. Lord. 2001. 'Tumours can act as adjuvants for humoral immunity', *Immunology*, 102: 486-97.

Buch, T., F. L. Heppner, C. Tertilt, T. J. Heinen, M. Kremer, F. T. Wunderlich, S. Jung, and A. Waisman. 2005. 'A Cre-inducible diphtheria toxin receptor mediates cell lineage ablation after toxin administration', *Nat Methods*, 2: 419-26.

Bule, P., S. I. Aguiar, F. Aires-Da-Silva, and J. N. R. Dias. 2021. 'Chemokine-Directed Tumor Microenvironment Modulation in Cancer Immunotherapy', *Int J Mol Sci*, 22.

Cardell, S., S. Tangri, S. Chan, M. Kronenberg, C. Benoist, and D. Mathis. 1995. 'CD1-restricted CD4+ T cells in major histocompatibility complex class II-deficient mice', *J Exp Med*, 182: 993-1004.

Cerwenka, A., and L. L. Lanier. 2001. 'Natural killer cells, viruses and cancer', *Nat Rev Immunol*, 1: 41-9.

Chan, I. S., and A. J. Ewald. 2022. 'The changing role of natural killer cells in cancer metastasis', *J Clin Invest*, 132.

Chaplin, D. D. 2010. 'Overview of the immune response', *J Allergy Clin Immunol*, 125: S3-23.

'Chapter 7 - Antigen Processing and Presentation.' in. 2014. Tak W. Mak, Mary E. Saunders and Bradley D. Jett (eds.), *Primer to the Immune Response (Second Edition)* (Academic Cell: Boston).

Chen, X., and J. J. Oppenheim. 2014. 'Th17 cells and Tregs: unlikely allies', *J Leukoc Biol*, 95: 723-31.

Chenthamara, Dhrisya, Sadhasivam Subramaniam, Sankar Ganesh Ramakrishnan, Swaminathan Krishnaswamy, Musthafa Mohamed Essa, Feng-Huei Lin, and M. Walid Qoronfleh. 2019. 'Therapeutic efficacy of nanoparticles and routes of administration', *Biomaterials Research*, 23: 20.

Clarkson, M. R., and M. H. Sayegh. 2005. 'T-cell costimulatory pathways in allograft rejection and tolerance', *Transplantation*, 80: 555-63.

Cooper, G.M. 2000. 'The Cell: A Molecular Approach. 2nd edition. Sunderland (MA): Sinauer Associates; 2000. The Development and Causes of Cancer.'.

Costa, Pmds, S. L. A. Sales, D. P. Pinheiro, L. Q. Pontes, S. S. Maranhao, C. D. O. Pessoa, G. P. Furtado, and C. L. M. Furtado. 2023. 'Epigenetic reprogramming in cancer: From diagnosis to treatment', *Front Cell Dev Biol*, 11: 1116805.

Crotzer, V. L., and J. S. Blum. 2009. 'Autophagy and its role in MHC-mediated antigen presentation', *J Immunol*, 182: 3335-41.

Davis, M. M., and P. J. Bjorkman. 1988. 'T-cell antigen receptor genes and T-cell recognition', *Nature*, 334: 395-402.

de Visser, Karin E., and Johanna A. Joyce. 2023. 'The evolving tumor microenvironment: From cancer initiation to metastatic outgrowth', *Cancer Cell*, 41: 374-403.

Del Prete, Annalisa, Valentina Salvi, Alessandra Soriani, Mattia Laffranchi, Francesca Sozio, Daniela Bosisio, and Silvano Sozzani. 2023. 'Dendritic cell subsets in cancer immunity and tumor antigen sensing', *Cellular & Molecular Immunology*, 20: 432-47.

Delacher, M., C. D. Imbusch, D. Weichenhan, A. Breiling, A. Hotz-Wagenblatt, U. Träger, A. C. Hofer, D. Kägebein, Q. Wang, F. Frauhammer, J. P. Mallm, K. Bauer, C. Herrmann, P. A. Lang, B. Brors, C. Plass, and M. Feuerer. 2017. 'Genome-wide DNA-methylation landscape defines specialization of regulatory T cells in tissues', *Nat Immunol*, 18: 1160-72.

DeNardo, D. G., and B. Ruffell. 2019. 'Macrophages as regulators of tumour immunity and immunotherapy', *Nat Rev Immunol*, 19: 369-82.

Dine, Jennifer, RuthAnn Gordon, Yelena Shames, Mary K. Kasler, and Margaret Barton-Burke. 2017. 'Immune checkpoint inhibitors: An innovation in immunotherapy for the treatment and management of patients with cancer', *Asia-Pacific Journal of Oncology Nursing*, 4: 127-35.

Dolina, J. S., N. Van Braeckel-Budimir, G. D. Thomas, and S. Salek-Ardakani. 2021. 'CD8(+) T Cell Exhaustion in Cancer', *Frontiers in immunology*, 12: 715234.

Dowling, D. J. 2018. 'Recent Advances in the Discovery and Delivery of TLR7/8 Agonists as Vaccine Adjuvants', *Immunohorizons*, 2: 185-97.

Engel, A. L., G. E. Holt, and H. Lu. 2011. 'The pharmacokinetics of Toll-like receptor agonists and the impact on the immune system', *Expert Rev Clin Pharmacol*, 4: 275-89.

Fan, Ting, Mingna Zhang, Jingxian Yang, Zhounan Zhu, Wanlu Cao, and Chunyan Dong. 2023. 'Therapeutic cancer vaccines: advancements, challenges, and prospects', *Signal Transduction and Targeted Therapy*, 8: 450.

Farber, D. L., N. A. Yudanin, and N. P. Restifo. 2014. 'Human memory T cells: generation, compartmentalization and homeostasis', *Nat Rev Immunol*, 14: 24-35.

Foroozandeh, P., and A. A. Aziz. 2018. 'Insight into Cellular Uptake and Intracellular Trafficking of Nanoparticles', *Nanoscale Res Lett*, 13: 339.

Fujii, S. I., and K. Shimizu. 2019. 'Immune Networks and Therapeutic Targeting of iNKT Cells in Cancer', *Trends Immunol*, 40: 984-97.

Gadani, S. P., J. C. Cronk, G. T. Norris, and J. Kipnis. 2012. 'IL-4 in the brain: a cytokine to remember', *J Immunol*, 189: 4213-9.

Genardi, S., L. Visvabharathy, L. Cao, E. Morgun, Y. Cui, C. Qi, Y. H. Chen, L. Gapin, E. Berdyshev, and C. R. Wang. 2020. 'Type II Natural Killer T Cells Contribute to Protection Against Systemic Methicillin-Resistant Staphylococcus aureus Infection', *Frontiers in immunology*, 11: 610010.

Gerhard, G. M., R. Bill, M. Messemaker, A. M. Klein, and M. J. Pittet. 2021. 'Tumor-infiltrating dendritic cell states are conserved across solid human cancers', *J Exp Med*, 218.

Germain, R. N. 2012. 'Maintaining system homeostasis: the third law of Newtonian immunology', *Nat Immunol*, 13: 902-6.

Gizinski, A. M., D. A. Fox, and S. Sarkar. 2010a. 'Pharmacotherapy: concepts of pathogenesis and emerging treatments. Co-stimulation and T cells as therapeutic targets', *Best Pract Res Clin Rheumatol*, 24: 463-77.

Gizinski, Alison M., David A. Fox, and Sujata Sarkar. 2010b. 'Co-stimulation and T cells as therapeutic targets', *Best Practice & Research Clinical Rheumatology*, 24: 463-77.

Godfrey, D. I., H. R. MacDonald, M. Kronenberg, M. J. Smyth, and L. Van Kaer. 2004. 'NKT cells: what's in a name?', *Nat Rev Immunol*, 4: 231-7.

Guc, E., and J. W. Pollard. 2021. 'Redefining macrophage and neutrophil biology in the metastatic cascade', *Immunity*, 54: 885-902.

Gupta, P. B., I. Pastushenko, A. Skibinski, C. Blanpain, and C. Kuperwasser. 2019. 'Phenotypic Plasticity: Driver of Cancer Initiation, Progression, and Therapy Resistance', *Cell Stem Cell*, 24: 65-78.

Hailemichael, Y., Z. Dai, N. Jaffarzad, Y. Ye, M. A. Medina, X. F. Huang, S. M. Dorta-Estremera, N. R. Greeley, G. Nitti, W. Peng, C. Liu, Y. Lou, Z. Wang, W. Ma, B. Rabinovich, R. T. Sowell, K. S. Schluns, R. E. Davis, P. Hwu, and W. W. Overwijk. 2013. 'Persistent antigen at vaccination sites induces tumor-specific $CD8^+$ T cell sequestration, dysfunction and deletion', *Nat Med*, 19: 465-72.

Hanahan, D. 2022. 'Hallmarks of Cancer: New Dimensions', *Cancer Discov*, 12: 31-46.

Hanahan, D., and R. A. Weinberg. 2000. 'The hallmarks of cancer', *Cell*, 100: 57-70.

———. 2011. 'Hallmarks of cancer: the next generation', *Cell*, 144: 646-74.

Hartmann, A. K., J. Bartneck, J. Pielenhofer, S. L. Meiser, D. Arnold-Schild, M. Klein, M. Stassen, H. Schild, S. Muth, H. C. Probst, P. Langguth, S. Grabbe, and M. P. Radsak. 2023. 'Optimized dithranol-imiquimod-based transcutaneous immunization enables tumor rejection', *Frontiers in immunology*, 14: 1238861.

Hayes, E. T., C. E. Hagan, L. Khoryati, M. A. Gavin, and D. J. Campbell. 2020. 'Regulatory T Cells Maintain Selective Access to IL-2 and Immune Homeostasis despite Substantially Reduced CD25 Function', *J Immunol*, 205: 2667-78.

Hernandez, J. B., R. H. Newton, and C. M. Walsh. 2010. 'Life and death in the thymus--cell death signaling during T cell development', *Curr Opin Cell Biol*, 22: 865-71.

Heufler, C., F. Koch, U. Stanzl, G. Topar, M. Wysocka, G. Trinchieri, A. Enk, R. M. Steinman, N. Romani, and G. Schuler. 1996. 'Interleukin-12 is produced by dendritic cells and mediates T helper 1 development as well as interferon-gamma production by T helper 1 cells', *Eur J Immunol*, 26: 659-68.

Hilligan, Kerry L., and Franca Ronchese. 2020. 'Antigen presentation by dendritic cells and their instruction of CD4+ T helper cell responses', *Cellular & Molecular Immunology*, 17: 587-99.

Homet Moreno, B., J. M. Zaretsky, A. Garcia-Diaz, J. Tsoi, G. Parisi, L. Robert, K. Meeth, A. Ndoye, M. Bosenberg, A. T. Weeraratna, T. G. Graeber, B. Comin-Anduix, S. Hu-Lieskovan, and A. Ribas. 2016. 'Response to Programmed Cell Death-1 Blockade in a Murine Melanoma Syngeneic Model Requires Costimulation, CD4, and CD8 T Cells', *Cancer Immunol Res*, 4: 845-57.

Hou, A., K. Hou, Q. Huang, Y. Lei, and W. Chen. 2020. 'Targeting Myeloid-Derived Suppressor Cell, a Promising Strategy to Overcome Resistance to Immune Checkpoint Inhibitors', *Frontiers in immunology*, 11: 783.

Hsieh, C. S., A. B. Heimberger, J. S. Gold, A. O'Garra, and K. M. Murphy. 1992. 'Differential regulation of T helper phenotype development by interleukins 4 and 10 in an alpha beta T-cell-receptor transgenic system', *Proc Natl Acad Sci U S A*, 89: 6065-9.

Hubert, P., and S. Amigorena. 2012. 'Antibody-dependent cell cytotoxicity in monoclonal antibody-mediated tumor immunotherapy', *Oncoimmunology*, 1: 103-05.

Jaillon, Sebastien, Andrea Ponzetta, Diletta Di Mitri, Angela Santoni, Raffaella Bonecchi, and Alberto Mantovani. 2020. 'Neutrophil diversity and plasticity in tumour progression and therapy', *Nature Reviews Cancer*, 20: 485-503.

Jandl, C., C. Loetsch, and C. King. 2017. 'Cytokine Expression by T Follicular Helper Cells', *Methods Mol Biol*, 1623: 95-103.

Janeway, C. A., Jr. 1989. 'Approaching the asymptote? Evolution and revolution in immunology', *Cold Spring Harb Symp Quant Biol*, 54 Pt 1: 1-13.

Janeway, C. A., Jr., and R. Medzhitov. 2002. 'Innate immune recognition', *Annu Rev Immunol*, 20: 197-216.

Jiménez-Morales, S., I. S. Aranda-Uribe, C. J. Pérez-Amado, J. Ramírez-Bello, and A. Hidalgo-Miranda. 2021. 'Mechanisms of Immunosuppressive Tumor Evasion: Focus on Acute Lymphoblastic Leukemia', *Frontiers in immunology*, 12: 737340.

Joffre, Olivier P., Elodie Segura, Ariel Savina, and Sebastian Amigorena. 2012. 'Cross-presentation by dendritic cells', *Nature Reviews Immunology*, 12: 557-69.

Josefowicz, S. Z., L. F. Lu, and A. Y. Rudensky. 2012. 'Regulatory T cells: mechanisms of differentiation and function', *Annu Rev Immunol*, 30: 531-64.

Joseph, T. M., D. Kar Mahapatra, A. Esmaeili, Ł Piszczyk, M. S. Hasanin, M. Kattali, J. Haponiuk, and S. Thomas. 2023. 'Nanoparticles: Taking a Unique Position in Medicine', *Nanomaterials (Basel)*, 13.

Joshi, Neha, Vikas Duhan, Neelam Lingwal, Sangeeta Bhaskar, and Pramod Upadhyay. 2012. 'Adjuvant properties of thermal component of hyperthermia enhanced transdermal immunization: effect on dendritic cells', *PloS one*, 7: e32067-e67.

Jung, D., and F. W. Alt. 2004. 'Unraveling V(D)J recombination; insights into gene regulation', *Cell*, 116: 299-311.

Kai, F., A. P. Drain, and V. M. Weaver. 2019. 'The Extracellular Matrix Modulates the Metastatic Journey', *Dev Cell*, 49: 332-46.

Kaiko, G. E., J. C. Horvat, K. W. Beagley, and P. M. Hansbro. 2008. 'Immunological decision-making: how does the immune system decide to mount a helper T-cell response?', *Immunology*, 123: 326-38.

Kalluri, Raghu. 2016. 'The biology and function of fibroblasts in cancer', *Nature Reviews Cancer*, 16: 582-98.

Kaplan, S. S., R. P. Heine, and R. L. Simmons. 1999. 'Defensins impair phagocytic killing by neutrophils in biomaterial-related infection', *Infect Immun*, 67: 1640-5.

Kawai, T., and S. Akira. 2010. 'The role of pattern-recognition receptors in innate immunity: update on Toll-like receptors', *Nat Immunol*, 11: 373-84.

Kawano, T., J. Cui, Y. Koezuka, I. Toura, Y. Kaneko, K. Motoki, H. Ueno, R. Nakagawa, H. Sato, E. Kondo, H. Koseki, and M. Taniguchi. 1997. 'CD1d-restricted and TCR-mediated activation of valpha14 NKT cells by glycosylceramides', *Science*, 278: 1626-9.

Kaye, J., G. Kersh, I. Engel, and S. M. Hedrick. 1991. 'Structure and specificity of the T cell antigen receptor', *Semin Immunol*, 3: 269-81.

Kesh, K., V. K. Gupta, B. Durden, V. Garrido, B. Mateo-Victoriano, S. P. Lavania, and S. Banerjee. 2020. 'Therapy Resistance, Cancer Stem Cells and ECM in Cancer: The Matrix Reloaded', *Cancers (Basel)*, 12.

Kim, J. C., X. Liu, K. Fitzgerald, J. S. Eng, J. Orf, S. A. O'Brien, B. Belmontes, A. J. Casbon, S. V. Novitskiy, K. V. Tarbell, J. DeVoss, and J. G. Egen. 2023. 'Brief report: STING expressed in tumor and non-tumor compartments has distinct roles in regulating anti-tumor immunity', *Cancer Immunol Immunother*, 72: 1327-35.

Kim, Seohyun, Sumin Cho, and Ji Hyung Kim. 2023. 'CD1-mediated immune responses in mucosal tissues: molecular mechanisms underlying lipid antigen presentation system', *Experimental & Molecular Medicine*, 55: 1858-71.

Krishnaswamy, J. K., T. Chu, and S. C. Eisenbarth. 2013. 'Beyond pattern recognition: NOD-like receptors in dendritic cells', *Trends Immunol*, 34: 224-33.

Kurachi, Makoto. 2019. 'CD8+ T cell exhaustion', *Seminars in Immunopathology*, 41: 327-37.

La Cava, A., L. Van Kaer, and Shi Fu Dong. 2006. 'CD4+CD25+ Tregs and NKT cells: regulators regulating regulators', *Trends Immunol*, 27: 322-7.

Lantz, O., and A. Bendelac. 1994. 'An invariant T cell receptor alpha chain is used by a unique subset of major histocompatibility complex class I-specific CD4+ and CD4-8- T cells in mice and humans', *J Exp Med*, 180: 1097-106.

Laumont, Céline M., Allyson C. Banville, Mara Gilardi, Daniel P. Hollern, and Brad H. Nelson. 2022. 'Tumour-infiltrating B cells: immunological mechanisms, clinical impact and therapeutic opportunities', *Nature Reviews Cancer*, 22: 414-30.

Lee, J. H., E. Shklovskaya, S. Y. Lim, M. S. Carlino, A. M. Menzies, A. Stewart, B. Pedersen, M. Irvine, S. Alavi, J. Y. H. Yang, D. Strbenac, R. P. M. Saw, J. F. Thompson, J. S. Wilmott, R. A. Scolyer, G. V. Long, R. F. Kefford, and H. Rizos. 2020. 'Transcriptional downregulation of MHC class I and melanoma de- differentiation in resistance to PD-1 inhibition', *Nat Commun*, 11: 1897.

Lepeltier, Elise, Lutz Nuhn, Claus-Michael Lehr, and Rudolf Zentel. 2015. 'Not just for tumor targeting: Unmet medical needs and opportunities for nanomedicine', *Nanomedicine (London, England)*, 10.

Li, Chunxiao, Ping Jiang, Shuhua Wei, Xiaofei Xu, and Junjie Wang. 2020. 'Regulatory T cells in tumor microenvironment: new mechanisms, potential therapeutic strategies and future prospects', *Molecular Cancer*, 19: 116.

Li, L., R. Yu, T. Cai, Z. Chen, M. Lan, T. Zou, B. Wang, Q. Wang, Y. Zhao, and Y. Cai. 2020. 'Effects of immune cells and cytokines on inflammation and immunosuppression in the tumor microenvironment', *Int Immunopharmacol*, 88: 106939.

Li, Y., L. Zhao, and X. F. Li. 2021. 'Hypoxia and the Tumor Microenvironment', *Technol Cancer Res Treat*, 20: 15330338211036304.

Liu, Jian, Minyang Fu, Manni Wang, Dandan Wan, Yuquan Wei, and Xiawei Wei. 2022. 'Cancer vaccines as promising immuno-therapeutics: platforms and current progress', *Journal of Hematology & Oncology*, 15: 28.

Lugano, R., M. Ramachandran, and A. Dimberg. 2020. 'Tumor angiogenesis: causes, consequences, challenges and opportunities', *Cell Mol Life Sci*, 77: 1745-70.

Lynn, G. M., R. Laga, P. A. Darrah, A. S. Ishizuka, A. J. Balaci, A. E. Dulcey, M. Pechar, R. Pola, M. Y. Gerner, A. Yamamoto, C. R. Buechler, K. M. Quinn, M. G. Smelkinson, O. Vanek, R. Cawood, T. Hills, O. Vasalatiy, K. Kastenmüller, J. R. Francica, L. Stutts, J. K. Tom, K. A. Ryu, A. P. Esser-Kahn, T. Etrych, K. D. Fisher, L. W. Seymour, and R. A. Seder. 2015. 'In vivo characterization of the physicochemical properties of polymer-linked TLR agonists that enhance vaccine immunogenicity', *Nat Biotechnol*, 33: 1201-10.

Lythgoe, M. P., B. H. Mullish, A. E. Frampton, and J. Krell. 2022. 'Polymorphic microbes: a new emerging hallmark of cancer', *Trends Microbiol*, 30: 1131-34.

Macho-Fernandez, E., and M. Brigl. 2015. 'The Extended Family of CD1d-Restricted NKT Cells: Sifting through a Mixed Bag of TCRs, Antigens, and Functions', *Frontiers in immunology*, 6: 362.

Market, E., and F. N. Papavasiliou. 2003. 'V(D)J recombination and the evolution of the adaptive immune system', *PLoS Biol*, 1: E16.

McCullough, Kenneth C., and Artur Summerfield. 2005. 'Basic Concepts of Immune Response and Defense Development', *ILAR Journal*, 46: 230-40.

Medzhitov, R., and C. A. Janeway, Jr. 1997. 'Innate immunity: the virtues of a nonclonal system of recognition', *Cell*, 91: 295-8.

———. 1998. 'Innate immune recognition and control of adaptive immune responses', *Semin Immunol*, 10: 351-3.

Morse, Michael A., William R. Gwin, and Duane A. Mitchell. 2021. 'Vaccine Therapies for Cancer: Then and Now', *Targeted Oncology*, 16: 121-52.

Mueller, D. L. 2010. 'Mechanisms maintaining peripheral tolerance', *Nat Immunol*, 11: 21-7.

Mundekkad, D., and W. C. Cho. 2022. 'Nanoparticles in Clinical Translation for Cancer Therapy', *Int J Mol Sci*, 23.

Muz, B., P. de la Puente, F. Azab, and A. K. Azab. 2015. 'The role of hypoxia in cancer progression, angiogenesis, metastasis, and resistance to therapy', *Hypoxia (Auckl)*, 3: 83-92.

Nagata, S. 1999. 'Fas ligand-induced apoptosis', *Annu Rev Genet*, 33: 29-55.

Nagata, Shigekazu, and Pierre Golstein. 1995. 'The Fas Death Factor', *Science*, 267: 1449-56.

Narvekar, A., A. Pardeshi, R. Jain, and P. Dandekar. 2022. 'ADCC enhancement: A conundrum or a boon to mAb therapy?', *Biologicals*, 79: 10-18.

Nelson, A., J. D. Lukacs, and B. Johnston. 2021. 'The Current Landscape of NKT Cell Immunotherapy and the Hills Ahead', *Cancers (Basel)*, 13.

Nicholson, L. B. 2016. 'The immune system', *Essays Biochem*, 60: 275-301.

Nosbaum, A., N. Prevel, H. A. Truong, P. Mehta, M. Ettinger, T. C. Scharschmidt, N. H. Ali, M. L. Pauli, A. K. Abbas, and M. D. Rosenblum. 2016. 'Cutting Edge: Regulatory T Cells Facilitate Cutaneous Wound Healing', *J Immunol*, 196: 2010-4.

Nuhn, L., N. Vanparijs, A. De Beuckelaer, L. Lybaert, G. Verstraete, K. Deswarte, S. Lienenklaus, N. M. Shukla, A. C. Salyer, B. N. Lambrecht, J. Grooten, S. A. David, S. De Koker, and B. G. De Geest. 2016. 'pH-degradable imidazoquinoline-ligated nanogels for lymph node-focused immune activation', *Proc Natl Acad Sci U S A*, 113: 8098-103.

Paget, Christophe, Melvyn T. Chow, Helene Duret, Stephen R. Mattarollo, and Mark J. Smyth. 2012. 'Role of γδ T Cells in α-Galactosylceramide–Mediated Immunity', *The Journal of Immunology*, 188: 3928-39.

Park, H., Z. Li, X. O. Yang, S. H. Chang, R. Nurieva, Y. H. Wang, Y. Wang, L. Hood, Z. Zhu, Q. Tian, and C. Dong. 2005. 'A distinct lineage of CD4 T cells regulates tissue inflammation by producing interleukin 17', *Nat Immunol*, 6: 1133-41.

Philip, M., and A. Schietinger. 2022. 'CD8(+) T cell differentiation and dysfunction in cancer', *Nat Rev Immunol*, 22: 209-23.

Pimentel, J. A. A. 2010. 'Role of allergen-specific CD8+ T cells in the murine asthma model', *TU München, Dissertation*.

Pishesha, Novalia, Thibault J. Harmand, and Hidde L. Ploegh. 2022. 'A guide to antigen processing and presentation', *Nature Reviews Immunology*, 22: 751-64.

Popova, N. V., and M. Jücker. 2022. 'The Functional Role of Extracellular Matrix Proteins in Cancer', *Cancers (Basel)*, 14.

Ramirez-Valdez, R. A., F. Baharom, A. Khalilnezhad, S. C. Fussell, D. J. Hermans, A. M. Schrager, K. K. S. Tobin, G. M. Lynn, S. Khalilnezhad, F. Ginhoux, B. J. Van den Eynde, C. S. K. Leung, A. S. Ishizuka, and R. A. Seder. 2023. 'Intravenous heterologous prime-boost vaccination activates innate and adaptive immunity to promote tumor regression', *Cell Rep*, 42: 112599.

Raphael, I., S. Nalawade, T. N. Eagar, and T. G. Forsthuber. 2015. 'T cell subsets and their signature cytokines in autoimmune and inflammatory diseases', *Cytokine*, 74: 5-17.

Rastogi, I., D. Jeon, J. E. Moseman, A. Muralidhar, H. K. Potluri, and D. G. McNeel. 2022. 'Role of B cells as antigen presenting cells', *Frontiers in immunology*, 13: 954936.

Reddy, M., E. Eirikis, C. Davis, H. M. Davis, and U. Prabhakar. 2004. 'Comparative analysis of lymphocyte activation marker expression and cytokine secretion profile in stimulated human peripheral blood mononuclear cell cultures: an in vitro model to monitor cellular immune function', *J Immunol Methods*, 293: 127-42.

Renukaradhya, G. J., M. A. Khan, M. Vieira, W. Du, J. Gervay-Hague, and R. R. Brutkiewicz. 2008. 'Type I NKT cells protect (and type II NKT cells suppress) the host's innate antitumor immune response to a B-cell lymphoma', *Blood*, 111: 5637-45.

Robertson, F. C., J. A. Berzofsky, and M. Terabe. 2014. 'NKT cell networks in the regulation of tumor immunity', *Frontiers in immunology*, 5: 543.

Robinson, J. M. 2008. 'Reactive oxygen species in phagocytic leukocytes', *Histochem Cell Biol*, 130: 281-97.

Romagnani, S. 1999. 'Th1/Th2 cells', *Inflamm Bowel Dis*, 5: 285-94.

Rue-Albrecht, K., F. Marini, C. Soneson, and A. T. L. Lun. 2018. 'iSEE: Interactive SummarizedExperiment Explorer', *F1000Res*, 7: 741.

Sahai, Erik, Igor Astsaturov, Edna Cukierman, David G. DeNardo, Mikala Egeblad, Ronald M. Evans, Douglas Fearon, Florian R. Greten, Sunil R. Hingorani, Tony Hunter, Richard O. Hynes, Rakesh K. Jain, Tobias Janowitz, Claus Jorgensen, Alec C. Kimmelman, Mikhail G. Kolonin, Robert G. Maki, R. Scott Powers, Ellen Puré, Daniel C. Ramirez, Ruth Scherz-Shouval, Mara H. Sherman, Sheila Stewart, Thea D. Tlsty, David A. Tuveson, Fiona M. Watt, Valerie Weaver, Ashani T. Weeraratna, and Zena Werb. 2020. 'A framework for advancing our understanding of cancer-associated fibroblasts', *Nature Reviews Cancer*, 20: 174-86.

Schlosser, E., M. Mueller, S. Fischer, S. Basta, D. H. Busch, B. Gander, and M. Groettrup. 2008. 'TLR ligands and antigen need to be coencapsulated into the same biodegradable microsphere for the generation of potent cytotoxic T lymphocyte responses', *Vaccine*, 26: 1626-37.

Seder, R. A., W. E. Paul, M. M. Davis, and B. Fazekas de St Groth. 1992. 'The presence of interleukin 4 during in vitro priming determines the lymphokine-producing potential of CD4+ T cells from T cell receptor transgenic mice', *J Exp Med*, 176: 1091-8.

Shen, Z., G. Reznikoff, G. Dranoff, and K. L. Rock. 1997. 'Cloned dendritic cells can present exogenous antigens on both MHC class I and class II molecules', *J Immunol*, 158: 2723-30.

Shevach, E. M., and A. M. Thornton. 2014. 'tTregs, pTregs, and iTregs: similarities and differences', *Immunol Rev*, 259: 88-102.

Sohl, Julian, Ann-Kathrin Hartmann, Jennifer Hahlbrock, Joschka Bartneck, Michael Stassen, Matthias Klein, Matthias Bros, Stephan Grabbe, Federico Marini, Kevin Woods, Borhane Guezguez, Matthias Mack, Hansjörg Schild, Sabine Muth, Felix Melchior, Hans Christian Probst, Peter Langguth, and Markus P. Radsak. 2022. 'Dithranol as novel co-adjuvant for non-invasive dermal vaccination', *npj Vaccines*, 7: 112.

Starr, T. K., S. C. Jameson, and K. A. Hogquist. 2003. 'Positive and negative selection of T cells', *Annu Rev Immunol*, 21: 139-76.

Sterner, Robert C., and Rosalie M. Sterner. 2021. 'CAR-T cell therapy: current limitations and potential strategies', *Blood Cancer Journal*, 11: 69.

Stickdorn, Judith, Lara Stein, Danielle Arnold-Schild, Jennifer Hahlbrock, Carolina Medina-Montano, Joschka Bartneck, Tanja Ziß, Evelyn Montermann, Cinja Kappel, Dominika Hobernik, Maximilian Haist, Hajime Yurugi, Marco Raabe, Andreas Best, Krishnaraj Rajalingam, Markus P. Radsak, Sunil A. David, Kaloian Koynov, Matthias Bros, Stephan Grabbe, Hansjörg Schild, and Lutz Nuhn. 2022. 'Systemically Administered TLR7/8 Agonist and Antigen-Conjugated Nanogels Govern Immune Responses against Tumors', *ACS Nano*, 16: 4426-43.

Sultana, Afreen, Mina Zare, Vinoy Thomas, T. S. Sampath Kumar, and Seeram Ramakrishna. 2022. 'Nano-based drug delivery systems: Conventional drug delivery routes, recent developments and future prospects', *Medicine in Drug Discovery*, 15: 100134.

Sun, T., Y. S. Zhang, B. Pang, D. C. Hyun, M. Yang, and Y. Xia. 2014. 'Engineered nanoparticles for drug delivery in cancer therapy', *Angew Chem Int Ed Engl*, 53: 12320-64.

Tan, M. H., E. D. Holyoke, and M. H. Goldrosen. 1976. 'Murine Colon Adenocarcinomas: Methods for Selective Culture In Vitro2', *JNCI: Journal of the National Cancer Institute*, 56: 871-73.

Tan, W., C. Zhang, J. Liu, and Q. Miao. 2019. 'Regulatory T-cells promote pulmonary repair by modulating T helper cell immune responses in lipopolysaccharide-induced acute respiratory distress syndrome', *Immunology*, 157: 151-62.

Terabe, M., and J. A. Berzofsky. 2008. 'The role of NKT cells in tumor immunity', *Adv Cancer Res*, 101: 277-348.

Toes, R. E., R. Offringa, R. J. Blom, C. J. Melief, and W. M. Kast. 1996. 'Peptide vaccination can lead to enhanced tumor growth through specific T-cell tolerance induction', *Proc Natl Acad Sci U S A*, 93: 7855-60.

Uruga, H., and M. Mino-Kenudson. 2021. 'Predictive biomarkers for response to immune checkpoint inhibitors in lung cancer: PD-L1 and beyond', *Virchows Arch*, 478: 31-44.

van der Leun, A. M., D. S. Thommen, and T. N. Schumacher. 2020. 'CD8(+) T cell states in human cancer: insights from single-cell analysis', *Nat Rev Cancer*, 20: 218-32.

Veldhoen, M., R. J. Hocking, C. J. Atkins, R. M. Locksley, and B. Stockinger. 2006. 'TGFbeta in the context of an inflammatory cytokine milieu supports de novo differentiation of IL-17-producing T cells', *Immunity*, 24: 179-89.

Vivier, E., D. H. Raulet, A. Moretta, M. A. Caligiuri, L. Zitvogel, L. L. Lanier, W. M. Yokoyama, and S. Ugolini. 2011. 'Innate or adaptive immunity? The example of natural killer cells', *Science*, 331: 44-9.

Vogt, S., and J. Mattner. 2021. 'NKT Cells Contribute to the Control of Microbial Infections', *Front Cell Infect Microbiol*, 11: 718350.

Wagner, H., and S. Bauer. 2006. 'All is not Toll: new pathways in DNA recognition', *J Exp Med*, 203: 265-8.

Walker, Lucy S. K. 2022. 'The link between circulating follicular helper T cells and autoimmunity', *Nature Reviews Immunology*, 22: 567-75.

Wang, J., Y. Li, and G. Nie. 2021. 'Multifunctional biomolecule nanostructures for cancer therapy', *Nat Rev Mater*, 6: 766-83.

Wculek, S. K., F. J. Cueto, A. M. Mujal, I. Melero, M. F. Krummel, and D. Sancho. 2020. 'Dendritic cells in cancer immunology and immunotherapy', *Nat Rev Immunol*, 20: 7-24.

Weisheit, C. K., D. R. Engel, and C. Kurts. 2015. 'Dendritic Cells and Macrophages: Sentinels in the Kidney', *Clin J Am Soc Nephrol*, 10: 1841-51.

Whiteside, T. L. 2008. 'The tumor microenvironment and its role in promoting tumor growth', *Oncogene*, 27: 5904-12.

Wilson, J. T., S. Keller, M. J. Manganiello, C. Cheng, C. C. Lee, C. Opara, A. Convertine, and P. S. Stayton. 2013. 'pH-Responsive nanoparticle vaccines for dual-delivery of antigens and immunostimulatory oligonucleotides', *ACS Nano*, 7: 3912-25.

Wolf, Natalie K., Djem U. Kissiov, and David H. Raulet. 2023. 'Roles of natural killer cells in immunity to cancer, and applications to immunotherapy', *Nature Reviews Immunology*, 23: 90-105.

Wu, Xiangyu, Tianhang Li, Rui Jiang, Xin Yang, Hongqian Guo, and Rong Yang. 2023. 'Targeting MHC-I molecules for cancer: function, mechanism, and therapeutic prospects', *Molecular Cancer*, 22: 194.

Xiao, S., D. Qin, X. Hou, L. Tian, Y. Yu, R. Zhang, H. Lyu, D. Guo, X. Z. Chen, C. Zhou, and J. Tang. 2023. 'Cellular senescence: a double-edged sword in cancer therapy', *Front Oncol*, 13: 1189015.

Xing, Y., and K. A. Hogquist. 2012. 'T-cell tolerance: central and peripheral', *Cold Spring Harb Perspect Biol*, 4.

Yokoyama, W. M. 2005. 'Natural killer cell immune responses', *Immunol Res*, 32: 317-25.

Yuen, G. J., E. Demissie, and S. Pillai. 2016. 'B lymphocytes and cancer: a love-hate relationship', *Trends Cancer*, 2: 747-57.

Zahavi, D., and L. Weiner. 2020. 'Monoclonal Antibodies in Cancer Therapy', *Antibodies (Basel)*, 9.

Zhao, Y., J. Deng, S. Rao, S. Guo, J. Shen, F. Du, X. Wu, Y. Chen, M. Li, M. Chen, X. Li, W. Li, L. Gu, Y. Sun, Z. Zhang, Q. Wen, Z. Xiao, and J. Li. 2022. 'Tumor Infiltrating Lymphocyte (TIL) Therapy for Solid Tumor Treatment: Progressions and Challenges', *Cancers (Basel)*, 14.

Zhu, J., H. Yamane, and W. E. Paul. 2010. 'Differentiation of effector CD4 T cell populations (*)', *Annu Rev Immunol*, 28: 445-89.

Zinkernagel, R. M., and P. C. Doherty. 1997. 'The discovery of MHC restriction', *Immunol Today*, 18: 14-7.

8. Curriculum vitae

Publications

1. Stickdorn, Judith, **Lara Stein**, Danielle Arnold-Schild, Jennifer Hahlbrock, Carolina Medina-Montano, Joschka Bartneck, Tanja Ziß, Evelyn Montermann, Cinja Kappel, Dominika Hobernik, Maximilian Haist, Hajime Yurugi, Marco Raabe, Andreas Best, Krishnaraj Rajalingam, Markus P. Radsak, Sunil A. David, Kaloian Koynov, Matthias Bros, Stephan Grabbe, Hansjörg Schild, and Lutz Nuhn. **2022**. 'Systemically Administered TLR7/8 Agonist and Antigen-Conjugated Nanogels Govern Immune Responses against Tumors', *ACS Nano*, 16: 4426-43. DOI: 10.1021/acsnano.1c10709
2. Trzeciak, Emily R., Niklas Zimmer, Isabelle Gehringer, **Lara Stein**, Barbara Graefen, Jonathan Schupp, Achim Stephan, Stephan Rietz, Michael Prantner, and Andrea Tuettenberg. **2022**. 'Oxidative Stress Differentially Influences the Survival and Metabolism of Cells in the Melanoma Microenvironment', *Cells*, 11: 930. DOI: 10.3390/cells11060930
3. Bartneck, J., A. K. Hartmann, **L. Stein**, D. Arnold-Schild, M. Klein, M. Stassen, F. Marini, J. Pielenhofer, S. L. Meiser, P. Langguth, M. Mack, S. Muth, H. C. Probst, H. Schild, and M. P. Radsak. **2023**. 'Tumor-infiltrating CCR2(+) inflammatory monocytes counteract specific immunotherapy', *Frontiers in immunology*, 14: 1267866.
4. Stickdorn, J., C. Czysch, C. Medina-Montano, **L. Stein**, L. Xu, M. Scherger, H. Schild, S. Grabbe, and L. Nuhn. **2023**. 'Peptide-Decorated Degradable Polycarbonate Nanogels for Eliciting Antigen-Specific Immune Responses', *Int J Mol Sci*, 24.

9. Acknowledgements / Danksagung

Am Ende danke ich euch allen. Ihr ward ein Teil dieser Reise und ich bin jedem Einzelnen sehr dankbar für die Unterstützung.

10. Eidesstattliche Versicherung

Ich, Lara Stein, geboren am 21.05.1994 in Neunkirchen (Saar), erkläre hiermit, dass ich die vorliegende Arbeit selbstständig verfasst und dabei keine anderen als die von mir angegebenen Hilfsmittel benutzt habe. Sämtliche Stellen der Arbeit, die im Wortlaut oder dem Sinn nach aus Publikationen oder Vorträgen anderer Autoren entnommen sind, habe ich als solche gekennzeichnet. Außerdem versichere ich, dass die Arbeit bisher weder gesamt, noch in Teilen einer andern Prüfungsbehörde vorgelegt wurde.

Mainz, den 17.05.2024

11. Underlying Publication

ACSNANO

www.acsnano.org

ARTICLE

Systemically Administered TLR7/8 Agonist and Antigen-Conjugated Nanogels Govern Immune Responses against Tumors

Judith Stickdorn,[‡] Lara Stein,[‡] Danielle Arnold-Schild, Jennifer Hahlbrock, Carolina Medina-Montano, Joschka Bartneck, Tanja Ziß, Evelyn Montermann, Cinja Kappel, Dominika Hobernik, Maximilian Haist, Hajime Yurugi, Marco Raabe, Andreas Best, Krishnaraj Rajalingam, Markus P. Radsak, Sunil A. David, Kaloian Koynov, Matthias Bros, Stephan Grabbe,* Hansjörg Schild,* and Lutz Nuhn*

Cite This: *ACS Nano* 2022, 16, 4426–4443

Read Online

ACCESS | Metrics & More | Article Recommendations | Supporting Information

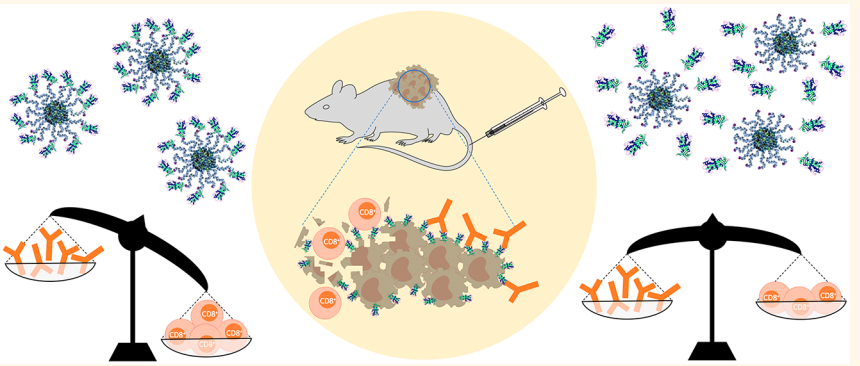

ABSTRACT: **The generation of specific humoral and cellular immune responses plays a pivotal role in the development of effective vaccines against tumors. Especially the presence of antigen-specific, cytotoxic T cells influences the outcome of therapeutic cancer vaccinations. Different strategies, ranging from delivering antigen-encoding mRNAs to peptides or full antigens, are accessible but often suffer from insufficient immunogenicity and require immune-boosting adjuvants as well as carrier platforms to ensure stability and adequate retention. Here, we introduce a pH-responsive nanogel platform as a two-component antitumor vaccine that is safe for intravenous application and elicits robust immune responses *in vitro* and *in vivo*. The underlying chemical design allows for straightforward covalent attachment of a model antigen (ovalbumin) and an immune adjuvant (imidazoquinoline-type TLR7/8 agonist) onto the same nanocarrier system. In addition to eliciting antigen-specific T and B cell responses that outperform mixtures of individual components, our two-component nanovaccine leads in prophylactic and therapeutic studies to an antigen-specific growth reduction of different tumors expressing ovalbumin intracellularly or on their surface. Regarding the versatile opportunities for functionalization, our nanogels are promising for the development of highly customized and potent nanovaccines.**

KEYWORDS: *nanogel, vaccine, immunotherapy, block copolymer, TLR agonist, polymer protein conjugate*

Endeavors in cancer immunotherapy seek to exploit the inherent capacity of immune cells to recognize and neutralize tumor cells. The individual background of each tumor as well as the diversity of each patients' immune status necessitates the development of personalized antitumor vaccines.[1] Research accomplishments of the last decades unveiled the role of immune evasion and checkpoint inhibition in tumorigenesis and drew attention to various immune cells as crucial targets in cancer immunotherapy.[2] To elicit a robust and persistent immune response, vaccines need to trigger an interlude of innate and adaptive immune events both cellularly

Received: December 2, 2021
Accepted: January 27, 2022
Published: February 1, 2022

https://doi.org/10.1021/acsnano.1c10709
ACS Nano 2022, 16, 4426–4443

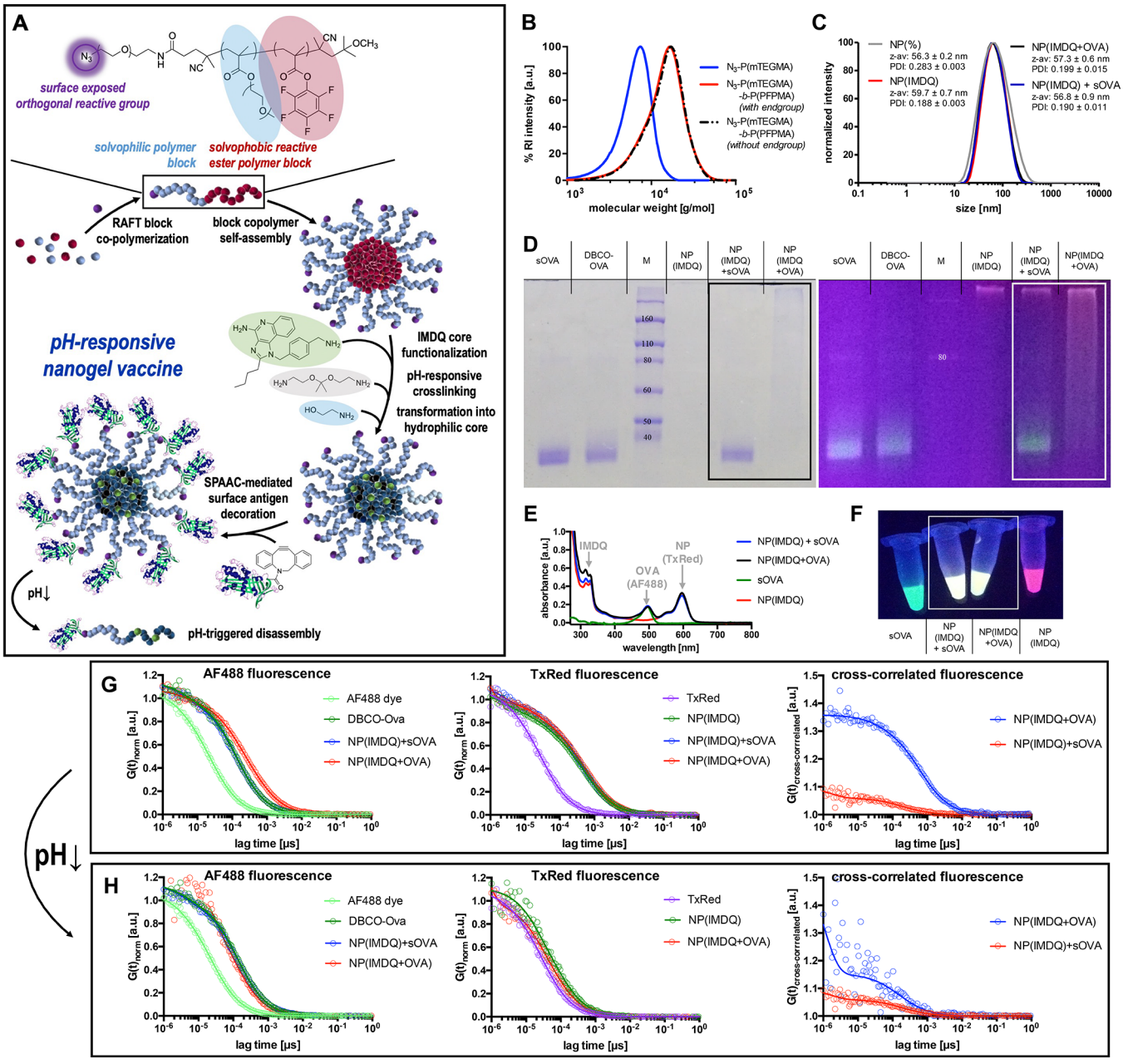

Figure 1. Characterization of TLR7/8-agonist- and protein conjugated nanogels for precise co-delivery of adjuvant and antigen during i.v. antitumor vaccination. (A) Synthetic design concept based on double reactive precursor block copolymers that self-assemble into block copolymer micelles with amine-reactive cores and a SPAAC-reactive corona. *Via* aminolysis of the pentafluorophenyl esters, the cores are covalently functionalized with the TLR 7/8 agonist IMDQ and Texas Red cadaverine and then sequentially cross-linked and transformed into pH-responsive nanogels. The corona is modified *via* click ligation of the surface-exposed azides to DBCO-modified (and Alexa Fluor 488-labeled) OVA as model antigen. (B) SEC chromatography of the RAFT-derived reactive homo and block copolymer (before and after removal of the dithiobenzoate end group). (C) DLS intensity size distribution plots of the resulting nanogels (with and without covalent IMDQ loading), mixed or covalently modified with OVA. (D) SDS-PAGE of modified OVA (labeled with Alexa Fluor 488) mixed or covalently conjugated to IMDQ-loaded nanogels (labeled with Texas Red) (left, Coomassie staining; right, UV excitation of the fluorescent dyes (red, Texas Red-labeled nanogel; green, Alex Fluor 488-labeled OVA). (E) UV−vis spectrum of the fluorescently labeled samples and (F) corresponding image of the samples upon excitation by a UV lamp. (G) FCS correlograms derived from Alexa Fluor 488 and Texas Red fluorescence, as well as their cross-correlated correlogram indicating successful OVA conjugation to the nanogel. (H) FCS correlograms and corresponding cross-correlated correlogram upon exposure to endosomal acidic pH conditions indicating successful particle degradation.

and humorally.[3] While the positive contributions of humoral antitumor responses and the function of B cells are currently still discussed,[4] the effective priming of cytotoxic $CD8^+$ T cells against tumor-specific antigens through MHC class I-restricted presentation of antigenic peptides on dendritic cells (DCs), so-called cross-priming,[5] is of particular importance since the existence of $CD8^+$ T cells in the tumor microenvironment can be correlated to improved tumor outcome and patient survival.[6−9] Recent attempts succeeded by applying antigen encoding mRNAs,[10−12] however, depending on efficient translation and potent presentation through antigen-presenting cells (APCs).[13,14] Alternatively, peptide- or protein-based

https://doi.org/10.1021/acsnano.1c10709
ACS Nano 2022, 16, 4426−4443

anticancer vaccine strategies have been explored even longer.[15,16] Unfortunately, they mostly suffer from insufficient immune activation with risk of tolerance[17,18] and tumor relapse.[19] Consequently, the development of improved carrier systems and the investigation of potent immune modulators such as Toll-like receptor (TLR) agonists as new vaccine adjuvants are addressed to boost vaccination outcome.[20,21]

Small-molecule imidazoquinoline-based TLR7/8 agonists are promising adjuvant candidates efficiently activating a broad spectrum of APCs, including different types of DCs.[22] Moreover, they have been demonstrated to trigger high levels of cytokines like TNF-α, INF-γ, IL-6, IL-12, and type I interferon, resulting in Th1-mediated immune responses[23] and cytotoxic T cells that act against intracellular pathogens or cancer cells.[24] Nevertheless, clinical use of those small-molecule adjuvants is hampered based on their pharmacokinetic profile causing severe systemic inflammation.[25−27] Covalent conjugation of TLR7/8 agonists to polymer scaffolds, however, has been shown to amend their safety profile and hinder fast clearance.[28]

The delivery of not only small-molecule adjuvants but also antigenic components including proteins or peptides provides several advantages when combined with polymer-based platforms.[29] In addition to prolonged circulation and improved pharmacokinetics, nanoparticular systems benefit from accumulation in lymphatic organs and uptake in immune cells based on their morphological and compositional similarities to pathogens.[28,30,31] If designed properly, they enable co-delivery of adjuvant and antigen to the same DC or other APCs and, thus, foster essential priming of $CD8^+$ T cells.[32,33] Carrier designs range from peptide- or lipid- to synthetic polymer-based systems including self-assembling micelles as well as core-cross-linked structures, which either physically encapsulate or covalently bind the desired cargo.[34−38] Incorporation of pH-responsive units that trigger disintegration after endosomal uptake seem to enhance antigen presentation and improve priming of $CD8^+$ T cells,[35] in addition to prevent undesired long-term accumulation.[39] Several studies emphasize that not only co-delivery of adjuvant and antigen to APCs plays a pivotal role in the effectiveness of a vaccine, but also the application of the nanocarrier itself already benefits its efficacy when compared to co-administration of the mixed components without a nanocarrier.[34,36,40]

One straightforward method to obtain amphiphilic, self-assembling polymers for nanocarrier syntheses is the reversible addition−fragmentation chain transfer (RAFT)-polymerization.[41] RAFT procedures allow the adjustable fabrication of copolymers regarding posterior nanoparticle size and tolerate the introduction of a great variety of functionalities.[42] While a tailored design of applied chain-transfer agents (CTAs) enables corona modifications, the introduction of reactive monomers allows core-functionalization in post-polymerization reactions.[43−47] We have combined RAFT-derived hetero-telechelic block copolymers with a post-polymerization modification approach[46] to generate core-cross-linked nanogels[48] and recently demonstrated that covalent nanogel conjugation with the TLR7/8 agonist 1-(4-(aminomethyl)-benzyl)-2-butyl-1*H*-imidazo[4,5-*c*]quinolin-4-amine (IMDQ) leads to localized immune activation after subcutaneous (s.c.) injection with safe antiviral and antitumor immune responses.[30,45,49]

In this study, we report on the evolution of this pH-responsive nanogel platform toward a multi-component antitumor vaccine that is even safe for intravenous (i.v.) administration and facilitates co-delivery of TLR7/8 agonist IMDQ and ovalbumin (OVA) as model antigen for improved generation of $CD8^+$ T cells *in vitro*. While the nanogel platform itself is immunologically silent, the nanoparticular co-delivery of IMDQ and OVA induces robust immune responses *in vitro* that outperform soluble mixtures of components. Prophylactic and therapeutic immunization against OVA-expressing tumors revealed the efficacy and specificity of this multi-component vaccine *in vivo*. Based on its chemical design, the herein described nanogel platform allows versatile adjustments regarding the introduced small molecules and attached antigens without morphological changes of the carrier and, therefore, might be an interesting candidate even for personalized anticancer immunotherapies.

RESULTS AND DISCUSSION

Core and Surface Modification of pH-Degradable Nanogel Platform for Dual Delivery of TLR7/8 Agonist and OVA Antigen. To realize quantifiable co-delivery of antigen and immune stimulant *via* a precise nanoscale carrier, we applied a tunable nanogel platform based on amphiphilic reactive precursor block copolymers that enable both core and corona functionalization *via* post-polymerization modifications. Through covalent conjugations, these nanogels ensure co-delivery of the attached TLR7/8 agonist and OVA as model protein antigen to immune cells both *in vitro* and *in vivo* (Figure 1A).

The underlying block copolymer is accessible through RAFT block copolymerization of methoxy tri(ethylene glycol) methacrylate (mTEGMA) and pentafluorophenyl methacrylate (PFPMA).[47,50] While the hydrophilic P(mTEGMA) block provides micellar stability and shielding properties, the solvophobic P(PFPMA)-block drives self-assembly to micelles in polar-aprotic solvents like DMSO and facilitates posterior core functionalization of the nanosized precursors by aminolysis of the reactive esters.[51] When applying the azide-functionalized chain-transfer agent 1-azido-16-cyano-13-oxo-3,6,9-trioxa-12-azaheptadecan-16-yl benzodithioate (azide-CTA) during the RAFT polymerization process,[50] click-reactive functionalities are installed on the surface of the resulting nanogels allowing for orthogonal surface-modifications through strain-promoted azide−alkyne cycloaddition (SPAAC)[52] with dibenzyl cyclooctyne (DBCO)-modified counterparts (Figure 1A).

RAFT block copolymerization of mTEGMA and PFPMA using the low-temperature initiator 2,2′-azobis(4-methoxy-2,4-dimethylvaleronitrile (AMDVN) afforded monodisperse block copolymers with a moderate PDI of 1.3 and a number-average molecular weight of around 12 kDa after removal of the dithiobenzoate end groups (Figure 1B; for detailed characterization of $P(mTEGMA)_{25}$ and block copolymer $P(mTEGMA)_{25}$-*b*-$P(PFPMA)_{34}$ compare Figures S1−S10). Formation of reactive precursor micelles after block copolymer self-assembly in DMSO was assessed by dynamic light scattering (DLS) (Figure S12). Subsequent covalent attachment of IMDQ as well as fluorescent labeling with Texas Red dye was achieved through aminolysis of the reactive esters inside the core (Figure 1A). Integrity of the P(mTEGMA) segment during aminolysis of PFP esters was confirmed by ^{1}H NMR measurements (Figure S10) in addition to a detailed characterization of the sequential aminolysis of PFP esters by ^{19}F NMR monitoring (Figure S9). Further core-cross-linking

https://doi.org/10.1021/acsnano.1c10709
ACS Nano 2022, 16, 4426−4443

with the acid-sensitive cross-linker 2,2-bis(aminoethoxy)-propane and conversion of the remaining PFP esters into fully hydrophilic moieties by 2-aminoethanol yielded the hydrophilic, pH-labile IMDQ-loaded nanogels that could be purified by dialysis and stored as dry powder after lyophilization. The introduction of the ketal-based cross-linker locks in the nanogels' morphology and size but at the same time assures disassembly of nanogels into single polymer chains after endosomal uptake.[53] Particle formation of IMDQ-loaded nanogels as well as their degradation behavior upon an acidic stimulus and long-term stability under physiological conditions were analyzed by DLS and FCS (Figures S13–S15). IMDQ-loading of redispersed nanogels was quantified *via* UV–vis spectroscopy as 9.5 wt% (Figure S11).

In a subsequent experiment, we verified the accessibility of the RAFT CTA-derived, surface-exposed azide groups for SPAAC conjugation. For this purpose, IMDQ-loaded nanogels were incubated with cyclooctyne-modified Oregon Green dye. UV–vis measurements after removal of unbound dye confirmed covalent attachment of the Oregon Green dye and, hence, preserved accessibility of azide-groups for covalent conjugation (Figure S16; a negative control sample of unmodified Oregon Green showed almost complete dye removal). Based on these results, we proceeded with the generation of the envisaged two-component antitumor vaccine composed of IMDQ-nanogels and surface attached model antigen.

Especially for i.v. administration, adjuvants and antigens should be combined into the same carrier system to guarantee co-delivery to the same immune cell subpopulations.[54] Prior to conjugation of the model antigen OVA to the nanogels, the protein's lysine-derived amino side chains were exploited through NHS ester chemistry for modification with a SPAAC-reactive DBCO-PEG_4 linker and an Alexa Fluor 488 label for monitoring (note that OVA is equipped with 20 potential lysine modification sites, and on average one Alexa Fluor 488 and five DBCO-PEG_4 linkers were attached according to UV–vis spectroscopy; Figure S17). DBCO modification did not alter the integrity or stability of the protein (Figure S18), and it was also well accessible for azide-terminated polymers for conjugation reactions (Figure S19). Interestingly, although one of the modification sites is localized in the $CD8^+$ T cell epitope region (compare Supporting Information), DBCO modification did not alter the protein's antigenicity (Figure S20).

Consequently, covalent conjugation of OVA to the azide-surface exposed nanogels could be performed by simply mixing both components dissolved in PBS, resulting in a protein to azide molar ratio of 1:20. Note that mixing the individually labeled compounds (Texas Red-labeled nanogel and the Alexa Fluor 488-labeled proteins) provided a yellow fluorescent sample (Figure 1E,F and Figure S21) from which successful conjugation could be validated macroscopically by sodium dodecyl sulfate–polyacrylamide gel electrophoresis (SDS-PAGE) (Figure 1D). Soluble ovalbumin (sOVA) as well as DBCO-modified ovalbumin (DBCO-OVA) showed distinct bands after UV excitation as well as after Coomassie staining. The disappearance of unbound DBCO-OVA after SPAAC reaction (NP(IMDQ+OVA)) indicated complete conjugation of DBCO-OVA to azide nanogels NP(IMDQ), while the mixture of sOVA and NP(IMDQ) did not lead to any ligation of sOVA (Figure 1D). In-depth characterization of various protein to azide molar ratios revealed no cross-linking between particles and confirmed the necessity of the excess azide (Figure S24). Further conjugate characterization by DLS revealed monodisperse nanogel formation with sizes around 58 nm that were independent of IMDQ and OVA loading (Figure 1C). Zeta potential measurements revealed a slight decrease in surface charge after conjugation of ovalbumin from −4 to −9.5 mV (Figure S23). Moreover, OVA-bearing particles still showed an acidic degradation profile upon exposure to endosomal pH (Figure S22).

In agreement with the gel electrophoresis experiment, subsequent fluorescence correlation spectroscopy (FCS) measurements[55] were performed to affirm covalent conjugation of IMDQ-loaded nanogels and DBCO-OVA on a molecular level (Figure 1G). The selection of fluorescent dyes allowed to monitor independently from each other the autocorrelation of the Texas Red-labeled NP(IMDQ) as well as the Alexa Fluor 488-labeled OVA (Figure 1E and Figure S18). Based on this setup, we found for the Alexa Fluor 488-derived OVA autocorrelation a quantitative shift to higher lag times which corresponds to larger species after SPAAC reaction, demonstrating covalent association of OVA to the nanogels (Figure 1G). This shift was independent from IMDQ-loading (compare to FCS measurement of nanogels without IMDQ, Figure S25). *Via* Texas Red-derived nanogel autocorrelation, also a slight increase in size was found (Figure 1G and Figure S26), indicating successful OVA conjugation. In addition, simultaneous analysis of both channels *via* fluorescent cross-correlation spectroscopy (FCCS) revealed an exclusive cross-correlation for NP(IMDQ+OVA) in comparison to the mixture of NP(IMDQ) and sOVA, thus manifesting dual-loading of nanogels also on a molecular level (Figure 1G and Figure S27). Upon acidification, the previously observed cross-correlation dropped and almost disappeared (Figure 1H), reflecting the pH-responsiveness of the nanogels and their disintegration into many non-cross-correlating single polymer chains, as observed also by the Texas Red-derived autocorrelation of NP(IMDQ) before (Figure 1H). Similar results were found again for empty nanogels without IMDQ NP(−) and are summarized in the Supporting Information (Figures S25–S27). Moreover, detailed calculation of the hydrodynamic radii derived from the resulting autocorrelation functions confirmed both conjugation of DBCO-modified OVA to the nanogel as well as degradation of IMDQ-loaded nanogels upon acidification (compare Tables S1 and S2 in the Supporting Information). Summarizing, the underlying chemical design allows for a well-defined and also reproducible fabrication process (compare Figure S28) toward precise co-delivery of immune stimulant and immunogenic part within one nanogel carrier system that is pre-defined in morphology and guarantees control over the co-delivery of each vaccine component.

IMDQ-Loaded, OVA-Decorated Nanogels Enable Co-delivery and Lead to Activation and Maturation of Immune Cells through TLR7/8-Dependent Signaling. After successful conjugation of IMDQ and OVA to the pH-responsive nanogels, we wanted to evaluate the system's co-delivering capacity and initiation of immune responses by its interaction with immune cells. While it has already been demonstrated that IMDQ-loaded nanogels outperform IMDQ-loaded polymer chains regarding TLR activation *in vivo*,[45] we first sought to investigate the influence of OVA co-administration, either covalently attached to the nanogel surface or solely admixed, on a TLR reporter cell line (Figure 2). Engineered RAW-Blue macrophages allow for a broad

https://doi.org/10.1021/acsnano.1c10709
ACS Nano 2022, 16, 4426–4443

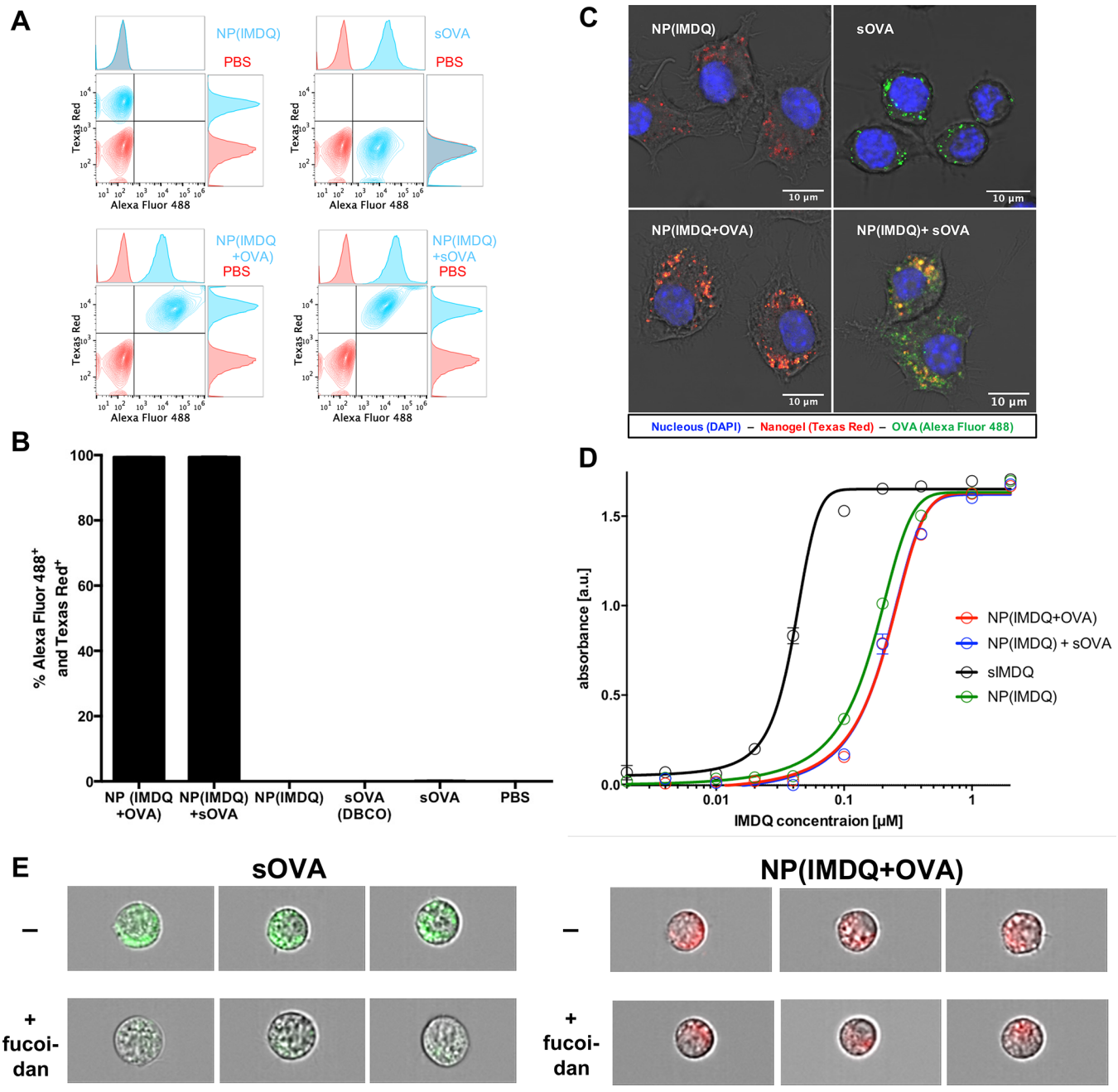

Figure 2. Nanogel-mediated co-delivery and immune cell stimulation by TLR7/8-agonist IMDQ and model protein antigen OVA in an immune reporter cell line. (A) Flow cytometric plots, (B) corresponding percentage of particle and antigen positive RAW-Blue macrophages, and (C) fluorescent confocal microscopy images after incubation with the respective nanogel conjugates and single compounds. (D) TLR agonistic activity measured by NF-kB activation *via* the RAW-Blue reporter assay. (E) Fluorescence imaging of DCs that have internalized soluble OVA (green) (left) or NP(IMDQ+OVA) nanogels. In the presence of the scavenger receptor inhibitor fucoidan (300 μg/mL) the uptake of sOVA is inhibited, but the nanogel sample is still internalized (for quantification, compare Figures S45 and S46).

screening of TLR activity and were, therefore, selected. *Via* MTT assay, no influence on the cells' viability was found in the relevant concentration range (Figure S29). By flow cytometry and fluorescent confocal microscopy experiments, RAW macrophages could be characterized to concomitantly internalize nanogels and co-delivered OVA. For that purpose, cells were incubated for 16 h with nanogel and OVA samples. We found that both nanogels and OVA were taken up independently from each other (Figure 2A and Figure S31). Interestingly, both co-delivery of covalently attached or co-administered soluble sOVA provided almost 100% Alexa Fluor 488 and Texas Red positive cells (Figure 2B). Additionally, by confocal microscopy both nanogel and OVA-derived fluorescence could be found internalized by cells (Figure 2C and Figure S32). While for the mixture of NP(IMDQ) and sOVA separate and co-localized fluorescent signals could be found for each species inside the cells, only the NP(IMDQ+OVA) sample with covalently attached OVA provided co-localization of both components inside same compartments. This could also be further confirmed on other antigen-presenting cell

https://doi.org/10.1021/acsnano.1c10709
ACS Nano 2022, 16, 4426–4443

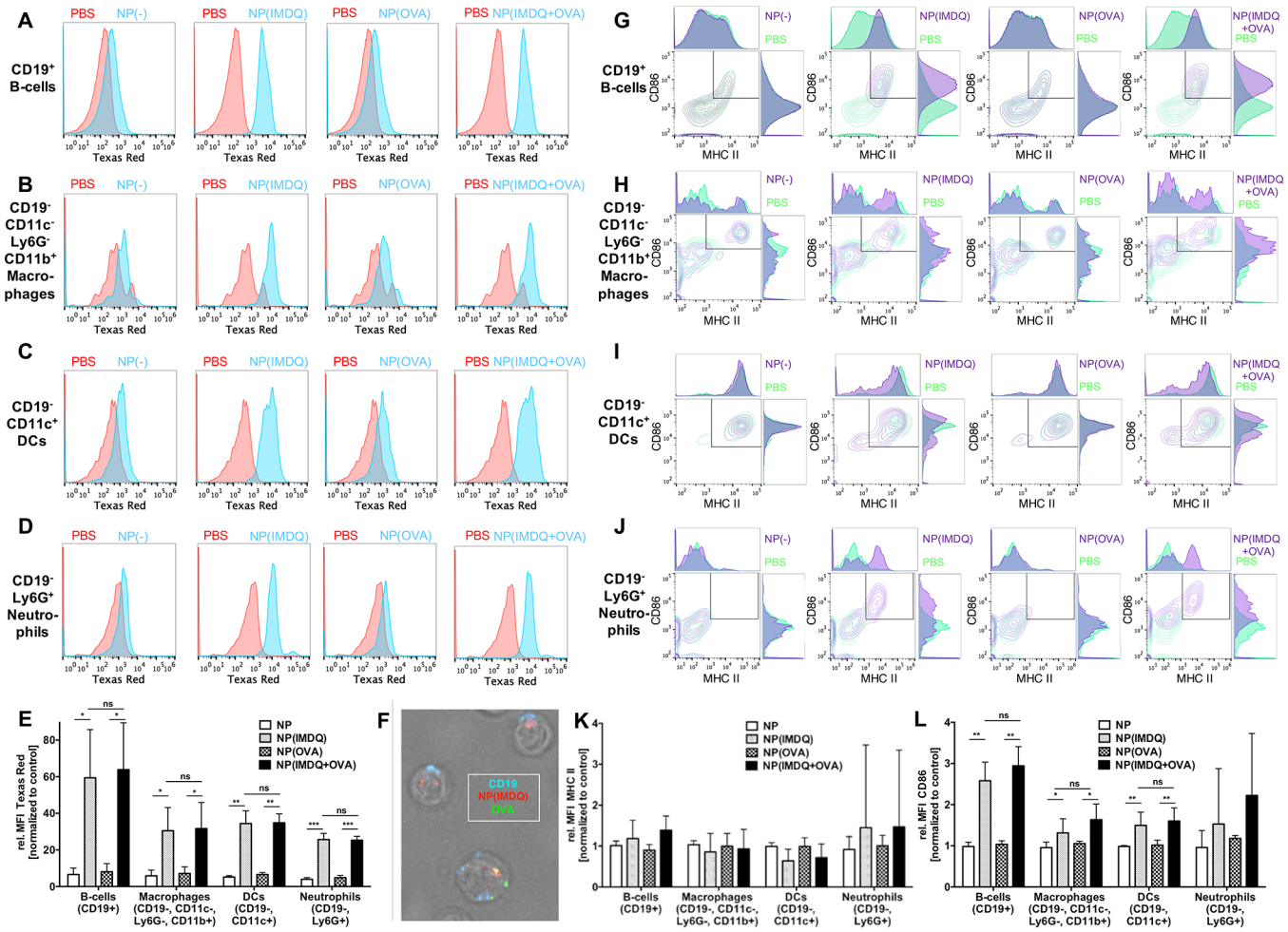

Figure 3. Nanogel-mediated co-delivery and immune cell stimulation by TLR7/8-agonist IMDQ and model protein antigen OVA in primary heterogeneous immune cells. Flow cytometric histograms of particle uptake in B cells (A), macrophages (B), DCs (C), and neutrophils (D) obtained from incubating spleen cells *ex vivo* with the respective nanogel conjugates. (E) Summary of particle-derived relative mean fluorescence intensity (MFI, normalized to PBS as control) of respective immune cells. (F) Fluorescent microscopy image of spleen cells identified as B cells (by CD19 expression, blue) which have internalized both NP(IMDQ) (red) and OVA (green) after incubation of total spleen cells *ex vivo* with NP(IMDQ+OVA). Flow cytometric plots of maturation status by CD86 and MHC-II expression of B cells (G), macrophages (H), DCs (I), and neutrophils (J) after incubating spleen cells with the respective nanogel conjugates. Summary of (K) MHC-II- and (L) CD86-derived relative mean fluorescence intensity (MFI, normalized to PBS as control). Due to immune cell preparation, CD86 serves as appropriate maturation marker for the respective immune cells after incubation with respective nanogel conjugates.

lines, *e.g.*, on DC2.4 (compare Figure S33). By flow cytometric analysis applying the ImageStream technology, overlays of OVA-derived fluorescence with bright field imaging confirmed again an intracellular localization of the antigen both in its soluble or particle-bound version (Figure S44). We additionally compared the uptake of sOVA (Alexa Fluor 488-labeled) with the NP(IMDQ+OVA) nanogel conjugate (Cy5-labeled) in the presence of fucoidan, a potent scavenger receptor inhibitor.[56] In Figure 2E (as well as in Figure S45) scavenger receptor inhibition caused a reduction of internalization for the sOVA, while for the nanogel sample NP(IMDQ+OVA) particles could still get internalized independent from the scavenger receptor (Figure S46). Note that scavenger receptors are usually associated with phagocytosis of bacterial pathogens and other extracellular antigens.[57] They further afford an intracellular processing leading to more MHC-II antigen presentation than MHC-I presentation. This would favor $CD4^+$ T cell responses at the expense of cytotoxic $CD8^+$ T cell immune responses.[58] Circumventing this intracellular processing by using the nanogel-bound version seems to be more attractive in order to enhance cross-presentation and generate a higher amount of antigen-specific $CD8^+$ T cells (see Figure 4). These observations underline again that the dual functionalized carriers guarantee successful co-delivery of both antigen and adjuvant into the same immune cell simultaneously.

Moreover, the co-delivered IMDQ is able to stimulate TLR receptor for an effective maturation of the APCs that are required for the induction of cellular and humoral immune responses. This could be monitored by RAW-Blue macrophages *via* secretion of the embryonic alkaline phosphatase (SEAP) in the cell culture supernatant caused by the NF-kB signaling. Compared to non-conjugated IMDQ, nanoparticular conjugated agonist led to a slightly reduced but still highly potent TLR activation in the sub-micromolar regime (Figure 2D). Similarly, OVA-decorated IMDQ nanogels also induced significant TLR activation comparable to IMDQ-loaded nanogels without OVA loading. Hence, OVA loading did not interfere with the TLR agonist−receptor interaction.

https://doi.org/10.1021/acsnano.1c10709
ACS Nano 2022, 16, 4426−4443

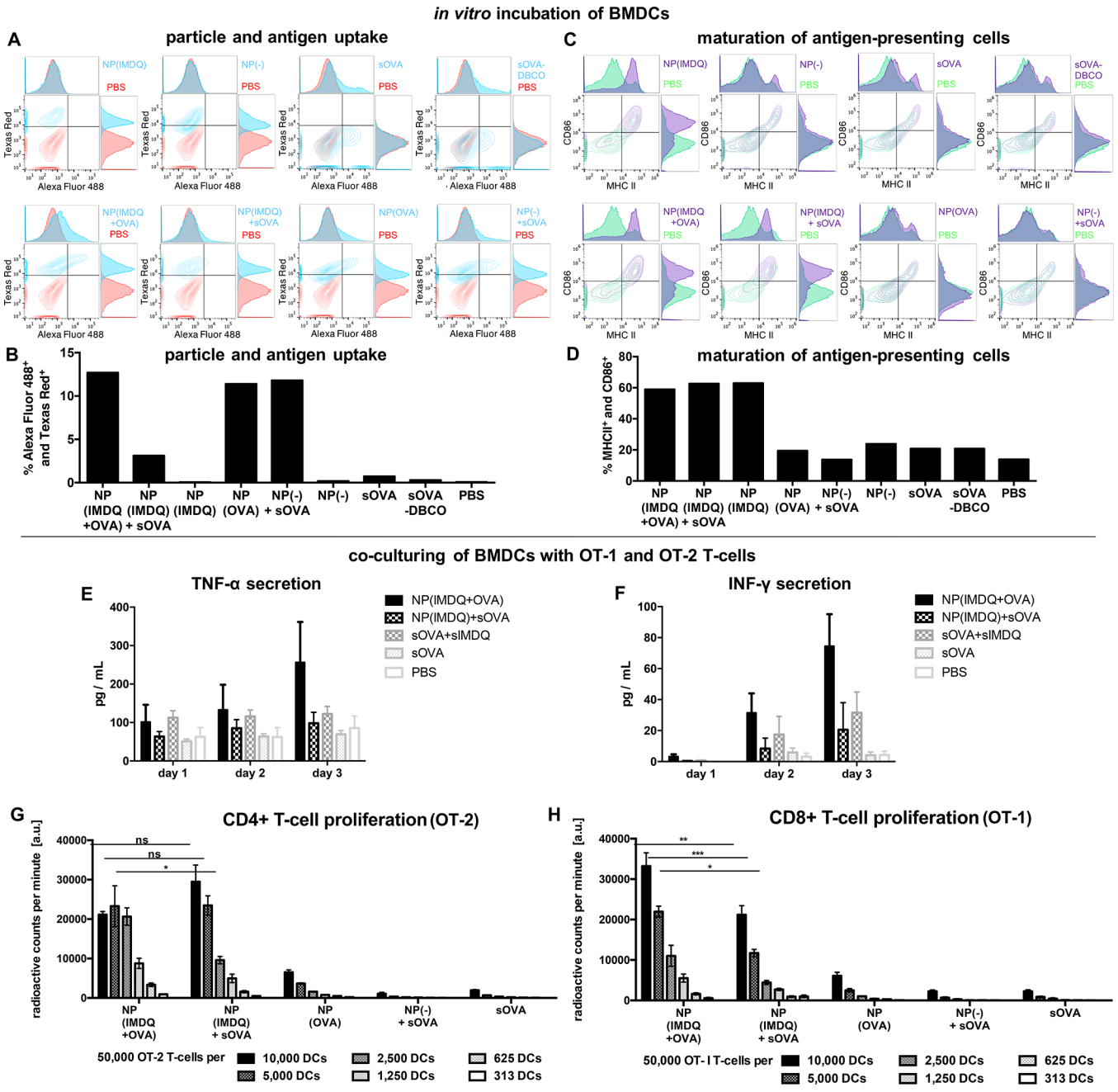

Figure 4. Nanogel-mediated co-delivery of antigen and adjuvant triggers maturation of primary dendritic cells and T cell proliferation *in vitro*. (A) Flow cytometric histogram and (B) percentage of both particle and antigen positive BMDCs after incubation with the respective nanogel conjugates and single compounds. (C) Flow cytometric histogram and (D) percentage of CD86 and MHC-II positive BMDCs after incubation with the respective nanogel conjugates. After co-culturing of nanogel-pulsed BMDCs with OVA-specific T cells secreted cytokines tumor necrosis factor TNF-α (E) and interferon INF-γ (F) were determined from the cell culture supernatant. OVA-specific T cell proliferation was determined at different ratio BMDC to T cell ratios with (G) OT-2 T cells for $CD4^+$ T cell proliferation and (H) OT-1 T cells for $CD8^+$ T cell proliferation. For the latter, covalently attached OVA seems to favor the secretion of pro-inflammatory cytokines and the induction of a $CD8^+$ T cell immune response pathway.

To assess the interaction of the nanogels with immune cells that are more relevant for successful *in vivo* immunization, we next performed similar studies using primary APCs *in vitro*. For that purpose, we selected murine splenocytes as heterogeneous primary immune cell population and incubated them with our nanogel samples (Figure 3), followed by flow cytometric analysis to identify each immune cell population (Figure S34). As visualized by the histogram plots in Figure 3A–D, a boosted nanogel uptake could generally be found when they were loaded with IMDQ in comparison to "empty" nanogels, independently from their additional OVA payload. A more in-depth evaluation of the involved immune cell subsets revealed that this is especially the case for B cells ($CD19^+$), but also macrophages ($CD19^-$, $CD11c^-$, $CD11b^+$, $Ly6G^-$), DCs ($CD11c^+$), and neutrophils ($Ly6G^+$) seem to follow this trend (Figure 3E). Interestingly, a pre-incubation of the nanogel samples with mouse serum prior to addition to spleen cells did not affect this uptake behavior (Figure S35). Besides,

https://doi.org/10.1021/acsnano.1c10709
ACS Nano 2022, 16, 4426–4443

also by fluorescent microscopy a preferential interaction with B cells could be observed, as both Texas Red-derived nanogel fluorescence and Alexa Fluor 488-derived OVA fluorescence were generally associated with $CD19^+$ B cells (Figure 3F and Figure S38). In fact, similar preferential association to B cells has also been found for IMDQ-loaded nanogels *in vivo* after s.c. injection and subsequent analysis of the draining lymph nodes before.[30]

We then also looked at maturation markers in the corresponding immune cell subpopulations by staining them for the expression of the co-stimulatory molecules CD86 and MHC-II, typical maturation markers for successful antigen presentation (Figure 3G–J). Particle-delivered IMDQ triggered the expression levels especially of CD86 in almost all analyzed APCs. MHC-II expression alone was already at relatively high basal levels in the negative control samples due to the applied splenic isolation conditions (Figure S37) and, thus, showed only a minor trend toward IMDQ-mediated maturation (Figure 3K). However, CD86 expression is much more sensitive and was exclusively stimulated by the nanogel-bound IMDQ in almost all immune cell populations (Figure 3L and Figure S36). Interestingly, B cells increased again most strikingly their maturation status. Taken into account their vigorous uptake of IMDQ- and OVA-loaded nanogels, these observations make them promising candidates for successful antigen presenting after i.v. applications, as nanogel pre-incubation with serum did also not alter this behavior either (Figures S36 and S37).

Two-Component Nanogel Platform Favors $CD8^+$ over $CD4^+$ T Cell Proliferation *In Vitro*. To further elucidate the downstream immune responses triggered by co-delivering antigen and adjuvant through our pH-degradable nanogel platform *in vitro*, we selected bone marrow-derived primary dendritic cells (BMDCs) and incubated them again for 16 h with the nanogel system (Figure 4). The previously observed simultaneous uptake of IMDQ-nanogels and OVA could again be confirmed. Interestingly, flow cytometry analysis revealed that for nanoparticle conjugated IMDQ the percentage of double positive cells (both particle/Texas Red and antigen/Alexa Fluor 488) was increased when OVA was covalently attached to the nanogels' surface. The amount of internalized sOVA is reduced when cells were already stimulated by NP(IMDQ) (Figure 4A,B and Figure S40). This is in agreement with other studies where maturation of APCs has been shown to reduce additional particle uptake capacities[59] and, thus, underlines the necessity of antigen and adjuvant co-delivery.

The cells' maturation profile could again be identified during flow cytometry analysis (Figure S41; for BMDCs, MHC-II expression is now also more reliable). Only for BMDCs pulsed with IMDQ-containing samples, both MHC-II and CD86 maturation markers were upregulated concurrently, while nanogels without TLR7/8 agonist did not trigger BMDC maturation independent of co-administration of OVA, demonstrating again that the nanogel system itself is immunogenically silent (Figure 4C,D).

Moreover, the BMDC maturation approach allowed us to further characterize *in vitro* antigen-specific $CD4^+$ and $CD8^+$ T cell immune responses, an assumed pre-requisite for successful induction of tumor immunity. Therefore, after stimulation with our IMDQ- and OVA-loaded nanogels overnight, BMDCs were then co-cultivated with dilutions of OVA-specific T cell receptor transgenic OT-1 and OT-2 T cells, isolated from the spleen of OT-1 or OT-2 mice, corresponding to the induction of OVA-specific $CD4^+$ (OT-2) and $CD8^+$ (OT-1) T cells. On the following days, cell culture supernatants were quantified for pro-inflammatory cytokines that support Th1-biased immune responses, and interestingly the nanogel conjugate of NP-(IMDQ+OVA) yielded highest secretion of tumor necrosis factor TNF-α and interferon INF-γ (Figure 4E,F). The T cell proliferation triggered by BMDC maturation and corresponding antigen presentation (either the $CD4^+$ epitope for OT-2 or the $CD8^+$ epitope for OT-1) could be measured radioactively *via* incorporation of ^{3}H-thymidine (Figures S42 and S43). Interestingly, the enhanced co-delivery and stimulation of our two-component nanogel vaccine had again a significant impact on the co-applied T cells. Only the combination of OVA with IMDQ-containing samples led to an increased proliferation of OT-1 and OT-2 cells, emphasizing the importance of co-administering antigen and adjuvant (Figure 4G,H).

Furthermore, covalent attachment of OVA to IMDQ-nanogels led to a significantly increased proliferation of OVA-specific OT-1/$CD8^+$ T cells compared to the mixture of sOVA and NP(IMDQ) (Figure 4H). For OT-2 cells ($CD4^+$ T cells), however, similar elevated proliferation levels were found for the covalent two-component system as well as the non-covalent mixture (Figure 4G). Consequently, our covalent NP(IMDQ+OVA) construct seems to boost OT-1/$CD8^+$ T cell proliferation significantly, probably by the increase in TNF-α and INF-γ secretion. This is in accordance with several previous reports demonstrating that a carrier-mediated co-delivery of OVA favors cross-presentation and the induction of $CD8^+$-governed immune responses.[60−62] Hence, under the applied *in vitro* settings our covalent nanogel platform which co-delivers antigen and adjuvant seems to amend the immune response in favor of $CD8^+$ T cell generation.

Two-Component Nanogel Platform Can Be Safely Applied Intravenously and Generates OVA-Specific Humoral and Cellular Immune Responses. Based on these promising *in vitro* results, we pursued *in vivo* applications for our nanovaccine. It is known that small-molecule TLR agonists are prone to cause systemic immune responses followed by systemic inflammation leading to severe side effects.[27] Conjugation of TLR7/8 agonists to polymeric carriers, however, has been shown to confine the subsequent immune response to draining lymph nodes after s.c. injection.[28,30] Interestingly, latest findings by Lynn and co-workers indicate that i.v. injection improves vaccine efficacy compared to s.c. immunization. Especially in case of a physical linkage between antigen and adjuvant affording nanosized particles, $CD8^+$ T cell responses were significantly higher after i.v. administration.[34] However, when applying carrier-bound TLR7/8 agonists into the bloodstream, their influence on hematologic toxicities should be monitored carefully in reflection to other reported systemic type I IFN responses.[63]

In this context, we injected our IMDQ-loaded nanogels i.v. into mice and first analyzed their biodistribution. For that purpose, we used Cy5-labeled nanogels and injected them with and without covalently attached ovalbumin (NP(IMDQ+OVA) and NP(IMDQ)+sOVA) into the tail vein of mice (for each sample an adjuvant dose corresponding to 10 μg of IMDQ was used according to our previous local immunization experiments[30,45]—additionally, an antigen dose corresponding to 30 μg of OVA was used, as at this ratio all antigen can quantitatively be conjugated to the nanogel, compare Figure S23). A mixture of soluble IMDQ and OVA (sIMDQ+sOVA)

https://doi.org/10.1021/acsnano.1c10709
ACS Nano 2022, 16, 4426−4443

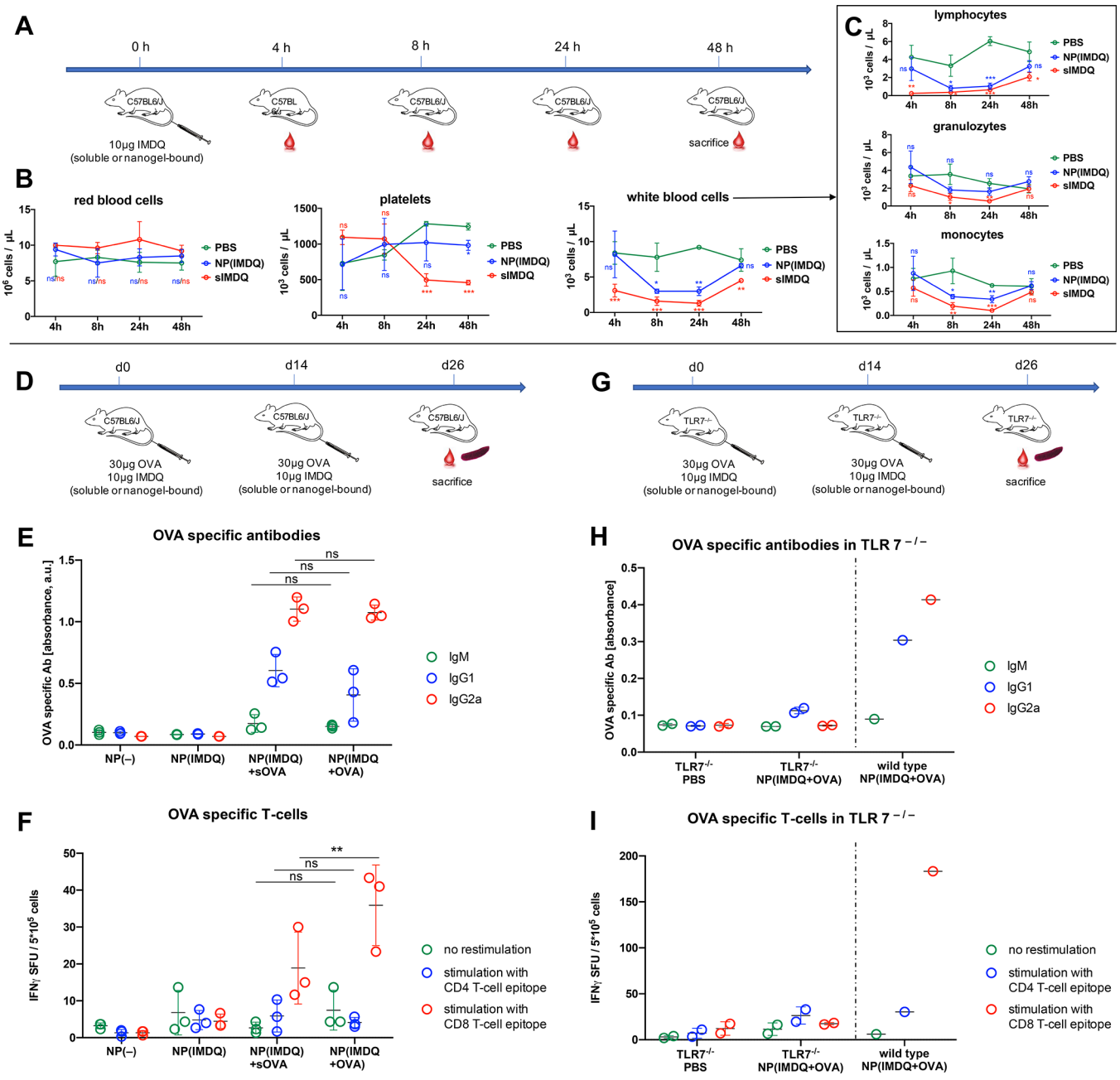

Figure 5. IMDQ- and OVA-loaded nanogel can be administered i.v. safely and generate OVA-specific humoral and superior cellular immune responses. (A) Schedule for analyzing hematologic toxicities of soluble or nanogel-bound TLR7/8 agonist IMDQ after single i.v. injection. (B) Corresponding blood cell results and (C) their differentiated white blood cells. (D) Immunization schedule for IMDQ- and OVA-loaded nanogel in wild-type mice and (E) the corresponding OVA specific antibodies determined by ELISA of the blood serum, as well as (F) the corresponding T cells determined by ELISpot of the isolated spleen cells. (G) Analogous immunization schedule for IMDQ- and OVA-loaded nanogel in TLR7$^{-/-}$ mice. (H) No OVA-specific antibodies could be found by ELISA in the blood serum as well as (I) no corresponding T cells could be determined by ELISpot of the isolated spleen cells, in contrast to a wild-type mouse serving as control during these experiments.

served as control. Cy5-labeling allowed us to monitor particle organ distribution after dissection using an IVIS imaging system (Figure S48). The majority of the particles were either found in the liver, a typical non-specific sink for systemically administered nanocarriers, and in the kidneys, probably due to the pH-induced particle degradation and unfolding into single polymer chains that can be cleared renally. Nonetheless, a significant amount could still be detected in the spleen as relevant lymphatic organ to induce antigen-specific immune responses.

We therefore conducted flow cytometry analyses of liver and spleen-derived single cell suspensions (Figures S54–S57) and observed an uptake of particles with and without OVA into various antigen-presenting immune cell subpopulations. Interestingly, co-delivery of IMDQ-functionalized particle (Cy5-labeled) with antigen (Alexa Fluor 488-labeled OVA) worked best for the covalent conjugate in most of these immune cells (Figures S55B and S57B). In analogy to the previous *ex vivo* incubation experiments on isolated spleen cells, we also analyzed maturation markers in the correspond-

https://doi.org/10.1021/acsnano.1c10709
ACS Nano 2022, 16, 4426–4443

ing immune cell subpopulations by staining them for co-stimulatory factors CD86 and MHC-II. Interestingly, none of these markers could be stimulated inside the liver, in line with its immunosuppressive microenvironment (Figure S55C,D). However, in the spleen, all IMDQ-containing NP increased the expression levels of CD86 in B cells, DCs, neutrophils ,and macrophages (MHC-II expression alone was again already at relatively high basal levels in the PBS control due to the applied splenic isolation conditions, Figure S57C,D). However, CD86 expression seems again to be more sensitive, as it was also exclusively most stimulated by the nanogel-bound IMDQ in almost all of these immune cell populations in the spleen (Figure S57C).

To further prove that nanogel-bound IMDQ on OVA-loaded nanogels has the potential to induce promising immune responses, we also checked for the cytokine profile of those mice 24 h after i.v. injection and found highest levels of the pro-inflammatory cytokines TNF-α and INF-γ for the dual-loaded nanogel NP(IMDQ+OVA) (Figure S51). These results are in accordance with the cytokine data of the *in vitro*-stimulated BMDCs (compare Figure 4E,F) and confirm that the nanogel-mediated co-delivery of both antigen and immune stimulant provides a good basis for successful immunizations. For additional insights into the innate immune response, we analyzed a larger panel of TLR7/8-driven cytokines also 4 h after the nanogel injection. Again, the nanovaccine led to elevated levels of most analyzed cytokines 24 h after i.v. injection. However, administration of sIMDQ+sOVA resulted in a rapid production of cytokines early after the injection (4 h), illustrating an undesired cytokine storm caused by sIMDQ when applied without a carrier system (Figure S52).

We further aimed to evaluate this toxicity after i.v. injection. Prompted by the strong accumulation of the nanogels in the liver (compare Figures S48 and S55), we looked at the liver enzyme parameters in the blood but could not observe any differences between different samples both after 4 and 24 h (Figures S49 and S50). Moreover, histopathological analyses by hematoxylin−eosin staining of liver, spleen, kidney, heart, and lung tissue showed no histological anomalies after i.v. injection of the nanovaccine (Figure S53).

However, a major impact especially for the i.v. administration of the soluble IMDQ could be detected on the composition of cells in the blood (Figure 5A−C). Earlier experiments revealed that, when bound to nanogels, the negative influence on the blood cell profile can be prevented and the immune response remains localized to draining lymph nodes after s.c. injection.[30,49] To provide an overview of IMDQ's impact after i.v. injection over time, mice were treated again with 100 μL of samples containing 10 μg equivalents of IMDQ, and blood samples were taken after 4, 8, 24, and 48 h for analysis of their red and white blood cell content as well as for the amount of platelets (Figure 5A). Systemic injection of TLR agonists resulting in uncontrolled release of type I interferons has been linked to strongly reduced numbers of platelets and white blood cells in the blood.[63]

While the number of red blood cells was not affected during all our studies (Figure 5B), the massive drop of platelets could be reconfirmed for the sIMDQ after 24 h, while the nanogel-bound TLR7/8 agonist had no effect, also after 48 h (Figure 5B). We relate this unfavorable site effect of the sIMDQ to the earlier detected massive cytokine expression when applied without a carrier system (Figure S52). Interestingly, such immunization-related severe thrombocytopenia is also associated as side effect of currently administered viral vector-based SARS-CoV-2 vaccines causing sinus vein thrombosis[64] and should therefore be circumvented already at an early stage of vaccine development.

Compared to sIMDQ, mice treated with nanogel-bound IMDQ (NP(IMDQ)) displaced no drop in platelets and only a reduced drop in lymphocytes that recovered more after 48 h effectively (Figure 5B). Specifically, white blood cell analyses revealed that the levels of lymphocytes, granulocytes and monocytes were also less affected by the nanogel-bound IMDQ than by sIMDQ and recovered to values of PBS-treated mice (Figure 5C). Moreover, empty nanogels or IMDQ-loaded nanogels decorated with OVA antigen never affected all hematologic parameters as much as sIMDQ after i.v. administration (Figure S47). Altogether, these findings highlight the enhanced safety profile of nanogel-bound IMDQ even after injection into the bloodstream, avoiding adverse systemic immune responses but instead providing more access to circulating immune cells for improved vaccination performance.

Proven effective and safe for i.v. injection, we used our two-component nanogels for immunizing naïve wild-type mice. On day 0 they were immunized i.v. with different nanogel samples, namely empty nanogels NP(−), IMDQ-loaded nanogels NP(IMDQ), two-component nanogels NP(IMDQ+OVA), and IMDQ nanogels mixed with sOVA (NP(IMDQ)+sOVA), followed by a boost immunization on day 14 (Figure 5D). On day 26 mice were sacrificed to analyze the generation of OVA-specific antibodies in the blood serum by ELISA (Figure 5E) and OVA-specific T cells in the spleen by ELISpot analysis (Figure 5F). As expected, only mice immunized with samples containing OVA and IMDQ showed secretion of OVA-specific antibodies. Both formulations, two-component vaccine and soluble mixture, led to increased secretion of IgG-type antibodies, especially the IgG2a subtype, which indicates a Th1-biased immune response. Here, covalent attachment of OVA did not have any drastic influence on the humoral response (Figure 5E). On the cellular level, however, spleen analysis of mice immunized with NP(IMDQ+OVA) revealed a significantly increased number of OVA-specific $CD8^+$ T cells compared to NP(IMDQ)+sOVA (Figure 5F). This observation is in accordance with our previous *in vitro* results (Figure 4G) indicating that OVA-bound IMDQ-nanogels mediate enhanced cross-presentation and favor a $CD8^+$ T cell response also *in vivo*.

Additionally, immunization experiments were repeated in $TLR7^{-/-}$ mice (Figure 5G) and revealed no priming of specific B cell (Figure 5H) and T cell (Figure 5I) immune responses. This clearly demonstrates that the nanogel-mediated Th1-biased humoral and cellular immune responses are mediated by TLR7 receptor stimulation triggered through nanogel-conjugated IMDQ.

Based on these results, we analyzed the effects of i.v. vaccination compared to s.c. vaccination on humoral and cellular responses, as similar systems have already been shown suitable for s.c. injection by us and others.[30,34] Hence, mice were injected twice with our nanovaccine. Again blood serum and spleen cells were tested for OVA-specific antibodies and T cells. This time, MHC-tetramer staining revealed $CD8^+$ T cells in blood after prime and boost immunization with our nanovaccine (Figure S58) but no significant differences between s.c. and i.v. administration. Similarly, recent data from Baharom *et al.* shows that i.v. vaccination does not trigger

https://doi.org/10.1021/acsnano.1c10709
ACS Nano 2022, 16, 4426−4443

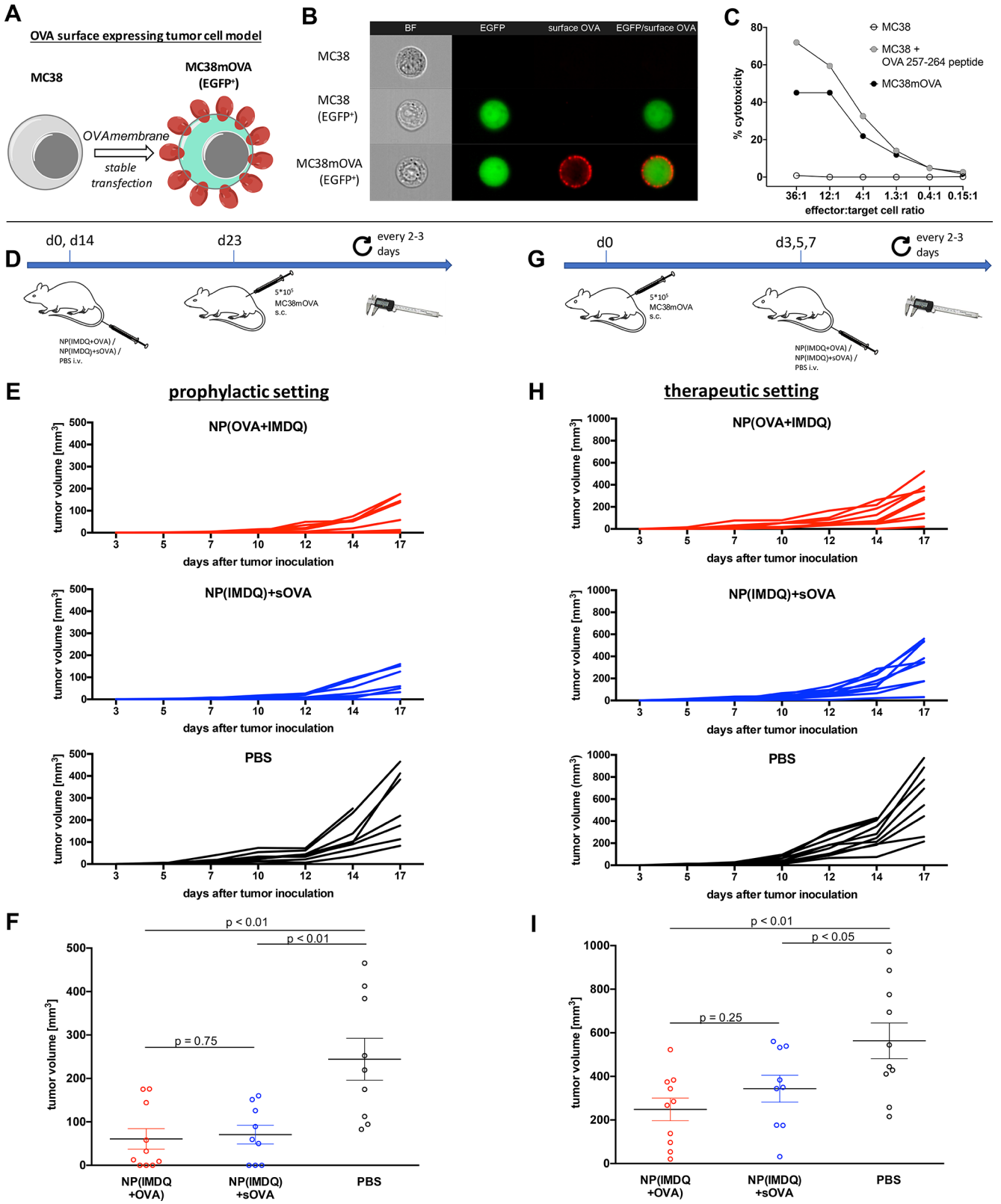

Figure 6. IMDQ- and OVA-loaded nanogels provide both prophylactic and therapeutic immunity toward a surface neoantigen-expressing tumor model. (A) MC38 cancer cells were genetically engineered to stably express OVA on their surface. (B) ImageStream analysis of wild-type MC38 cells (top), MC38 cells expressing only EGFP (middle) and MC38mOVA (EGFP$^+$, bottom) stained for surface OVA by OVA-specific antibodies. Image panels (left to right) show brightfield (BF, magnification 40×), EGFP expression (green), surface OVA expression (Alexa Fluor 647, red), and overlay image (EGFP/surface OVA). (C) CD8$^+$ T cell-mediated killing of MC38mOVA and control target cells (MC38 and peptide-pulsed MC38 (1 μM, 45 min at 37 °C)) after incubation with OT-I T cells at the indicated ratios (specific target lysis was calculated as described in the Supporting Information). (D) Prophylactic immunization schedule and challenge with MC38mOVA tumor cells. (E) Results of the individual tumors after prophylactic immunization with the corresponding nanogel samples or PBS (n = 10).

https://doi.org/10.1021/acsnano.1c10709
ACS Nano 2022, 16, 4426−4443

Figure 6. continued

(F) End point tumor volume showing reduced tumor growth for NP(IMDQ+OVA)- and NP(IMDQ)+sOVA-immunized mice compared to PBS group; however, no significant difference between NP(IMDQ+OVA) and NP(IMDQ)+sOVA could be found. (G) Therapeutic schedule for the treatment of mice challenged with MC38mOVA tumor cells (n = 10). (H) Results of the individual tumors after therapeutic treatment with the corresponding nanogel samples or PBS. (I) End point tumor volume showing reduced tumor growth for NP(IMDQ+OVA) and NP(IMDQ)+sOVA-treated mice compared to PBS group. A more significant difference between NP(IMDQ+OVA) and NP(IMDQ)+sOVA could be found compared to the prophylactic treatment.

higher numbers of antigen-specific T cells compared to s.c. vaccination but creates subtypes of $CD8^+$ T cells with superior antitumor capacity.[65] In our study, i.v. administration of NP(IMDQ+OVA) significantly outperformed s.c. injection in the generation of OVA-specific IgG2a antibodies (Figure S59A). Furthermore, investigating the INF-γ secretion of OVA-specific T cells *via* ELISpot, we found an improved performance of the i.v. immunization for both $CD4^+$ and $CD8^+$ T cells (Figure S59B).

In addition, mice body weight was monitored over time during these immunization studies. Note that NP(IMDQ+OVA) conjugate was well tolerated for i.v. and s.c. injection routes. However, the administration of sIMDQ as adjuvant led to a rapid drop in body weight and confirmed the necessity of covalent IMDQ-attachment once more (Figure S60) and its impact on generation of OVA-specific T cells (Figure S61).

Summarizing, our IMDQ nanogels could be demonstrated as safe for i.v. immunization and elicit robust humoral and cellular immune responses. Furthermore, our results are indicating that covalent attachment of OVA benefits the formation of OVA-specific cytotoxic $CD8^+$ T cells both *in vitro* and *in vivo*.

Prophylactic Immunization with Two-Component Nanovaccine Reduces Tumor Growth and Leads to Enhanced Tumor Protection during Therapeutic Vaccination. The presence and the activation of antigen-specific cytotoxic T cells in the tumor microenvironment is often correlated with improved tumor regression and therapy output.[66] Referring to superior generation of OVA-specific $CD8^+$ T cells after immunization with our two-component nanogels, we next asked whether this observation might be displayed by enhanced tumor regression *in vivo*, too. For that purpose, we first aimed to implement an OVA-dependent tumor model system that is accessible to both humoral and cellular immune responses (the classical B16-OVA model, for instance, has some limitations: its cytosolic OVA expression does not provide access for antibody-mediated immune responses[67] and its downregulated MHC-I expression allows only reduced CD8 epitope presentation[68]). We therefore first selected the MC38 colon cancer cell line and established an OVA antigen model for our studies (Figure 6).

Cancer immunotherapy seeks to enable immunization against tumor-specific antigens either as overexpressing antigens or as neoantigens. In contrast to patient-specific neoepitopes usually found intracellularly, we hypothesize that cancer-specific cell surface expressed neoantigens display better suited targets since they are accessible for both cellular as well as humoral immune responses. Hence, the MC38 tumor model was genetically engineered to stably express membrane-bound OVA and, thereby, allows the elimination by OVA-specific cellular as well as humoral immune responses (Figure 6A). OVA surface expression could be verified by ImageStream analysis, clearly showing OVA-dependent fluorescence at the cell surface after incubation with OVA-specific antibodies (non-transfected or EGFP transfected control cells could not be stained by OVA-specific antibodies on their surface) (Figure 6B). These data suggest that these tumor cells can be detected by humoral immune responses. Furthermore, OVA-expressing MC38 cells were also recognized and eliminated by OVA-specific $CD8^+$ T cells obtained from OT-1 mice. When co-incubated for 4 h with OT-1 T cells, OVA-surface-expressing MC38 cells (MC38mOVA) were killed in a T cell dose-dependent way, in analogy to wild-type MC38 cells externally loaded with MHC-I binding CD8 T cell epitope OVA 257-264 peptide. Non-treated MC38 cells lacking OVA expression were not lysed at all (Figure 6C). Consequently, these experiments confirm that also cellular immune responses are capable of recognizing and responding to our tumor model in an antigen-specific fashion. Summarizing, our OVA-expressing MC38 tumor cell model was considered to be suitable for analyzing tumor-specific humoral and cellular immune responses triggered by our two-component nanovaccine.

Subsequently, the OVA membrane-expressing MC38 cell line was applied to wild-type mice. We first assessed prophylactic tumor protection *in vivo* by immunization two times (on day 0 and day 14) with either NP(IMDQ+OVA) conjugate or the mixture NP(IMDQ)+sOVA (Figure 6D). On day 23 mice were then subcutaneously inoculated with membranous-expressing OVA MC38 cells and tumor growth was analyzed each 2−3 days. While tumors rapidly grew in the non-immunized control group (PBS) from day 12 after inoculation, prophylactic immunization against OVA with both nanogel samples resulted in significantly reduced tumor growth (Figure 6E). However, no significant differences in tumor protection based on the nature of OVA delivery, covalently attached or administered, could be observed by comparing final tumor volumes (Figure 6F). In accordance with our previous *in vivo* findings that both NP(IMDQ+OVA) conjugate or the mixture NP(IMDQ)+sOVA were able to induce similar humoral immune responses (Figure 5E), we hypothesize that these mechanisms might primarily be responsible here to inhibit growth of the surface antigen-expressing tumor cells under prophylactic conditions.

Alternatively, we further assessed the influence of NP(IMDQ+OVA) on tumor regression under therapeutic conditions. For that purpose, mice were first inoculated s.c. with OVA MC38 cells on day 0, and on day 3 palpable tumors could be detected at a volume below 5 mm^3. Next, i.v. immunization with NP(IMDQ+OVA) or NP(IMDQ)+sOVA was performed on days 3, 5, and 7 (Figure 6G). Again, analysis of tumor growth showed that both formulations could trigger significant tumor regression (Figure 6H). Interestingly, treatment with NP(IMDQ+OVA) seemed to have a slightly improved effect on controlling final tumor volumes than the mixture of NP(IMDQ)+sOVA (Figure 6I). This is in line with our previous finding that covalent attachment of OVA guarantees more efficient co-delivery of OVA and IMDQ

https://doi.org/10.1021/acsnano.1c10709
ACS Nano 2022, 16, 4426−4443

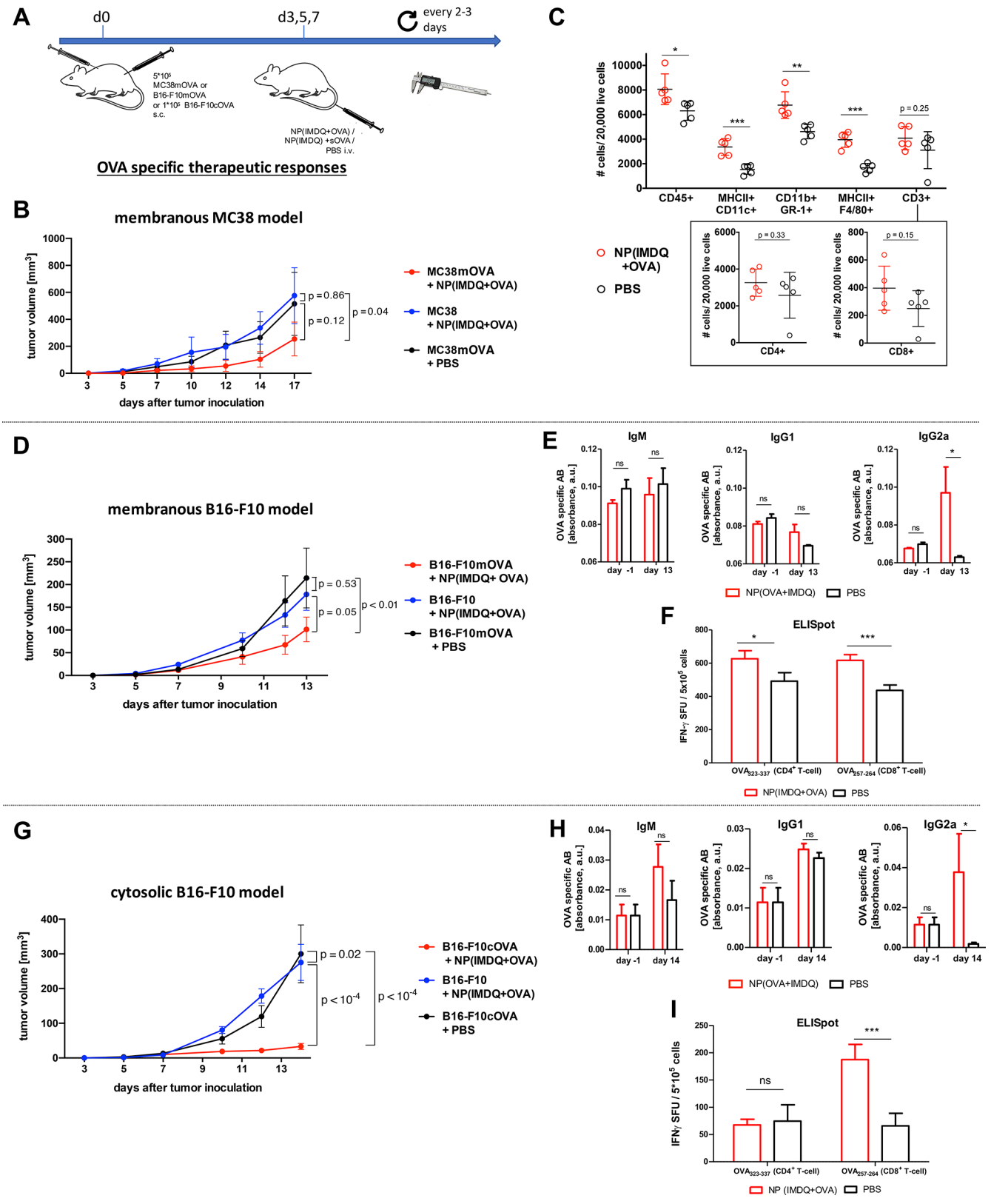

Figure 7. IMDQ- and OVA-loaded nanogels provide antigen-specific tumor immunity by induction of Th-1-biased immune responses with respect to increasing levels of antigen-specific IgG2a titers, increasing numbers of antigen-specific $CD8^+$ and $CD4^+$ T cells and increasing numbers of tumor-infiltrating immune cells. (A) Therapeutic schedule for the treatment of mice challenged with both MC38mOVA and wild-type MC38, B16-F10mOVA and wild-type B16-F10, or B16-F10cOVA and wild-type B16-F10 tumor cells. (B) Results of the MC38mOVA or MC38 tumor sizes after treatment either with NP(IMDQ+OVA) or PBS (n = 10). (C) Flow cytometric analysis of single-cell tumor suspensions derived from MC38mOVA tumors treated with NP(IMDQ+OVA) or PBS. (D) Results of B16-F10mOVA or B16-F10 tumor sizes after treatment with NP(IMDQ+OVA) or PBS (n = 9−11). (E) ELISA analysis of blood serum samples taken on day −1 (so before tumor inoculation and treatment with the nanogel) and day 13 after tumor inoculation from B16-F10mOVA-bearing mice treated

https://doi.org/10.1021/acsnano.1c10709
ACS Nano 2022, 16, 4426−4443

Figure 7. continued

with NP(IMDQ+OVA) or PBS. (F) ELISpot analysis of the isolated spleen cells taken on day 13 after tumor inoculation from B16-F10mOVA-bearing mice treated with NP(IMDQ+OVA) or PBS. (G) Results of B16-F10cOVA or B16-F10 tumor sizes after treatment with NP(IMDQ+OVA) or PBS (n = 10). (H) ELISA analysis of blood serum samples taken on day −1 and day 14 after tumor inoculation from B16-F10cOVA-bearing mice treated with NP(IMDQ+OVA) or PBS. (I) ELISpot analysis of the isolated spleen cells taken on day 14 after tumor inoculation from B16-F10cOVA-bearing mice treated with NP(IMDQ+OVA) or PBS.

followed by rapid immune cell stimulation, cross-presentation, and induction of OVA-dependent $CD8^+$ cells (Figure 5F).

OVA- and IMDQ-Loaded Two-Component Nanovaccine Governs Antigen-Specific Tumor Growth by Increasing the Number of Infiltrating Immune Cells into the Tumor Microenvironment. In a subsequent experiment, we wanted to confirm these observations and investigated whether the observed antitumor effects fully rely on OVA-specific immune responses. For that purpose, mice were inoculated on one flank with MC38mOVA cells and on the other flank with wild-type MC38 cells not expressing OVA. On days 3, 5, and 7, mice were then treated with NP(IMDQ+OVA) or PBS as control (Figure 7A). Whereas nanovaccine treatment induced again an immune response that recognized the OVA-expressing MC38 tumors selectively and caused reduced tumor growth, the MC38 tumors did not respond to the immunization and grew comparable to the MC38mOVA tumors of PBS-treated mice (Figure 7B).

Moreover, we looked at the immune status by determining the number of infiltrating immune cells in the MC38mOVA tumor micromilieu after treatment with NP(IMDQ+OVA) (Figure 7C and Figures S63 and S64). We generally observed a significant increase in the number of immune cells ($CD45^+$) compared to PBS-treated tumors, most notably in number of infiltrating myeloid cell populations, as reflected by an increase in numbers of MHC-II^+ $CD11c^+$ dendritic cells, $CD11b^+$ $Gr\text{-}1^+$ neutrophils, and MHC-II+$F4/80^+$ macrophages, all considered as antitumoral. Beyond that, also a slight increase in $CD3^+$ T cells was observed. When analyzing this population more carefully, we confirmed that the number of infiltrating $CD8^+$ T cells, but not of $CD4^+$ T cells, increased within the tumors after treatment with NP(IMDQ+OVA), reflecting the proposed enhanced cellular antitumoral immune response induced by NP(IMDQ+OVA).

Based on these results, we further applied the same experimental conditions using the commonly used B16-F10 tumor model but also engineered the cell line with a membrane expressing OVA in analogy to the MC38 model. Although the B16-F10 cell line is known to have down-regulated MHC-I expression and, thus, only reduced CD8 epitope presentation,[68] we observed again similar results for this B16-F10mOVA model as for the MC38mOVA model. Therapeutic treatment with our two-component vaccine led to an antigen-specific reduction of the transplanted B16-F10mOVA tumor, while the wild-type B16-F10 tumors were not affected in the same way as the untreated B16-F10mOVA tumors (Figure 7D). These results confirm that our IMDQ- and OVA-loaded nanogel fully guarantees selective antigen-specific antitumor responses in mice after i.v. administration, independent from the tumor source.

To shine further light on the immunologic mechanism behind these findings, we performed ELISA analysis of blood serum samples taken from of B16-F10mOVA-bearing mice before tumor inoculation (day −1) and after nanogel treatment (day 13 after tumor inoculation). Again, they revealed a significant increase especially of IgG2a antibodies after treatment with NP(IMDQ+OVA) (Figure 7E), indicating a Th1-biased immune response in analogy to the previous immunization experiments (Figure 5D). This was further proven by cytokine analysis of those blood samples revealing a significant induction of the pro-inflammatory cytokines TNF-α and INF-γ (Figure S62), as already demonstrated after nanogel treatment *in vitro* (Figure 4E,F) and *in vivo* (Figure S51). This finally resulted in an increase of the number of OVA-specific $CD4^+$ and $CD8^+$ T cells in the spleen determined by ELISpot analysis (Figure 7F), which are again in accordance with our immunization studies (Figure 5F).

Indicating that the antigen-specific generation of antibodies plays a crucial role in the rejection of tumors that present OVA on the cell surface, we decided to investigate the impact of humoral and cellular immune responses in a mice model lacking antibody production. Hence, antibody-deficient mice, referred to as IgMi mice,[69] were challenged with MC38mOVA tumors but in contrast to wild-type mice no tumor reduction was observable. Further analysis of spleen cells revealed that IgMi mice, besides lacking antibodies, also show reduced generation of antigen-specific $CD8^+$ T cells compared to wild-type mice (Figure S65). Hence, we propose that failed tumor rejection in IgMi mice cannot exclusively be attributed to antibody deficiency and might also depend on reduced generation of T cells. This makes it difficult to draw clear conclusions regarding the impact of antibodies and T cells on tumor control.

Therefore, we modified our tumor model by generating B16-F10 cells expressing OVA exclusively in the cytosol (B16-F10cOVA). Interestingly, we were also able to observe antigen-specific and robust reduction of tumors in this model, while control wild-type B16-F10 tumors were not affected (Figure 7G). Subsequent analysis of antibody secretion and OVA-specific T cell generation revealed again increased secretion of OVA-specific IgG2a antibodies and more importantly a rise in OVA-specific $CD8^+$ T cells (Figure 7H,I), giving evidence that the induction of cellular immune responses is primarily essential for the antitumor effect induced by our nanovaccine. These properties might therefore also become relevant when addressing currently investigated clinical settings of cancer-specific neoepitopes.

Altogether these results confirm that the i.v.-administered, co-delivering two-component nanovaccine NP(IMDQ+OVA) induces robust antigen-specific humoral and cellular immune responses *in vitro* and *in vivo* that install enhanced antitumor efficacy, after both prophylactic and therapeutic immunization.

CONCLUSION

Therapeutic vaccination against tumor-associated antigens is of great interest regarding the variety of tumor types and individual immune condition for each patient. Vaccines need to elicit antigen-specific stable humoral and cellular immune responses to ensure immunogenicity and avoid tolerance. Here, we reported on a RAFT-based nanogel system that

https://doi.org/10.1021/acsnano.1c10709
ACS Nano 2022, 16, 4426−4443

chemically allows covalent attachment of antigens and core functionalization with small molecules in a straightforward way, resulting in a two-component nanovaccine that is safe for i.v. immunization and allows physical co-delivery of antigen and adjuvant. We showed that covalent attachment of OVA to our IMDQ-loaded nanogels elicits robust humoral and cellular immune responses and, in addition, benefits the generation of antigen-specific $CD8^+$ T cells both *in vitro* and *in vivo*. These observations are in accordance with studies by other groups that emphasize the importance of incorporation of immune adjuvant and antigen into the same carrier system.[34−36] The development of well-defined OVA-dependent MC38 and B16-F10 tumors facilitated tumor studies with membrane-bound OVA, mimicking the expression of tumor-associated neo-antigens in clinical relevant tumors that are responsive toward both humoral and cellular immune responses as well as studying the exclusive impact of cellular immunity on cytosolically expressed OVA.

Our nanogels elicited OVA-dependent antitumor responses in both prophylactic and therapeutic approaches. The demand for personalized cancer vaccines promotes the need for customizable vaccine platforms. Regarding the chemical design of our nanogel platform, easy modifications toward co-delivery of other immune-interfering drugs and antigens or peptides are possible, since both components only need to exhibit either amino functionalities due to the reactive ester approach for core conjugation or DBCO modification for ligation to the particle surface. As well, multi-targeting by combination with immune checkpoint inhibitors or different antigens on one nanogel is conceivable. Based on the selected RAFT polymerization conditions and core-cross-linking of polymeric micelles, the size and morphology of our nanovaccines are pre-defined before functionalization; hence, the nanoparticulate formulation is fully independent of the immunologically relevant payload. Their pharmacokinetic profile will exclusively rely on the performance of the immunogenically silent carrier. In addition, the results of this study conclude that the pH-degradable nanogel system further facilitates a safe i.v. administration of highly immune stimulating imidazoquinoline-type TLR7/8 adjuvants in combination with co-delivered cancer-associated antigens and, thus, provides—in contrast to currently investigated antigen-free adjuvant treatments of tumors—opportunities to install cancer-specific immunity.

Overall, our nanogel approach can be considered as a highly versatile immunocarrier platform that is able to trigger antitumor capacities and might be interesting for the development of highly customized nanovaccines, not only for clinically more relevant tumors but also against other pandemic viral diseases.

MATERIALS AND METHODS

Detailed information on instrumentations, materials, cells and mice, as well as experimental procedures can be found in the Supporting Information.

ASSOCIATED CONTENT

Supporting Information

The Supporting Information is available free of charge at https://pubs.acs.org/doi/10.1021/acsnano.1c10709.

Instrumentation, materials, cells and mice, experimental procedures, and data, including Figures S1−S65 (PDF)

AUTHOR INFORMATION

Corresponding Authors

Stephan Grabbe − *Department of Dermatology, University Medical Center of Johannes Gutenberg-University Mainz, 55131 Mainz, Germany*; Email: stephan.grabbe@unimedizin-mainz.de

Hansjörg Schild − *Institute of Immunology, University Medical Center of Johannes Gutenberg-University Mainz, 55131 Mainz, Germany*; Email: schild@uni-mainz.de

Lutz Nuhn − *Max Planck Institute for Polymer Research, 55128 Mainz, Germany*; orcid.org/0000-0003-0761-1106; Email: lutz.nuhn@mpip-mainz.mpg.de

Authors

Judith Stickdorn − *Max Planck Institute for Polymer Research, 55128 Mainz, Germany*

Lara Stein − *Institute of Immunology, University Medical Center of Johannes Gutenberg-University Mainz, 55131 Mainz, Germany*

Danielle Arnold-Schild − *Institute of Immunology, University Medical Center of Johannes Gutenberg-University Mainz, 55131 Mainz, Germany*

Jennifer Hahlbrock − *Institute of Immunology, University Medical Center of Johannes Gutenberg-University Mainz, 55131 Mainz, Germany*

Carolina Medina-Montano − *Department of Dermatology, University Medical Center of Johannes Gutenberg-University Mainz, 55131 Mainz, Germany*

Joschka Bartneck − *IIIrd Department of Medicine - Hematology, Oncology, Pneumology, University Medical Center of the Johannes Gutenberg-University Mainz, 55131 Mainz, Germany*

Tanja Ziß − *Institute of Immunology, University Medical Center of Johannes Gutenberg-University Mainz, 55131 Mainz, Germany*

Evelyn Montermann − *Department of Dermatology, University Medical Center of Johannes Gutenberg-University Mainz, 55131 Mainz, Germany*

Cinja Kappel − *Department of Dermatology, University Medical Center of Johannes Gutenberg-University Mainz, 55131 Mainz, Germany*; orcid.org/0000-0002-9122-0601

Dominika Hobernik − *Department of Dermatology, University Medical Center of Johannes Gutenberg-University Mainz, 55131 Mainz, Germany*

Maximilian Haist − *Department of Dermatology, University Medical Center of Johannes Gutenberg-University Mainz, 55131 Mainz, Germany*

Hajime Yurugi − *Cell Biology Unit, University Medical Center of Johannes Gutenberg-University Mainz, 55131 Mainz, Germany*

Marco Raabe − *Max Planck Institute for Polymer Research, 55128 Mainz, Germany*; orcid.org/0000-0002-3677-6615

Andreas Best − *Max Planck Institute for Polymer Research, 55128 Mainz, Germany*

Krishnaraj Rajalingam − *Cell Biology Unit, University Medical Center of Johannes Gutenberg-University Mainz, 55131 Mainz, Germany*

Markus P. Radsak − *IIIrd Department of Medicine - Hematology, Oncology, Pneumology, University Medical Center of the Johannes Gutenberg-University Mainz, 55131 Mainz, Germany*

Sunil A. David − *ViroVax, LLC, Lawrence 66047-1620 Kansas, United States;* orcid.org/0000-0003-1655-4641
Kaloian Koynov − *Max Planck Institute for Polymer Research, 55128 Mainz, Germany;* orcid.org/0000-0002-4062-8834
Matthias Bros − *Department of Dermatology, University Medical Center of Johannes Gutenberg-University Mainz, 55131 Mainz, Germany*

Complete contact information is available at: https://pubs.acs.org/10.1021/acsnano.1c10709

Author Contributions

‡J.S. and L.S. contributed equally.

Funding

Open access funded by Max Planck Society.

Notes

The authors declare no competing financial interest.

ACKNOWLEDGMENTS

The authors gratefully acknowledge support through the DFG SFB 1066 Project B04. Moreover, L.N. would like to thank the DFG Emmy-Noether program, the Liebig Program of the Fonds der Chemischen Industrie (FCI), and the Max Buchner Research Foundation for their generous support. The authors thank Claudia Braun from the Histology Core Facility of the Research Center for Immunotherapy of the Johannes Gutenberg University Mainz for the preparation of tissue sections and H&E staining.

REFERENCES

(1) Sahin, U.; Türeci, Ö. Personalized Vaccines for Cancer Immunotherapy. *Science* **2018**, *359* (6382), 1355−1360.
(2) Parish, C. R. Cancer Immunotherapy: The Past, the Present and the Future. *Immunol. Cell Biol.* **2003**, *81* (2), 106−113.
(3) Guy, B. The Perfect Mix: Recent Progress in Adjuvant Research. *Nat. Rev. Microbiol.* **2007**, *5* (7), 396−397.
(4) Sharonov, G. V.; Serebrovskaya, E. O.; Yuzhakova, D. V.; Britanova, O. V.; Chudakov, D. M. B Cells, Plasma Cells and Antibody Repertoires in the Tumour Microenvironment. *Nat. Rev. Immunol.* **2020**, *20* (5), 294−307.
(5) Sánchez-Paulete, A. R.; Teijeira, A.; Cueto, F. J.; Garasa, S.; Pérez-Gracia, J. L.; Sánchez-Arráez, A.; Sancho, D.; Melero, I. Antigen Cross-Presentation and T cell Cross-Priming in Cancer Immunology and Immunotherapy. *Ann. Oncol.* **2017**, *28* (5), xii44−xii55.
(6) Sato, E.; Olson, S. H.; Ahn, J.; Bundy, B.; Nishikawa, H.; Qian, F.; Jungbluth, A. A.; Frosina, D.; Gnjatic, S.; Ambrosone, C.; et al. Intraepithelial CD8+ Tumor-Infiltrating Lymphocytes and a High CD8+/Regulatory T Cell Ratio Are Associated with Favorable Prognosis in Ovarian Cancer. *Proc. Natl. Acad. Sci. U. S. A.* **2005**, *102* (51), 18538−18543.
(7) Mahmoud, S. M. A.; Paish, E. C.; Powe, D. G.; Macmillan, R. D.; Grainge, M. J.; Lee, A. H. S.; Ellis, I. O.; Green, A. R. Tumor-Infiltrating CD8+ Lymphocytes Predict Clinical Outcome in Breast Cancer. *J. Clin. Oncol.* **2011**, *29* (15), 1949−1955.
(8) Naito, Y.; Saito, K.; Shiiba, K.; Ohuchi, A.; Saigenji, K.; Nagura, H.; Ohtani, H. CD8+ T Cells Infiltrated within Cancer Cell Nests as a Prognostic Factor in Human Colorectal Cancer. *Cancer Res.* **1998**, *58* (16), 3491−3494.
(9) Nakano, O.; Naito, Y.; Nagura, H.; Ohtani, H.; Nakano, O.; Sato, M.; Suzuki, K.; Orikasa, S.; Aizawa, M.; Suzuki, Y.; et al. Proliferative Activity of Intratumoral CD8+ T-Lymphocytes as a Prognostic Factor in Human Renal Cell Carcinoma: Clinicopathologic Demonstration of Antitumor Immunity. *Cancer Res.* **2001**, *61* (13), 5132−5136.
(10) Verbeke, R.; Lentacker, I.; De Smedt, S. C.; Dewitte, H. Three Decades of Messenger RNA Vaccine Development. *Nano Today* **2019**, *28*, 100766.
(11) Sahin, U.; Derhovanessian, E.; Miller, M.; Kloke, B. P.; Simon, P.; Löwer, M.; Bukur, V.; Tadmor, A. D.; Luxemburger, U.; Schrörs, B.; et al. Personalized RNA Mutanome Vaccines Mobilize Poly-Specific Therapeutic Immunity against Cancer. *Nature* **2017**, *547* (7662), 222−226.
(12) Grabbe, S.; Haas, H.; Diken, M.; Kranz, L. M.; Langguth, P.; Sahin, U. Translating Nanoparticulate-Personalized Cancer Vaccines into Clinical Applications: Case Study with RNA-Lipoplexes for the Treatment of Melanoma. *Nanomedicine* **2016**, *11* (20), 2723−2734.
(13) Pardi, N.; Hogan, M. J.; Porter, F. W.; Weissman, D. MRNA Vaccines — a New Era in Vaccinology. *Nat. Rev. Drug Discovery* **2018**, *17* (4), 261−279.
(14) Karikó, K.; Muramatsu, H.; Welsh, F. A.; Ludwig, J.; Kato, H.; Akira, S.; Weissman, D. Incorporation of Pseudouridine Into mRNA Yields Superior Nonimmunogenic Vector With Increased Translational Capacity and Biological Stability. *Mol. Ther.* **2008**, *16* (11), 1833−1840.
(15) Purcell, A. W.; McCluskey, J.; Rossjohn, J. More than One Reason to Rethink the Use of Peptides in Vaccine Design. *Nat. Rev. Drug Discovery* **2007**, *6* (5), 404−414.
(16) Hollingsworth, R. E.; Jansen, K. Turning the Corner on Therapeutic Cancer Vaccines. *npj Vaccines* **2019**, *4* (1), 7.
(17) Toes, R. E. M.; Offringa, R.; Blom, R. J. J.; Melief, C. J. M.; Kast, W. M. Peptide Vaccination Can Lead to Enhanced Tumor Growth through Specific T cell Tolerance Induction. *Proc. Natl. Acad. Sci. U. S. A.* **1996**, *93* (15), 7855−7860.
(18) Hailemichael, Y.; Dai, Z.; Jaffarzad, N.; Ye, Y.; Medina, M. A.; Huang, X.-F.; Dorta-Estremera, S. M.; Greeley, N. R.; Nitti, G.; Peng, W.; et al. Persistent Antigen at Vaccination Sites Induces Tumor-Specific CD8+ T Cell Sequestration, Dysfunction and Deletion. *Nat. Med.* **2013**, *19* (4), 465−472.
(19) Li, W.; Joshi, M. D.; Singhania, S.; Ramsey, K. H.; Murthy, A. K. Peptide Vaccine: Progress and Challenges. *Vaccines (Basel)* **2014**, *2* (3), 515−536.
(20) Gnjatic, S.; Sawhney, N.; Bhardwaj, N. TLR Agonists: Are They Good Adjuvants? *Cancer J.* **2010**, *16* (4), 382−391.
(21) Foged, C. Subunit Vaccines of the Future: The Need for Safe, Customized and Optimized Particulate Delivery Systems. *Ther. Delivery* **2011**, *2* (8), 1057−1077.
(22) Beesu, M.; Salyer, A. C. D.; Brush, M. J. H.; Trautman, K. L.; Hill, J. K.; David, S. A. Identification of High-Potency Human TLR8 and Dual TLR7/TLR8 Agonists in Pyrimidine-2,4-Diamines. *J. Med. Chem.* **2017**, *60* (5), 2084−2098.
(23) Dowling, D. J. Recent Advances in the Discovery and Delivery of TLR7/8 Agonists as Vaccine Adjuvants. *ImmunoHorizons* **2018**, *2* (6), 185−197.
(24) Zitvogel, L.; Galluzzi, L.; Kepp, O.; Smyth, M. J.; Kroemer, G. Type I Interferons in Anticancer Immunity. *Nat. Rev. Immunol.* **2015**, *15* (7), 405−414.
(25) Harrison, L. I.; Astry, C.; Kumar, S.; Yunis, C. Pharmacokinetics of 852A, an Imidazoquinoline Toll-like Receptor 7-Specific Agonist, Following Intravenous, Subcutaneous, and Oral Administrations in Humans. *J. Clin. Pharmacol.* **2007**, *47* (8), 962−969.
(26) Weigel, B. J.; Cooley, S.; DeFor, T.; Weisdorf, D. J.; Panoskaltsis-Mortari, A.; Chen, W.; Blazar, B. R.; Miller, J. S. Prolonged Subcutaneous Administration of 852A, a Novel Systemic Toll-like Receptor 7 Agonist, to Activate Innate Immune Responses in Patients with Advanced Hematologic Malignancies. *Am. J. Hematol.* **2012**, *87* (10), 953−956.
(27) Engel, A. L.; Holt, G. E.; Lu, H. The Pharmacokinetics of Toll-like Receptor Agonists and the Impact on the Immune System. *Expert Rev. Clin. Pharmacol.* **2011**, *4* (2), 275−289.
(28) Lynn, G. M.; Laga, R.; Darrah, P. A.; Ishizuka, A. S.; Balaci, A. J.; Dulcey, A. E.; Pechar, M.; Pola, R.; Gerner, M. Y.; Yamamoto, A.; et al. In Vivo Characterization of the Physicochemical Properties of

Polymer-Linked TLR Agonists That Enhance Vaccine Immunogenicity. *Nat. Biotechnol.* **2015**, *33* (11), 1201−1210.
(29) Lybaert, L.; Vermaelen, K.; De Geest, B. G.; Nuhn, L. Immunoengineering through Cancer Vaccines − A Personalized and Multi-Step Vaccine Approach towards Precise Cancer Immunity. *J. Controlled Release* **2018**, *289* (May), 125−145.
(30) Nuhn, L.; Vanparijs, N.; De Beuckelaer, A.; Lybaert, L.; Verstraete, G.; Deswarte, K.; Lienenklaus, S.; Shukla, N. M.; Salyer, A. C. D.; Lambrecht, B. N.; et al. PH-Degradable Imidazoquinoline-Ligated Nanogels for Lymph Node-Focused Immune Activation. *Proc. Natl. Acad. Sci. U. S. A.* **2016**, *113* (29), 8098−8103.
(31) Lepeltier, E.; Nuhn, L.; Lehr, C.-M.; Zentel, R. Not Just for Tumor Targeting: Unmet Medical Needs and Opportunities for Nanomedice. *Nanomedicine (Lond).* **2015**, *10* (20), 3147−3166.
(32) Wilson, J. T.; Keller, S.; Manganiello, M. J.; Cheng, C.; Lee, C.; Opara, C.; Convertine, A.; Stayton, P. S. pH-Responsive Nanoparticle Vaccines for Dual-Delivery of Antigens and Immunostimulatory Oligonucleotides. *ACS Nano* **2013**, *7* (5), 3912−3925.
(33) Schlosser, E.; Mueller, M.; Fischer, S.; Basta, S.; Busch, D. H.; Gander, B.; Groettrup, M. TLR Ligands and Antigen Need to Be Coencapsulated into the Same Biodegradable Microsphere for the Generation of Potent Cytotoxic T Lymphocyte Responses. *Vaccine* **2008**, *26*, 1626−1637.
(34) Lynn, G. M.; Sedlik, C.; Baharom, F.; Zhu, Y.; Ramirez-Valdez, R. A.; Coble, V. L.; Tobin, K.; Nichols, S. R.; Itzkowitz, Y.; Zaidi, N.; et al. Peptide−TLR-7/8a Conjugate Vaccines Chemically Programmed for Nanoparticle Self-Assembly Enhance CD8 T cell Immunity to Tumor Antigens. *Nat. Biotechnol.* **2020**, *38* (3), 320−332.
(35) Knight, F. C.; Gilchuk, P.; Kumar, A.; Becker, K. W.; Sevimli, S.; Jacobson, M. E.; Suryadevara, N.; Wang-Bishop, L.; Boyd, K. L.; Crowe, J. E.; et al. Mucosal Immunization with a PH-Responsive Nanoparticle Vaccine Induces Protective CD8+ Lung-Resident Memory T Cells. *ACS Nano* **2019**, *13* (10), 10939−10960.
(36) Wilson, D. S.; Hirosue, S.; Raczy, M. M.; Bonilla-Ramirez, L.; Jeanbart, L.; Wang, R.; Kwissa, M.; Franetich, J. F.; Broggi, M. A. S.; Diaceri, G.; et al. Antigens Reversibly Conjugated to a Polymeric Glyco-Adjuvant Induce Protective Humoral and Cellular Immunity. *Nat. Mater.* **2019**, *18* (2), 175−185.
(37) Traini, G.; Ruiz-de-Angulo, A.; Blanco-Canosa, J. B.; Zamacola Bascarán, K.; Molinaro, A.; Silipo, A.; Escors, D.; Mareque-Rivas, J. C. Cancer Immunotherapy of TLR4 Agonist−Antigen Constructs Enhanced with Pathogen-Mimicking Magnetite Nanoparticles and Checkpoint Blockade of PD-L1. *Small* **2019**, *15* (4), 1803993.
(38) Moon, J. J.; Suh, H.; Bershteyn, A.; Stephan, M. T.; Liu, H.; Huang, B.; Sohail, M.; Luo, S.; Ho Um, S.; Khant, H.; et al. Interbilayer-Crosslinked Multilamellar Vesicles as Synthetic Vaccines for Potent Humoral and Cellular Immune Responses. *Nat. Mater.* **2011**, *10* (3), 243−251.
(39) Sharifi, S.; Behzadi, S.; Laurent, S.; Laird Forrest, M.; Stroeve, P.; Mahmoudi, M. Toxicity of Nanomaterials. *Chem. Soc. Rev.* **2012**, *41* (6), 2323−2343.
(40) Conniot, J.; Scomparin, A.; Peres, C.; Yeini, E.; Pozzi, S.; Matos, A. I.; Kleiner, R.; Moura, L. I. F.; Zupančič, E.; Viana, A. S.; et al. Immunization with Mannosylated Nanovaccines and Inhibition of the Immune-Suppressing Microenvironment Sensitizes Melanoma to Immune Checkpoint Modulators. *Nat. Nanotechnol.* **2019**, *14* (9), 891−901.
(41) Moad, G.; Rizzardo, E.; Thang, S. H. RAFT Polymerization and Some of Its Applications. *Chem. - An Asian J.* **2013**, *8* (8), 1634−1644.
(42) York, A.; Kirkland, S.; McCormick, C. Advances in the Synthesis of Amphiphilic Block Copolymers via RAFT Polymerization: Stimuli-Responsive Drug and Gene Delivery. *Adv. Drug Delivery Rev.* **2008**, *60* (9), 1018−1036.
(43) York, A. W.; Huang, F.; McCormick, C. L. Rational Design of Targeted Cancer Therapeutics through the Multiconjugation of Folate and Cleavable SiRNA to RAFT-Synthesized (HPMA-s-APMA) Copolymers. *Biomacromolecules* **2010**, *11* (2), 505−514.
(44) Vanparijs, N.; Nuhn, L.; Paluck, S. J.; Kokkinopoulou, M.; Lieberwirth, I.; Maynard, H. D.; De Geest, B. G. Core/Shell Protein-Reactive Nanogels via a Combination of RAFT Polymerization and Vinyl Sulfone Postmodification. *Nanomedicine* **2016**, *11* (20), 2631−2645.
(45) Nuhn, L.; Van Hoecke, L.; Deswarte, K.; Schepens, B.; Li, Y.; Lambrecht, B. N.; De Koker, S.; David, S. A.; Saelens, X.; De Geest, B. G. Potent Anti-Viral Vaccine Adjuvant Based on PH-Degradable Nanogels with Covalently Linked Small Molecule Imidazoquinoline TLR7/8 Agonist. *Biomaterials* **2018**, *178*, 643−651.
(46) Das, A.; Theato, P. Activated Ester Containing Polymers: Opportunities and Challenges for the Design of Functional Macromolecules. *Chem. Rev.* **2016**, *116* (3), 1434−1495.
(47) Nuhn, L.; Bolli, E.; Massa, S.; Vandenberghe, I.; Movahedi, K.; Devreese, B.; Van Ginderachter, J. A.; De Geest, B. G. Targeting Protumoral Tumor-Associated Macrophages with Nanobody-Functionalized Nanogels through Strain Promoted Azide Alkyne Cycloaddition Ligation. *Bioconjugate Chem.* **2018**, *29* (7), 2394−2405.
(48) Stickdorn, J.; Nuhn, L. Reactive-Ester Derived Polymer Nanogels for Cancer Immunotherapy. *Eur. Polym. J.* **2020**, *124*, 109481.
(49) Nuhn, L.; De Koker, S.; Van Lint, S.; Zhong, Z.; Catani, J. P.; Combes, F.; Deswarte, K.; Li, Y.; Lambrecht, B. N.; Lienenklaus, S.; et al. Nanoparticle-Conjugate TLR7/8 Agonist Localized Immunotherapy Provokes Safe Antitumoral Responses. *Adv. Mater.* **2018**, *30* (45), 1803397.
(50) Nuhn, L.; Kaps, L.; Diken, M.; Schuppan, D.; Zentel, R. Reductive Decationizable Block Copolymers for Stimuli-Responsive MRNA Delivery. *Macromol. Rapid Commun.* **2016**, *37* (11), 924−933.
(51) Nuhn, L.; Hirsch, M.; Krieg, B.; Koynov, K.; Fischer, K.; Schmidt, M.; Helm, M.; Zentel, R. Cationic Nanohydrogel Particles as Potential siRNA Carriers for Cellular Delivery. *ACS Nano* **2012**, *6* (3), 2198−2214.
(52) Agard, N. J.; Prescher, J. A.; Bertozzi, C. R. A Strain-Promoted [3 + 2] Azide-Alkyne Cycloaddition for Covalent Modification of Biomolecules in Living Systems. *J. Am. Chem. Soc.* **2004**, *126* (46), 15046−15047.
(53) Nuhn, L.; Van Herck, S.; Best, A.; Deswarte, K.; Kokkinopoulou, M.; Lieberwirth, I.; Koynov, K.; Lambrecht, B. N.; De Geest, B. G. FRET Monitoring of Intracellular Ketal Hydrolysis in Synthetic Nanoparticles. *Angew. Chemie Int. Ed.* **2018**, *57* (33), 10760−10764.
(54) Deres, K.; Schild, H.; Wiesmüller, K.-H.; Jung, G.; Rammensee, H.-G. In Vivo Priming of Virus-Specific Cytotoxic T Lymphocytes with Synthetic Lipopeptide Vaccine. *Nature* **1989**, *342* (6249), 561−564.
(55) Koynov, K.; Butt, H. Current Opinion in Colloid & Interface Science Fluorescence Correlation Spectroscopy in Colloid and Interface Science. *Curr. Opin. Colloid Interface Sci.* **2012**, *17* (6), 377−387.
(56) Bermudez, L. E.; Parker, A.; Goodman, J. R. Growth within Macrophages Increases the Efficiency of Mycobacterium Avium in Invading Other Macrophages by a Complement Receptor-Independent Pathway. *Infect. Immun.* **1997**, *65* (5), 1916−1925.
(57) Peiser, L.; Gough, P. J.; Kodama, T.; Gordon, S. Macrophage Class A Scavenger Receptor-Mediated Phagocytosis of Escherichia Coli: Role of Cell Heterogeneity, Microbial Strain, and Culture Conditions in Vitro. *Infect. Immun.* **2000**, *68* (4), 1953−1963.
(58) Wang, X. Y.; Facciponte, J.; Chen, X.; Subjeck, J. R.; Repasky, E. A. Scavenger Receptor-A Negatively Regulates Antitumor Immunity. *Cancer Res.* **2007**, *67* (10), 4996−5002.
(59) Diken, M.; Kreiter, S.; Selmi, A.; Britten, C. M.; Huber, C.; Türeci, Ö.; Sahin, U. Selective Uptake of Naked Vaccine RNA by Dendritic Cells Is Driven by Macropinocytosis and Abrogated upon DC Maturation. *Gene Ther.* **2011**, *18* (7), 702−708.
(60) Shen, H.; Ackerman, A. L.; Cody, V.; Giodini, A.; Hinson, E. R.; Cresswell, P.; Edelson, R. L.; Saltzman, W. M.; Hanlon, D. J. Enhanced and Prolonged Cross-Presentation Following Endosomal

https://doi.org/10.1021/acsnano.1c10709
ACS Nano 2022, 16, 4426−4443

Escape of Exogenous Antigens Encapsulated in Biodegradable Nanoparticles. *Immunology* **2006**, *117* (1), 78−88.
(61) Hirosue, S.; Kourtis, I. C.; van der Vlies, A. J.; Hubbell, J. A.; Swartz, M. A. Antigen Delivery to Dendritic Cells by Poly(Propylene Sulfide) Nanoparticles with Disulfide Conjugated Peptides: Cross-Presentation and T Cell Activation. *Vaccine* **2010**, *28* (50), 7897−7906.
(62) De Koker, S.; De Geest, B. G.; Singh, S. K.; De Rycke, R.; Naessens, T.; Van Kooyk, Y.; Demeester, J.; De Smedt, S. C.; Grooten, J. Polyelectrolyte Microcapsules as Antigen Delivery Vehicles to Dendritic Cells: Uptake, Processing, and Cross-Presentation of Encapsulated Antigens. *Angew. Chemie - Int. Ed.* **2009**, *48* (45), 8485−8489.
(63) Cauwels, A.; Van Lint, S.; Paul, F.; Garcin, G.; De Koker, S.; Van Parys, A.; Wueest, T.; Gerlo, S.; Van der Heyden, J.; Bordat, Y.; et al. Delivering Type I Interferon to Dendritic Cells Empowers Tumor Eradication and Immune Combination Treatments. *Cancer Res.* **2018**, *78* (2), 463−474.
(64) Greinacher, A.; Thiele, T.; Warkentin, T. E.; Weisser, K.; Kyrle, P. A.; Eichinger, S. Thrombotic Thrombocytopenia after ChAdOx1 NCov-19 Vaccination. *N. Engl. J. Med.* **2021**, *384* (22), 2092−2101.
(65) Baharom, F.; Ramirez-Valdez, R. A.; Tobin, K. K. S.; Yamane, H.; Dutertre, C. A.; Khalilnezhad, A.; Reynoso, G. V.; Coble, V. L.; Lynn, G. M.; Mulè, M. P.; et al. Intravenous Nanoparticle Vaccination Generates Stem-like TCF1+ Neoantigen-Specific CD8+ T Cells. *Nat. Immunol.* **2021**, *22* (1), 41−52.
(66) Fridman, W. H.; Pages, F.; Sautès-Fridman, C.; Galon, J. The Immune Contexture in Human Tumours: Impact on Clinical Outcome. *Nat. Rev. Cancer* **2012**, *12* (4), 298−306.
(67) Brown, D. M.; Fisher, T. L.; Wei, C.; Frelinger, J. G.; Lord, E. M. Tumours Can Act as Adjuvants for Humoral Immunity. *Immunology* **2001**, *102* (4), 486−497.
(68) Seliger, B.; Wollscheid, U.; Momburg, F.; Blankenstein, T.; Huber, C. Characterization of the Major Histocompatibility Complex Class I Deficiencies in B16 Melanoma Cells. *Cancer Res.* **2001**, *61* (3), 1095−1099.
(69) Waisman, A.; Croxford, A. L.; Demircik, F. New Tools to Study the Role of B Cells in Cytomegalovirus Infections. *Med. Microbiol. Immunol.* **2008**, *197* (2), 145−149.

https://doi.org/10.1021/acsnano.1c10709
ACS Nano 2022, 16, 4426−4443